

Identification of Partial-Differential-Equations-Based Models from Noisy Data via Splines

Yujie Zhao¹, Xiaoming Huo², Yajun Mei²

¹ *Biostatistics and Research Decision Sciences Department, Merck & Co., Inc*

² *H. Milton Stewart School of Industrial and Systems Engineering, Georgia Tech*

Abstract: We propose a two-stage method called *Spline-Assisted Partial Differential Equations-based Model Identification* that can be used to identify models based on partial differential equations (PDEs) from noisy data. In the first stage, we employ cubic splines to estimate unobservable derivatives. The underlying PDE is based on a subset of these derivatives. This stage is computationally efficient. Its computational complexity is the product of a constant and the sample size, which is the lowest possible order of computational complexity. In the second stage, we apply the least absolute shrinkage and selection operator to identify the underlying PDE-based model. Statistical properties are developed, including the model identification accuracy. We validate our theory using numerical examples and a real-data case study based on an National Aeronautics and Space Administration data set.

Key words and phrases: partial differential equations, model identification, cubic splines, Lasso.

1. Introduction

Partial differential equations (PDEs) are widely used to model physical processes in fields such as engineering (Wang et al., 2019), physics (Xun et al., 2013), and biology (Lagergren et al., 2020). In these applications, there are two classes of technical issues: the *forward problem* and the *inverse problem*. The forward problem studies the properties of functions that PDEs determine. It has been extensively studied by mathematicians (Olver, 2014; Wang et al., 2014). Different from forward problems, inverse problems try to identify PDE-based models from the observed noisy data. Research on the inverse problem is relatively sparse, and the corresponding statistical property is notably less known. In this paper, we propose a method for solving the inverse problem, which we refer to as a *PDE identification problem*.

With the rise of big data, the PDE identification problem has become indispensable. A good PDE identification approach offers at least the following two benefits. First, we can predict future trends using the identified PDE model, conditional that such a model reflects the underlying processes. Second, interpretable PDE models enable scientists to validate/reexamine the underlying physical/biological laws governing the process.

We propose a new method for the PDE identification problem, called

Spline Assisted Partial Differential Equation based Model Identification (SAPDEMI).

SAPDEMI can efficiently identify the underlying PDE model from noisy data \mathcal{D} :

$$\begin{aligned} \mathcal{D} = \{ & (x_i, t_n, u_i^n) : x_i \in (0, X_{\max}) \subseteq \mathbb{R}, \forall i = 0, \dots, M-1, \\ & t_n \in (0, T_{\max}) \subseteq \mathbb{R}, \forall n = 0, \dots, N-1\} \in \Omega, \end{aligned} \quad (1.1)$$

where $x_i \in \mathbb{R}$ is a spatial variable, with $x_i \in (0, X_{\max})$, for $i = 0, 1, \dots, M-1$, and we call M the *spatial resolution*. The variable $t_n \in \mathbb{R}$ is a temporal variable, with $t_n \in (0, T_{\max})$, for $n = 0, 1, \dots, N-1$, and we call N the *temporal resolution*. We use T_{\max} and X_{\max} to denote the upper bound of the temporal variable and the spatial variable, respectively. The variable u_i^n is a representation of the ground truth $u(x_i, t_n)$, contaminated by the noise that follows a normal distribution with mean zero and stand deviation σ :

$$u_i^n = u(x_i, t_n) + \epsilon_i^n, \quad \epsilon_i^n \stackrel{i.i.d.}{\sim} N(0, \sigma^2). \quad (1.2)$$

Here, $u(x, t)$ is the ground truth function, which is determined by an underlying PDE model, and is assumed to satisfy the following equation:

$$\begin{aligned} \frac{\partial}{\partial t} u(x, t) = & \beta_{00}^* + \sum_{k=0}^{q_{\max}} \sum_{i=1}^{p_{\max}} \beta_{ki}^* \left[\frac{\partial^k}{\partial x^k} u(x, t) \right]^i + \\ & \sum_{\substack{i+j \leq p_{\max} \\ i, j > 0}} \sum_{\substack{0 < k < l \\ l \leq q_{\max}}} \beta_{k^i, l^j}^* \left[\frac{\partial^k}{\partial x^k} u(x, t) \right]^i \left[\frac{\partial^l}{\partial x^l} u(x, t) \right]^j. \end{aligned} \quad (1.3)$$

The left-hand side of the above equation is the first-order partial derivative of the underlying function with respect to the temporal variable t ,

and the right-hand side is the p_{\max} th-order polynomial of the derivatives with respect to the spatial variable x up to the q_{\max} th total order. For notational simplicity, we denote the ground truth coefficient vector, $\boldsymbol{\beta}^* = (\beta_{00}^*, \beta_{01}^*, \beta_{1^1}^*, \dots, \beta_{q_{\max}^{p_{\max}}}^*)$, as $\boldsymbol{\beta}^* = (\beta_1^*, \beta_2^*, \beta_3^*, \dots, \beta_K^*)^\top$, where $K = 1 + (p_{\max} + 1)q_{\max} + \frac{1}{2}q_{\max}(q_{\max} + 1)(p_{\max} - 1)!$ is the total number of coefficients on the right-hand side. Noted that, in practice, the majority of the entries in $\boldsymbol{\beta}^*$ are zero. For instance, in the transport equation $\frac{\partial}{\partial t}u(x, t) = a\frac{\partial}{\partial x}u(x, t)$, with any $a \neq 0$, we have only $\beta_3^* \neq 0$ and $\beta_i^* = 0$, for any $i \neq 3$ (see Olver, 2014, Section 2.2). Therefore, it is reasonable to assume that the coefficient $\boldsymbol{\beta}^*$ in (1.3) is sparse.

To identify the above model, we need to overcome two technical challenges. First, the derivatives in (1.3) are unobservable, and need to be estimated from the noisy observations. Second, we need to identify the underlying model, which is presumably simple (i.e., sparse).

We design our proposed SAPDEMI method as a two-stage method to identify the underlying PDE models from the noisy data \mathcal{D} . The first stage is called the *functional estimation stage*, where we estimate all the derivatives from the noisy data \mathcal{D} , including $\frac{\partial}{\partial t}u(x, t)$, $\frac{\partial}{\partial x}u(x, t)$, and so on. In this stage, we first use cubic splines (Shridhar and Balatoni, 1974) to fit the noisy data \mathcal{D} , and then we approximate the derivatives of the underly-

ing function from the derivatives of the estimated cubic splines. The second stage is called the *model identification stage*, where we apply the least absolute shrinkage and selection operator (Lasso) (Tibshirani, 1996) to identify the derivatives (or their combinations) that should be included in the PDE-based models. To ensure accuracy, we develop sufficient conditions for correct identification and the asymptotic properties of the identified models. The main tool used in our theoretical analysis is the primal-dual witness (PDW) method (see Hastie et al., 2015, Chapter 11).

The rest of this section is organized as follows. In Section 1.1, we review existing methods related to the PDE identification problem. In Section 1.2, we summarize our contributions.

1.1 Literature Review

A pioneering work in identifying underlying dynamic models from noisy data is that of Liang and Wu (2008). Their method is also a two-stage method. In the functional estimation stage, they use a local polynomial regression to estimate the value of the function and its derivatives. Subsequently, in the model identification stage, they use the least squares method. Following this work, various extensions have been proposed.

The first class of extensions modifies the functional estimation stage

of Liang and Wu (2008), and can be divided into three categories. **(F1)**. In the numerical differentiation category (Wu et al., 2012), the derivative $\frac{\partial}{\partial x}u(x, t)$ is simply approximated as $\frac{\partial}{\partial x}u(x, t) \approx \frac{u(x+\Delta x, t) - u(x-\Delta x, t)}{2\Delta x}$, where $(x + \Delta x, t)$ and $(x - \Delta x, t)$ are the two closest points to (x, t) in the x -domain. The essence of numerical differentiation is to approximate the first-order derivative as the slope of a nearby secant line. Although the implementation is easy, the approximation results can be highly biased, because its accuracy depends greatly on Δx : a small value of Δx yields large rounding errors in the subtraction (Ueberhuber, 2012), and a large value of Δx leads to poor performance when estimating the tangent slope using secants. Thus, this naive numerical differentiation is not preferred owing to its bias. **(F2)**. In the basis expansion category, researchers first approximate the unknown functions using basis expansion methods, and then approximate the derivatives of the underlying function as those of the approximated functions. There are multiple options for the choice of bases. The most popular basis is the local polynomial basis (see Liang and Wu, 2008; Bär et al., 1999; Schaeffer, 2017; Rudy et al., 2017; Parlitz and Merkwirth, 2000). Another popular choice is the spline basis (see Wu et al., 2012; Xun et al., 2013; Wang et al., 2019). Our proposed method belongs here. In this category, the major limitation of existing approaches is the potentially high

computational complexity. For instance, the local polynomial basis requires computational complexity of order $\max\{O(M^2N), O(MN^2)\}$ in the functional estimation stage. However, we show that our proposed SAPDEMI method requires only $O(MN)$. The sample size of the dataset \mathcal{D} is MN , so it takes at least MN numerical operations to read \mathcal{D} . Consequently, the lowest possible bound, in theory, is $O(MN)$, As achieved by our proposed SAPDEMI method. **(F3)**. In the machine or deep learning category, researchers first fit unknown functions using machine/deep learning methods, and then approximate the derivatives of the underlying functions as those of the approximated functions. A popular machine/deep learning method is the neural network (NN) approach. For instance, Srivastava et al. (2020) use an artificial neural network (ANN). These methods are limited by potential overfitting and the selection of the hyper-parameters.

The second class of extensions modifies the model identification stage of Liang and Wu (2008). Here, existing methods fall within the framework of the (penalized) least squares method, and we can again divide them into three categories. **(M1)**. In the least squares category, researchers study ordinary differential equation (ODE) identification (Miao et al., 2009) and PDE identification (Bär et al., 1999; Wu et al., 2012) , although they too have problems with overfitting. **(M2)**. In the ℓ_2 -penalized least squares cat-

egory, Xun et al. (2013) and Wang et al. (2019) penalize the smoothness of the unknown function, which is assumed to be in a prescribed reproducing kernel Hilbert space (RKHS). Essentially, this method falls within the framework of the ℓ_2 -penalized least squares method. Although this method helps to avoid overfitting by introducing the ℓ_2 -penalty, it has limited power in terms of “model selection”. **(M3)**. In the ℓ_1 -penalized least squares method category, Schaeffer (2017) identifies unknown dynamic models (i.e., functions) using the ℓ_1 -penalized least squares method. The author provides an efficient algorithm, based on the proximal mapping method, but does not discuss the statistical proprieties of the identified model. Recently, Kang et al. (2019) use a similar method to that of Schaeffer (2017), and demonstrate empirical successes. However, the derivation of the statistical theory is still missing. Our study addresses this gap in the literature.

In addition to the ℓ_2 - or ℓ_1 -penalized least squares methods, other methods have been proposed for the model selection stage, but are not as widely used. Here, examples include the Akaike information criterion (AIC) in Mangan et al. (2017), smoothly clipped absolute deviation (SCAD) in Lu et al. (2011), and hard-thresholding in Rudy et al. (2017). The first two approaches may lead to NP-hard problems in numerical implementation. The last one is ad-hoc, and may be difficult to analyze. Thus, we do

not address these alternative approaches.

Although our proposed SAPDEMI method applies to the PDE model, other nonparametric models are possible. Here, we take PDEs as an initial research project mainly because they are deterministic. Thus, we can compare our identified model with the true model, and show the model notification accuracy. As our initial research project, we prefer the PDE to machine learning (ML) models (e.g., neural network, random forest), because a PDE offers insight into the physical law. However, the ML models are usually black-box methods (Loyola-Gonzalez, 2019). We also prefer the PDE to the time series models, because it behaves like a “continuous version” of a time series model (Perona et al., 2000; Chen et al., 2018) at a high level. Furthermore, we prefer the PDE to the Gaussian process (GP) model, because the GP model restricts its response variables to follow a Gaussian distribution (Liu et al., 2020; Wei et al., 2018). Again, although we take the PDE as our initial research project, we are open to using the aforementioned nonparametric models in future work.

1.2 Our Contributions

Here, we summarize the contributions of our proposed method. **(1)** In the functional estimation stage, our proposed SAPDEMI method is com-

putationally efficient. Specifically, we require computational complexity of order $O(MN)$, which is the lowest possible order in this stage. In comparison, the aforementioned local polynomial regression requires computational complexity of order $\max\{O(M^2N), O(MN^2)\}$, which is higher. **(2)** For our proposed SAPDEMI method, we establish a theoretical guarantee of the model identification accuracy, which, to the best of our knowledge, is a novel result. **(3)** We extend our method to PDE-based model identification, and compare it with ODE-based model identification. The latter has more related work, whereas the former is not yet well understood.

The rest of the paper is organized as follows. In Section 2, we describe the technical details of our proposed SAPDEMI method. In Section 3, we present our main theory, including the sufficient conditions for correct identification, and the statistical properties of the identified models. In Section 4, we conduct numerical experiments to validate the theory from Section 3. In Section 5, we apply SAPDEMI to a real-world case study using data downloaded from the National Aeronautics and Space Administration (NASA). In Section 6, we conclude the paper and discuss some future research.

2. Proposed Method: SAPDEMI

The proposed SAPDEMI method is a two-stage method for identifying the underlying PDE model from noisy data \mathcal{D} . The first stage is called the *functional estimation stage*. Here, we estimate the function and its derivatives from the noisy data \mathcal{D} in (1.1), and use these as input in the second stage. The second stage is called the *model identification stage*, where we identify the underlying PDE-based model.

In our notation, scalars are denoted by lowercase letters (e.g., β). Vectors are denoted by lowercase bold face letters (e.g., $\boldsymbol{\beta}$), and its i th entry is denoted as β_i . Matrices are denoted by uppercase boldface letter (e.g., \mathbf{B}), and its (i, j) th entry is denoted as B_{ij} . For the vector $\boldsymbol{\beta} \in \mathbb{R}^p$, its k th norm is defined as $\|\boldsymbol{\beta}\|_k := (\sum_{i=1}^p |\beta_i|^k)^{1/k}$. For the matrix $\mathbf{B} \in \mathbb{R}^{m \times n}$, its Frobenius norm is defined as $\|\mathbf{B}\|_F = \sqrt{\sum_{i=1}^m \sum_{j=1}^n |B_{ij}|^2}$. We write $f(n) = O(g(n))$ if there exists a $G \in \mathbb{R}^+$ and an n_0 such that $|f(n)| \leq Gg(x)$, for all $n > n_0$.

This section is organized as follows. In Section 2.1, we introduce the functional estimation stage, and in Section 2.2, we describe the model identification stage.

2.1 Functional Estimation Stage

In this section, we describe the functional estimation stage of our proposed SAPDEMI method. In this stage, we estimate the functional values and their derivatives from the noisy data \mathcal{D} in (1.1). These derivatives include the derivatives with respect to the spatial/temporal variable x/t . We take derivatives with respect to the spatial variable x as an example; the derivatives with respect to the temporal variable t can be derived similarly.

The main tool that we use is the cubic spline. Suppose there is a cubic spline $s(x)$ over the knots $\{(x_i, u_i^n)\}_{i=0,1,\dots,M-1}$ satisfying the properties in McKinley and Levine (1998): **(1)** $s(x) \in C^2[x_0, x_{M-1}]$, where $C^2[x_0, x_{M-1}]$ denotes the sets of function whose 0th, first, and second derivatives are continuous in $[x_0, x_{M-1}]$; **(2)** For any $i = 1, \dots, M-1$, $s(x)$ is a polynomial of degree three in $[x_{i-1}, x_i]$; **(3)**. For the two end-points, x_0 and x_{M-1} , we have $s''(x_0) = s''(x_{M-1}) = 0$, where $s''(x)$ is the second derivative of $s(x)$.

By fitting the data $\{(x_i, u_i^n)\}_{i=0,1,\dots,M-1}$ (with a general fixed $n \in \{0, 1, \dots, N-1\}$) into the above cubic spline $s(x)$, one can solve $s(x)$ as the minimizer of the following optimization problem:

$$J_\alpha(s) = \alpha \sum_{i=0}^{M-1} w_i [u_i^n - s(x_i)]^2 + (1 - \alpha) \int_{x_0}^{x_{M-1}} s''(x)^2 dx, \quad (2.4)$$

where the first term $\alpha \sum_{i=0}^{M-1} w_i [u_i^n - s(x_i)]^2$ is the weighted sum of squares

2.1 Functional Estimation Stage

for the residuals, and we take the weight $w_0 = w_1 = \dots = w_{M-1} = 1$. In the second term, $(1 - \alpha) \int_{x_0}^{x_{M-1}} s''(x)^2 dx$, the function $s''(x)$ is the second derivative of $s(x)$, and this term is the penalty of the smoothness. In the above optimization problem, the parameter $\alpha \in (0, 1]$ controls the trade-off between the goodness of fit and the smoothness of the cubic spline. By minimizing the above optimization problem, we obtain an estimate of $s(x)$, together with its first derivative $s'(x)$ and its second derivative $s''(x)$. If the cubic spline approximates the underlying PDE curves well, we can declare that the derivatives of the underlying dynamic system can be approximated by the derivatives of the cubic spline $s(x)$, that is, we have $\widehat{u(x, t_n)} \approx \widehat{s(x)}$, $\frac{\partial}{\partial x} \widehat{u(x, t_n)} \approx \widehat{s'(x)}$, $\frac{\partial^2}{\partial x^2} \widehat{u(x, t_n)} \approx \widehat{s''(x)}$ (Ahlberg et al., 1967; Rubin and Graves Jr, 1975; Rashidinia and Mohammadi, 2008). Following a similar procedure to obtain the derivatives with respect to the spatial variable x , we can get the derivatives with respect to the temporal variable t , that is, $\frac{\partial}{\partial t} \widehat{u(x_i, t_n)}$, for any $i = 0, \dots, M-1$ and $n = 0, \dots, N-1$.

A nice property of the cubic spline is that there is a closed-form solution for (2.4). First, the value of the cubic spline $s(x)$ at the point $\{x_0, x_1, \dots, x_{M-1}\}$, that is, $\widehat{\mathbf{s}} = \left(\widehat{s(x_0)}, \widehat{s(x_1)}, \dots, \widehat{s(x_{M-1})} \right)^\top$, can be solved as

$$\widehat{\mathbf{s}} = [\alpha \mathbf{W} + (1 - \alpha) \mathbf{A}^\top \mathbf{M} \mathbf{A}]^{-1} \alpha \mathbf{W} \mathbf{u}^n. \quad (2.5)$$

2.1 Functional Estimation Stage

The above closed-form estimation can be used to approximate the function

that corresponds to the underlying PDE model, that is, $\widehat{\mathbf{s}} \approx \widehat{\mathbf{f}}$

$= \left(u(\widehat{x_0, t_n}), u(\widehat{x_1, t_n}), \dots, u(\widehat{x_{M-1}, t_n}) \right)^\top$. Here, $\mathbf{W} = \text{diag}(w_0, \dots, w_{M-1}) \in \mathbb{R}^{M \times M}$, vector $\mathbf{u}^n = (u_0^n, \dots, u_{M-1}^n)^\top \in \mathbb{R}^M$, and the matrices $\mathbf{A} \in \mathbb{R}^{(M-2) \times M}$

and $\mathbf{M} \in \mathbb{R}^{(M-2) \times (M-2)}$ are

$$\mathbf{A} = \begin{pmatrix} \frac{1}{h_0} & \frac{-1}{h_0} - \frac{1}{h_1} & \frac{1}{h_1} & \dots & 0 & 0 & 0 \\ 0 & \frac{1}{h_1} & \frac{-1}{h_1} - \frac{1}{h_2} & \dots & 0 & 0 & 0 \\ \vdots & \vdots & \vdots & \ddots & \vdots & \vdots & \vdots \\ 0 & 0 & 0 & \dots & \frac{1}{h_{M-3}} & \frac{-1}{h_{M-3}} - \frac{1}{h_{M-2}} & \frac{1}{h_{M-2}} \end{pmatrix}, \quad (2.6)$$

$$\mathbf{M} = \begin{pmatrix} \frac{h_0+h_1}{3} & \frac{h_1}{6} & 0 & \dots & 0 & 0 \\ \frac{h_1}{6} & \frac{h_1+h_2}{3} & \frac{h_2}{6} & \dots & 0 & 0 \\ \vdots & \vdots & \vdots & \ddots & \vdots & \vdots \\ 0 & 0 & 0 & \dots & \frac{h_{M-3}}{6} & \frac{h_{M-3}+h_{M-2}}{3} \end{pmatrix}, \quad (2.7)$$

respectively, with $h_i = x_{i+1} - x_i$, for $i = 0, 1, \dots, M-2$.

For the mathematical derivation of (2.5) from (2.4), and the derivation of first- and second-order derivatives, please refer to the Supplementary Material A.2.

The advantage of the cubic spline is that its computational complexity is only a linear polynomial of the sample size MN .

Proposition 2.1. Given the data \mathcal{D} in (1.1), if we use the cubic spline in (2.4) in the functional estimation stage, the computation complexity is of order

$$\max\{O(p_{\max}MN), O(K^3)\},$$

where p_{\max} is the highest polynomial order in (1.3), M/N is the spatial/temporal resolution, and K is the number of covariates in (1.3).

The proof can be found in the online Supplementary Material A.10.1.

As suggested by Proposition 2.1, when $p_{\max}, K \ll M, N$ (which is often the case in practice), it only requires $O(MN)$ numerical operations in the functional estimation stage. This is the lowest possible order of complexity in this stage, because MN is exactly the sample size of \mathcal{D} , and reading the data is a task of order $O(MN)$. Therefore, it is very efficient to use a cubic spline, because its computational complexity achieves the lowest possible order of complexity.

By way of comparisons, we discuss the computational complexity of the local polynomial regression, which is widely used in the literature (Liang and Wu, 2008; Bär et al., 1999; Schaeffer, 2017; Rudy et al., 2017; Parlitz and Merkwirth, 2000). This computational complexity is

$\max\{O(M^2N), O(MN^2), O(p_{\max}MN), O(K^3)\}$, which is much higher than ours for a generalized polynomial order p_{\max} . Specifically, if one restricts

2.2 Model Identification Stage

the local polynomial regression method to the same order as that of the cubic spline, its computational complexity is

$$\max\{O(M^2N), O(MN^2), O(K^3)\},$$

which is still higher than that of the cubic spline method in Proposition 2.1.

The related proposition and proof are available in Supplementary Materials A.10. We summarize the pros and cons of the cubic spline and the local polynomial regression in Table 1.

Table 1: Pros and cons of the cubic spline and the local polynomial regression in the functional estimation stage (assume that $p_{\max}, q_{\max}, K \ll M, N$)

Method	Cubic spline	Local polynomial regression
Pros	Computational complexity is $O(MN)$	Derivatives up to any order
Cons	If higher-than-2 order is required, need extensions beyond cubic splines.	Computational complexity is $\max\{(M^2N), O(MN^2)\}$

2.2 Model Identification Stage

In this section, we discuss the model identification stage of our proposed SAPDEMI method. In this stage, we identify the PDE model in (1.3).

Note that the model in (1.3) can be regarded as a linear regression model with a response variable that is the first-order derivative with respect to the

2.2 Model Identification Stage

temporal variable t , that is, $\frac{\partial u(x,t)}{\partial t}$, and the covariates are the derivative(s) with respect to the spatial variable x , including $\frac{\partial}{\partial x}u(x_i, t_n), \frac{\partial^2}{\partial x^2}u(x_i, t_n), \dots, \left(\frac{\partial^2}{\partial x^2}u(x_i, t_n)\right)^{p_{\max}}$. Because we have MN observations in the data set \mathcal{D} in (1.1), the response vector is of length MN :

$$\nabla_t \mathbf{u} = \left(\widehat{\frac{\partial u(x_0, t_0)}{\partial t}}, \dots, \widehat{\frac{\partial u(x_{M-1}, t_0)}{\partial t}}, \dots, \widehat{\frac{\partial u(x_{M-1}, t_{N-1})}{\partial t}} \right)^\top, \quad (2.8)$$

and the design matrix is of dimension $MN \times K$:

$$\mathbf{X} = \left(\widehat{\mathbf{x}}_0^0, \widehat{\mathbf{x}}_1^0, \dots, \widehat{\mathbf{x}}_{M-1}^0, \widehat{\mathbf{x}}_1^0, \dots, \widehat{\mathbf{x}}_{M-1}^{N-1} \right)^\top \in \mathbb{R}^{MN \times K}. \quad (2.9)$$

For the above design matrix \mathbf{X} , its $(nN + i + 1)$ st row is $\widehat{\mathbf{x}}_i^n = \left(1, \widehat{u(x_i, t_n)}, \frac{\partial}{\partial x} \widehat{u(x_i, t_n)}, \frac{\partial^2}{\partial x^2} \widehat{u(x_i, t_n)}, \left(\widehat{u(x_i, t_n)} \right)^2, \dots, \left(\frac{\partial^2}{\partial x^2} \widehat{u(x_i, t_n)} \right)^{p_{\max}} \right)^\top$. The K components of $\widehat{\mathbf{x}}_i^n$ are candidate terms in the PDE model. Note that all of the derivatives listed in (2.8) and (2.9) are estimated from the functional estimation stage described in Section 2.1.

Next, we use the Lasso to identify the nonzero coefficients in (1.3):

$$\widehat{\boldsymbol{\beta}} = \arg \min_{\boldsymbol{\beta}} \frac{1}{2MN} \|\nabla_t \mathbf{u} - \mathbf{X}\boldsymbol{\beta}\|_2^2 + \lambda \|\boldsymbol{\beta}\|_1, \quad (2.10)$$

where $\lambda > 0$ is a turning parameter that controls the trade-off between the sparsity of $\boldsymbol{\beta}$ and the goodness of fit. Given the ℓ_1 penalty in (2.10), $\widehat{\boldsymbol{\beta}}$ is sparse, that is, only a few of its entries are likely to be nonzero. Accordingly, we can identify the underlying PDE model as

$$\frac{\partial}{\partial t} u(x, t) = \mathbf{x}^\top \widehat{\boldsymbol{\beta}}, \quad (2.11)$$

where $\mathbf{x} = \left(1, u(x, t), \frac{\partial}{\partial x}u(x, t), \frac{\partial^2}{\partial x^2}u(x, t), (u(x, t))^2, \dots, \left(\frac{\partial^2}{\partial x^2}u(x, t)\right)^{p_{\max}}\right)^\top \in \mathbb{R}^K$. To solve equation (2.10), one can use the coordinate descent method (Beck and Tetrushvili, 2013; Tseng, 2001); see the online Supplementary Material A.4.

3. Theory on Statistical Properties

The theoretical evaluation is performed from two aspects. **(S1)**. First, we check whether our identified PDE model contains derivatives that are included in the “true” underlying PDE model. This is called the *support set recovery* property. Mathematically, we check whether $\text{supp}(\widehat{\boldsymbol{\beta}}) \subseteq \text{supp}(\boldsymbol{\beta}^*)$, where $\widehat{\boldsymbol{\beta}}$ is the minimizer of (2.10), $\boldsymbol{\beta}^*$ is the ground truth, and $\text{supp}(\boldsymbol{\beta}) = \{i : \beta_i \neq 0, \forall i, 1 \leq i \leq K\}$, for a general vector $\boldsymbol{\beta} \in \mathbb{R}^K$. However, the support recovery depends on the choice of the penalty parameter λ : a large value of λ leads to $\text{supp}(\widehat{\boldsymbol{\beta}}) = \emptyset$ (empty set), whereas a small value of λ results in a nonsparse $\widehat{\boldsymbol{\beta}}$. A proper selection of λ hopefully leads to the correct recovery of the support set recovery, that is, we have $\text{supp}(\widehat{\boldsymbol{\beta}}) \subseteq \text{supp}(\boldsymbol{\beta}^*)$. We discuss the selection of λ to achieve the above goal in Theorem 3.1. **(S2)**. Second, we are interested in an upper bound of the estimation error of our estimator. Specifically, we consider $\left\|\widehat{\boldsymbol{\beta}}_{\mathcal{S}} - \boldsymbol{\beta}_{\mathcal{S}}^*\right\|_{\infty}$, where $\mathcal{S} = \text{supp}(\boldsymbol{\beta}^*)$, and the vectors $\widehat{\boldsymbol{\beta}}_{\mathcal{S}}$ and $\boldsymbol{\beta}_{\mathcal{S}}^*$ are subvectors of $\widehat{\boldsymbol{\beta}}$ and

β^* , respectively, and contain only elements with indices that are in \mathcal{S} . An upper bound of the above estimation error is discussed in Theorem 3.2.

This section is organized as follows. In Section 3.1, we present the conditions for the theorems. In Section 3.2, we state two theorems.

3.1 Conditions for the Theorems

In this section, we introduce the conditions we use for our theorems. We begin with three frequently used conditions in ℓ_1 -regularized regression models. These conditions provide sufficient conditions for exact sparse recovery (see Hastie et al., 2015, Chapter 11). Subsequently, we introduce three conditions that are widely used in cubic spline-based functional estimation (see Silverman, 1984, (2.5)-(2.8)).

Condition 3.1 (Mutual Incoherence Condition). For some *incoherence parameter* $\mu \in (0, 1]$ and $P_\mu \in [0, 1]$, we have $\mathbb{P} \left(\|\mathbf{X}_{\mathcal{S}^c}^\top \mathbf{X}_{\mathcal{S}} (\mathbf{X}_{\mathcal{S}}^\top \mathbf{X}_{\mathcal{S}})^{-1}\|_\infty \leq 1 - \mu \right) \geq P_\mu$, where the matrix $\mathbf{X}_{\mathcal{S}^c}$ is the complement of $\mathbf{X}_{\mathcal{S}}$.

Condition 3.2 (Minimal Eigenvalue Condition). There exists some constant $C_{\min} > 0$ such that $\Lambda_{\min} \left(\frac{1}{NM} \mathbf{X}_{\mathcal{S}}^\top \mathbf{X}_{\mathcal{S}} \right) \geq C_{\min}$, almost surely. Here, $\Lambda_{\min}(\mathbf{A})$ denotes the minimal eigenvalue of a square matrix $\mathbf{A} \in \mathbb{R}^{n \times n}$. This condition can be considered a stronger version of the invertibility condition (see Hastie et al., 2015, Chapter 11).

3.1 Conditions for the Theorems

Condition 3.3 (Knots c.d.f. Convergence Condition). Suppose the sequence of the empirical distribution function over the design points $a = x_0 < \dots < x_{M-1} = b$, with different sample size M , is denoted as $F_M(x)$, that is, we have $F_M(x) = \frac{1}{M} \sum_{i=0}^{M-1} \mathbb{1}\{x_i \leq x\}$. Then, there exists an absolutely continuous distribution function F on $[a, b]$ such that $F_M \rightarrow F$ uniformly as $M \rightarrow +\infty$. Here, $\mathbb{1}\{A\}$ is the indicator of event A . A similar condition holds for the temporal variable: suppose the sequence of the empirical distribution function over the design points $\bar{a} = t_0 < \dots < t_{N-1} = \bar{b}$, with different sample size N , is denoted as $G_N(x)$. Then, there exists an absolutely continuous distribution function G on $[\bar{a}, \bar{b}]$ such that $G_N \rightarrow G$ uniformly as $N \rightarrow +\infty$.

Condition 3.4 (Knots p.d.f. Convergence Condition). Suppose the first derivatives of the functions F and G (defined in Condition 3.3) are denoted as f and g , respectively. Then we have

$$0 < \inf_{[x_0, x_{M-1}]} f \leq \sup_{[x_0, x_{M-1}]} f < +\infty \text{ and } 0 < \inf_{[t_0, t_{N-1}]} g \leq \sup_{[t_0, t_{N-1}]} g < +\infty,$$

and f and g also have bounded first derivatives on $[x_0, x_{M-1}]$, $[t_0, t_{N-1}]$.

Condition 3.5 (Gentle Decrease of Smoothing Parameter Condition). Suppose that $\zeta(M) = \sup_{[x_0, x_{M-1}]} |F_M - F|$. The smoothing parameter α in (2.4) depends on M in such a way that $\alpha \rightarrow 0$ and $\alpha^{-1/4} \zeta(M) \rightarrow 0$ as $M \rightarrow +\infty$.

A similar condition also holds for the temporal variable.

3.2 Main Theory

In the first theorem, we develop the lower bound of λ to realize the correct recovery of the support set, that is, $\mathcal{S}(\hat{\beta}) \subseteq \mathcal{S}(\beta^*)$.

Theorem 3.1. Given the data in (1.1), suppose the conditions in Lemma A.2 and Corollary A.1 (see the online Supplementary Material A.6) hold, as do Condition 3.1 - 3.5. If we take $M = O(N)$, then there exists a constant $\mathcal{C}_{(\sigma, \|u\|_{L^\infty(\Omega)})} > 0$ that is independent of the spatial resolution M and the temporal resolution N . Thus, if we set the cubic spline smoothing parameter with the spatial variable x in (2.4) as $\alpha = O\left((1 + M^{-4/7})^{-1}\right)$, set the cubic spline smoothing parameter with temporal variable t as $\bar{\alpha} = O\left((1 + N^{-4/7})^{-1}\right)$, and set the turning parameter

$$\lambda \geq \mathcal{C}(\sigma, \|u\|_{L^\infty(\Omega)}) \frac{\sqrt{K} \log(N)}{\mu N^{3/7-r}} \quad (3.12)$$

to identify the PDE model in (2.10), for some $r \in (0, \frac{3}{7})$, with sufficient large N , then with probability greater than $P_\mu - \underbrace{O(Ne^{-N^r})}_{P'}$, we have $\mathcal{S}(\hat{\beta}) \subseteq \mathcal{S}(\beta^*)$. Here, K is the number of columns of the design matrix \mathbf{X} in (2.10), and μ and P_μ are defined in Condition 3.1.

The proof of the above theorem can be found in the Supplementary

Material A.10, along with several lemmas, the conditions of which are standardized in cubic splines. The above theorem provides the lower bound of λ to realize the correct recovery of the support set. As indicated by (3.12), the lower bound is affected by several factors. First, it is affected by the temporal resolution N : as N increases, there is greater flexibility in tuning the penalty parameter λ . Second, the lower bound in (3.12) is affected by the incoherence parameter μ : if μ is small, then the lower bound increases. This is because a small μ means that the feature variable candidates are similar to each other. This phenomenon is called *multicollinearity*. In this case, we have a very limited choice in terms of selecting λ . However, we cannot increase the value of μ , because this is decided by the data set \mathcal{D} (see Condition 3.1). Third, the lower bound in (3.12) is affected by the number of columns of the matrix \mathbf{X} . If its number of columns is very large, then it requires a larger λ to identify the significant feature variables from among potential feature variables.

Note too that the probability $P_\mu - P'$ converges to P_μ as $N \rightarrow +\infty$. This limiting probability P_μ is determined by the data \mathcal{D} (see Condition (3.1)). Thus, when N is very large, our proposed SAPDEMI method can realize $\mathcal{S}(\hat{\beta}) \subseteq \mathcal{S}(\beta^*)$ with probability close to P_μ .

In the second theorem, we develop an upper bound for the estimating

error.

Theorem 3.2. Suppose the conditions in Theorem 3.1 hold. Then with probability greater than $1 - O(Ne^{-Nr}) \rightarrow 1$, there exists an $\dot{N} > 0$, such that when $N > \dot{N}$, we have

$$\left\| \widehat{\boldsymbol{\beta}}_{\mathcal{S}} - \boldsymbol{\beta}_{\mathcal{S}}^* \right\|_{\infty} \leq \sqrt{K} C_{\min} \left(\sqrt{K} \mathcal{C}_{(\sigma, \|u\|_{L^{\infty}(\Omega)})} \frac{\log(N)}{N^{3/7-r}} + \lambda \right),$$

where K is the number of columns of the matrix \mathbf{X} , $\mathcal{S} := \{i : \beta_i^* \neq 0, \forall i = 1, \dots, K\}$ and the vectors $\widehat{\boldsymbol{\beta}}_{\mathcal{S}}$, and $\boldsymbol{\beta}_{\mathcal{S}}^*$ are subvectors of $\widehat{\boldsymbol{\beta}}$ and $\boldsymbol{\beta}^*$, respectively, that contain only those elements with indices that are in \mathcal{S} . The theorem shows that when $N \rightarrow +\infty$, the error bound converges to 0.

The proof can be found in the Supplementary Material A.10. The previous theorem shows that the estimation error bound for the ℓ_{∞} -norm of the coefficient error in (3.13) consists of two components. The first component is affected by the temporal resolution N and the number of feature variable candidates K . As $N \rightarrow +\infty$, this first component converges to zero without an explicit dependence on the feature variable selected from (2.10). The second component is $\sqrt{K} C_{\min} \lambda$. When N increases to $+\infty$, this second component also converges to zero. This is because, as stated in Theorem 3.1, when $N \rightarrow +\infty$, the lower bound of λ , which realizes the correct support recovery, converges to zero. Thus, the accuracy of the

coefficient estimation improves as we increase N .

By combining Theorems 3.1 and 3.2, we find that when the minimum absolute value of the nonzero entries of β^* is sufficiently large, with an adequate choice of λ , we can guarantee the exact recovery. Mathematically, when $\min_{i \in \mathcal{S}} |(\beta_S^*)_i| > \sqrt{K} C_{\min} \left(\sqrt{K} \mathcal{C}_{(\sigma, \|u\|_{L^\infty(\Omega)})} \frac{\log(N)}{N^{3/7-r}} + \lambda \right)$, where $(\beta_S^*)_i$ refers to the i th element in the vector β_S^* , we have a correct signed support of $\hat{\beta}$. This helps when selecting the penalty parameters λ . In addition, the plot of the solution paths helps with the selection of the penalty parameters λ ; see Section 4.

4. Numerical Examples

We conduct numerical experiments to verify the computational efficiency and the statistical accuracy of our proposed SAPDEMI method.

Our examples are based on (1) the transport equation, (2) the inviscid Burgers' equation, and (3) the viscous Burgers' equation. We select these three PDE models as representatives, because they all play fundamental roles in modeling physical phenomena and demonstrate characteristic behaviors of a more complex system, such as dissipation and shock formation (Haberman, 1983). In addition to wide applications, they cover a wide range of categories, including the first-order PDE, second-order PDE, lin-

4.1 Example 1: Transport Equation

ear PDE, and nonlinear PDE, which cover most of the PDEs frequently seen in practice. Furthermore, the difficulty of identifying the above PDE models increases from the first example—the transport equation—to the last example—the viscous Burgers’ equation. We set $p_{\max} = 2$ and $q_{\max} = 2$ in (1.3) for the three numerical examples (see the full formula of the full model in the Supplementary Material A.11), that is, we identify the PDE model from the full model.

In terms of computational efficiency, the results of these three examples are the same, so we present only the result for the first example. We also verify Conditions 3.1 - 3.5 for the above three examples. The details of the verification are provided in the Supplementary Material A.12.

4.1 Example 1: Transport Equation

The PDE problem studied in this section is the transport equation. It is a linear first-order PDE model. Given its simplicity and straightforward physical meaning, it is widely used to model the concentration of a substance flowing in a fluid at a constant rate. For example, it can model a pollutant in a uniform fluid flow that is moving with velocity a (Olver, 2014,

Section 2.2):

$$\begin{cases} \frac{\partial}{\partial t}u(x, t) = a\frac{\partial}{\partial x}u(x, t), \quad \forall 0 \leq x \leq X_{\max}, 0 \leq t \leq T_{\max}; \\ u(x, 0) = f(x). \end{cases} \quad (4.13)$$

Here, $a \in \mathbb{R}$ is a fixed nonzero constant, known as the *wave speed*. In this section, we set $a = -2$, $f(x) = 2 \sin(4x)$, $X_{\max} = 1$ and $T_{\max} = 0.1$. Given these settings, there is a closed-form solution, $u(x, t) = 2 \sin(4x - 8t)$.

The dynamic pattern of the above transport equation is visualized in Fig. 1, where the subfigures (a), (b), and (c) show the ground truth and noisy observations under $\sigma = 0.05$ and $\sigma = 0.1$, respectively. The figure shows that a larger noise results in the shape of the transport equation being less smooth, potentially leading to additional difficulties in the PDE model identification.

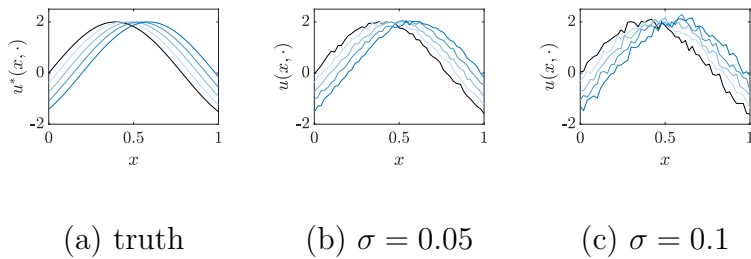


Figure 1: Noisy/True curves from (4.13) ($M = N = 100$).

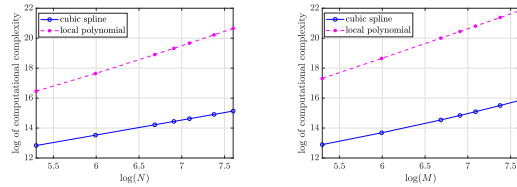
First, we consider the computational complexity of the functional estimation stage. We select the local polynomial regression as a benchmark, and visualize the number of numerical operations of the two methods in

4.1 Example 1: Transport Equation

Fig. 2, where the x-axis is $\log(M)$ or $\log(N)$, and the y-axis is the logarithm of the number of numerical operations. In Fig. 2, two scenarios are discussed: (1) M is fixed as 20, and N varies from 200 to 2000; and (2) N is fixed as 20, and M varies from 200 to 2000. Fig. 2 shows that, as M or N increases, so does the number of numerical operations in the functional estimation stage. We find that the cubic splines method needs fewer numerical operations, compared with the local polynomial regression. Furthermore, a simple linear regression of the four lines in Fig. 2 shows that in (a), the slope of the cubic spline is 0.9998, and as N goes to infinity, the slope gets get closer to one. This validates that the computational complexity of the cubic splines-based method is of order $O(N)$ when M is fixed. The result in (b) is similar. Thus, we numerically verify that the computational complexity of the cubic spline method is of order $O(MN)$. Similarly, for a local polynomial, we can numerically validate its computational complexity, which is $\max\{O(M^2N), O(MN^2)\}$.

We now verify numerically that with high probability, our SAPDEMI can correctly identify the underlying PDE models. From the formula of the transport equation in equation (4.13), we know that the correct feature variable is $\frac{\partial}{\partial x}u(x, t)$, and that other feature variables should not be identified. We discuss the identification accuracy under different sample sizes and

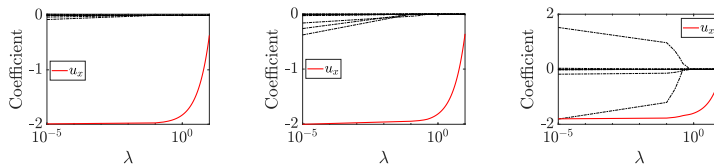
4.2 Example 2: Inviscid Burgers' Equation



(a) fixed $M = 20$ (b) fixed $N = 20$

Figure 2: Computational complexity of the cubic spline and a local polynomial.

magnitudes of noise. We find that the accuracy stays at 100%. To explain the high accuracy, we plot the solution paths in Fig. 3 under different σ , namely, $\sigma = 0.01, 0.1, 1$. From Fig. 3, we can increase λ to overcome this difficulty, and thus achieve a correct PDE identification.



(a) $\sigma = 0.01$ (b) $\sigma = 0.1$ (c) $\sigma = 1$

Figure 3: Solution paths in the transport equation under different σ and $M = N = 100$. The notation u_x is a simplification of $\frac{\partial}{\partial x}u(x, t)$.

4.2 Example 2: Inviscid Burgers' Equation

In this section, we investigate the inviscid Burgers' equation (see Olver, 2014, Section 8.4), which is representative of a first-order nonlinear PDE

4.2 Example 2: Inviscid Burgers' Equation

and is used frequently in applied mathematics, such as fluid mechanics, nonlinear acoustics, gas dynamics, and traffic flow. This PDE model was first introduced by Harry Bateman in 1915, and later studied by Johannes Martinus Burgers in 1948 (Whitham, 2011). The formula of the inviscid Burgers' equation is listed below:

$$\begin{cases} \frac{\partial}{\partial t}u(x, t) = -\frac{1}{2}u(x, t)\frac{\partial}{\partial x}u(x, t) \\ u(x, 0) = f(x) & 0 \leq x \leq X_{\max} \\ u(0, t) = u(1, t) = 0 & 0 \leq t \leq T_{\max} \end{cases}, \quad (4.14)$$

where we set $f(x) = \sin(2\pi x)$, $X_{\max} = 1$ and $T_{\max} = 0.1$. Fig. 4(a), (b), and (c) show the ground truth and noisy observations under $\sigma = 0.05$ and 0.1, respectively. Compared with our first example (transport equation in

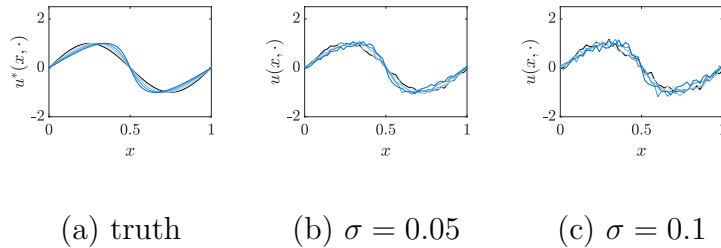


Figure 4: Noisy/True curves from (4.14) ($M = 50, N = 50$).

(4.13)), the inviscid Burgers' equation can be regarded an extension from the linear transport equation to a nonlinear transport equation. Specifically, if we set a in (4.13) as $a = -\frac{1}{2}u(x, t)$, then (4.13) is equivalent to (4.14). In the literature, this PDE model is considerably more challenging than the

4.3 Example 3: Viscous Burgers' Equation

linear transport PDE in (4.13): the wave speed in (4.13) depends only on the spatial variable x , whereas the wave speed in (4.14) depends on both the spatial variable x and the size of the disturbance $u(x, t)$. Given the complicated wave speed in (4.14), it can model more complicated dynamic patterns. For example, larger waves move faster, and overtake smaller, slow-moving waves.

In this example, SAPDEMI correctly identifies with an accuracy above 99% (see Fig. 8(a)). The effect of σ is also reflected in Fig. 5, where the length of the λ -interval for correct identification decreases as σ increases.

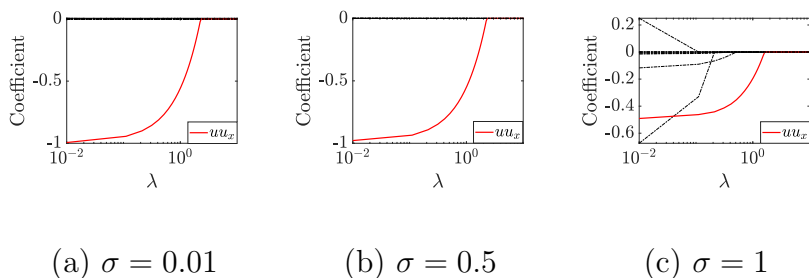


Figure 5: Solution paths in the inviscid Burgers' equation under different σ and $M = N = 100$. Here u and u_x are simplifications of $u(x, t)$ and $\frac{\partial}{\partial x}u(x, t)$, respectively.

4.3 Example 3: Viscous Burgers' Equation

In this section, we investigate the more challenging viscous Burgers' equation (see Olver, 2014, Section 8.4), which is a fundamental second-order

4.3 Example 3: Viscous Burgers' Equation

semilinear PDE. It is frequently employed to model physical phenomena in fluid dynamics (Bonkile et al., 2018) and nonlinear acoustics in dissipative media (Rudenko and Soluian, 1975). For example, in fluid and gas dynamics, we can interpret the term $\nu \frac{\partial^2}{\partial x^2} u(x, t)$ as modeling the effect of viscosity (Olver, 2014, Section 8.4). Thus, the viscous Burgers' equation represents a version of the equations of the viscous fluid flows, including the celebrated and widely applied Navier-Stokes equations (Whitham, 2011):

$$\left\{ \begin{array}{l} \frac{\partial u(x,t)}{\partial t} = -\frac{1}{2}u(x,t)\frac{\partial}{\partial x}u(x,t) + \nu\frac{\partial^2}{\partial x^2}u(x,t) \\ u(x,0) = f(x) \\ u(0,t) = u(1,t) = 0 \end{array} \right. \quad \begin{array}{l} 0 \leq x \leq X_{\max} \\ \\ 0 \leq t \leq T_{\max} \end{array} \quad , \quad (4.15)$$

where we set $f(x) = \sin^2(4\pi x) + \sin^3(2\pi x)$, $X_{\max} = 1$, $T_{\max} = 0.1$ and $\nu = 0.1$. Fig. 6 shows the corresponding curves, where (a), (b), and (c) are the ground truth and noisy observations under $\sigma = 0.05$ and $\sigma = 0.1$, respectively.

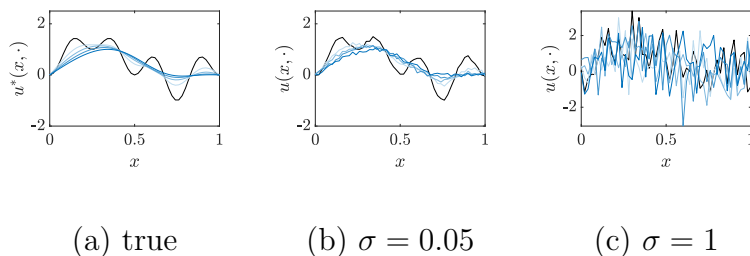


Figure 6: Noisy/True curves from (4.15) ($M = 50$, $N = 50$).

Compared with the previous two PDE models (transport equation in

4.3 Example 3: Viscous Burgers' Equation

(4.13) and inviscid Burgers' equation in (4.14)), the above PDE is more complicated and challenging. This is because the viscous Burgers' equation involves not only the first-order derivative, but also the second-order derivatives. Our simulations provide sufficiently complicated examples.

Based on Fig. 8(b), we conclude that with high probability, our proposed SAPDEMI can correctly identify the underlying viscous Burgers' equation, for the following reasons. When $M = N = 200$ or 150 , the accuracy stays above 90% for all levels of $\sigma \in [0.01, 1]$. When $M = N = 100$, the accuracy is above 70% when $\sigma \in [0.01, 0.5]$, and reduces to 50% when $\sigma = 1$. This makes sense, because as shown in Fig. 7, when σ increases from 0.01 to 1, the length of the λ -interval for correct identification decreases, making it more difficult to realize a correct identification. Thus, if we encounter a very noisy data set \mathcal{D} , a larger sample size is preferred.

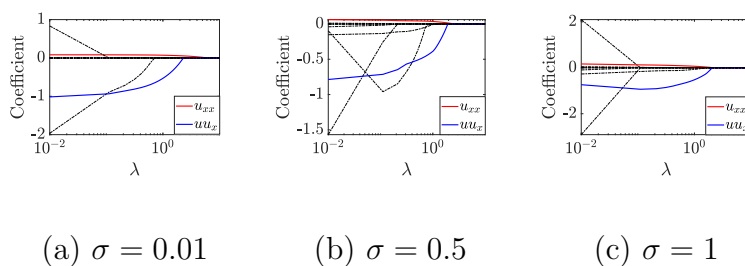
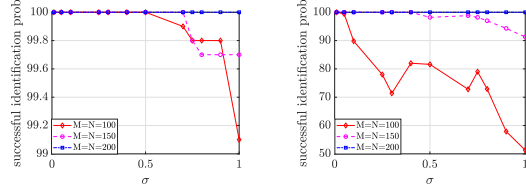


Figure 7: Solution paths in the viscous Burgers' equation under different σ and $M = N = 100$. The notation u_{xx} and uu_x stand for $u(x, t) \frac{\partial}{\partial x} u(x, t)$ and $\frac{\partial^2}{\partial x^2} u(x, t)$, respectively.

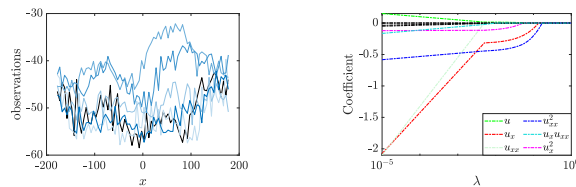


(a) example 2 (b) example 3

Figure 8: Curves of successful identification probability.

5. Case Study

In this section, we apply SAPDEMI to a real-world data set that is a subset of the Cloud-Aerosol Lidar and Infrared Pathfinder Satellite Observations (CALIPSO) data set downloaded from NASA. The CALIPSO reports the monthly mean of temperature in 2017 at 34°N and 110.9418 meters above the Earth’s surface over a uniform spatial grid from 180°W to 180°E, with equally spaced 5° intervals. The missing data are handled either by direct imputation or by using the instrument methods Chen et al. (2018, 2021); Chen and Fang (2019); Chen et al. (2018).



(a) observed temperature (b) solution path

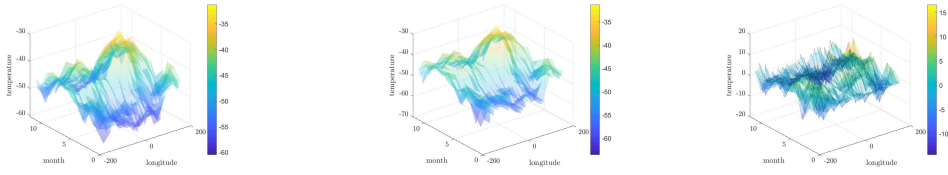
Figure 9: Visualization and identification of the CALIPSO data.

The identified PDE model ($N = 12, M = 72$), reasonably speaking, is

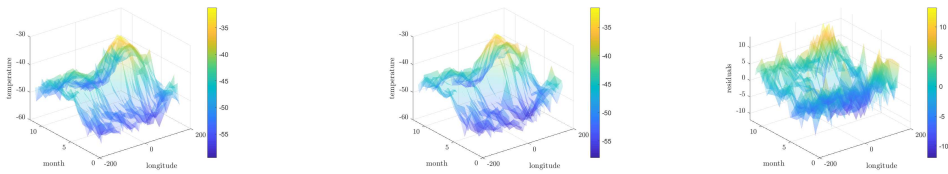
$$\frac{\partial}{\partial t}u(x, t) = a \frac{\partial}{\partial x}u(x, t) + b \left(\frac{\partial^2}{\partial x^2}u(x, t) \right)^2, \quad (5.16)$$

where the values of a and b can be estimated using a simple linear regression on the selected derivatives, that is, $\frac{\partial}{\partial x}u(x, t)$ and $\left(\frac{\partial^2}{\partial x^2}u(x, t) \right)^2$. The linear regression suggests reasonable values of $a = -0.2505$ and $b = 1.7648$. Note that we focus on identification, that is, identifying $\frac{\partial}{\partial x}u(x, t)$ and $\left(\frac{\partial^2}{\partial x^2}u(x, t) \right)^2$ from many derivative candidates, rather than estimating the coefficients. Therefore, we use $a = -0.2505$ and $b = 1.7648$ as a reference.

Because the CALIPSP is a real-world data set, we do not know the ground truth of the underlying PDE model. Here we provide some justifications. First, from the solution path in Fig. 9(b), the coefficients of $\frac{\partial}{\partial x}u(x, t)$ and $\left(\frac{\partial^2}{\partial x^2}u(x, t) \right)^2$ remain nonzeros under $\lambda = 0.05$, whereas the other coefficients are all zero. Second, the identified PDE model in (5.16) fits well to the training data (see Fig. 10 (a.1)-(a.3)). Third, the identified PDE model in (5.16) predicts well in the testing data (see Fig 10 (b.1)-(b.3)). Thus, our proposed SAPDEMI method performs well in the CALIPSO data set, because it adequately predicts the feature values in 2018.



(a.1) observed 2017 temp (a.2) fitted 2017 temp (a.3) 2017 residual



(b.1) observed 2018 temp (b.2) predicted 2018 temp (b.3) 2018 residual

Figure 10: 3D surface plots of the temperatures in 2017/2018.

6. Conclusion

We have proposed an SAPDEMI method for identifying underlying PDE models from noisy data. The proposed method is computationally efficient, and we derive a statistical guarantee on its performance. We realize there are many promising future research directions, including, but not limited to, incorporating a multivariate spatial variable ($\mathbf{x} \in \mathbb{R}^d$ with $d \geq 2$) (Habermann and Kindermann, 2007), and the interactions between spatial and temporal variables. In our paper, we aim at showing the methodology to solve the PDE identification, so we skip discuss the above future research and our paper should provide a good starting point for these further

research.

Supplementary Material

There is an online supplementary material for this paper, which includes (1) lemmas to derive the main theory; (2) numerical details of the figures in the simulation; (3) proofs and other technical details which is not covered in the main body of the paper due to the page limitation.

Acknowledgments

The authors gratefully acknowledge the support of NSF grants DMS-2015405, DMS-2015363, and the TRIAD (a part of the TRIPODS program at NSF, located at Georgia Tech and enabled by the NSF grant CCF-1740776).

References

- Ahlberg, J., J. Walsh, R. Bellman, and E. N. Nilson (1967). *The theory of splines and their applications*. Academic press.
- Aydin, D., M. Memmedli, and R. E. Omay (2013). Smoothing parameter selection for nonparametric regression using smoothing spline. *European Journal of Pure and applied mathematics* 6(2), 222–238.

REFERENCES

- Bär, M., R. Hegger, and H. Kantz (1999). Fitting partial differential equations to space-time dynamics. *Physical Review E* 59(1), 337.
- Beck, A. and L. Tretuashvili (2013). On the convergence of block coordinate descent type methods. *SIAM journal on Optimization* 23(4), 2037–2060.
- Bonkile, M. P., A. Awasthi, C. Lakshmi, V. Mukundan, and V. Aswin (2018). A systematic literature review of burgers' equation with recent advances. *Pramana* 90(6), 1–21.
- Butcher, J. C. and N. Goodwin (2008). *Numerical methods for ordinary differential equations*, Volume 2. Wiley Online Library.
- Chen, J. and F. Fang (2019). Semiparametric likelihood for estimating equations with non-ignorable non-response by non-response instrument. *Journal of Nonparametric Statistics* 31(2), 420–434.
- Chen, J., F. Fang, and Z. Xiao (2018). Semiparametric inference for estimating equations with nonignorable missing covariates. *Journal of Nonparametric Statistics* 30(3), 796–812.
- Chen, J., D. Ohlssen, and Y. Zhou (2018). Functional mixed effects model for the analysis of dose-titration studies. *Statistics in Biopharmaceutical Research* 10(3), 176–184.
- Chen, J., J. Shao, and F. Fang (2021). Instrument search in pseudo-likelihood approach for nonignorable nonresponse. *Annals of the Institute of Statistical Mathematics* 73(3), 519–533.
- Chen, J., B. Xie, and J. Shao (2018). Pseudo likelihood and dimension reduction for data with

REFERENCES

- nonignorable nonresponse. *Statistical Theory and Related Fields* 2(2), 196–205.
- Craven, P. and G. Wahba (1978). Smoothing noisy data with spline functions. *Numerische mathematik* 31(4), 377–403.
- Fan, J., T. Gasser, I. Gijbels, M. Brockmann, and J. Engel (1997). Local polynomial regression: optimal kernels and asymptotic minimax efficiency. *Annals of the Institute of Statistical Mathematics* 49(1), 79–99.
- Friedman, J., T. Hastie, and R. Tibshirani (2010). Regularization paths for generalized linear models via coordinate descent. *Journal of statistical software* 33(1), 1.
- Haberman, R. (1983). *Elementary applied partial differential equations*, Volume 987. Prentice Hall Englewood Cliffs, NJ.
- Habermann, C. and F. Kindermann (2007). Multidimensional spline interpolation: Theory and applications. *Computational Economics* 30(2), 153–169.
- Hastie, T., R. Tibshirani, and M. Wainwright (2015). *Statistical learning with sparsity: the lasso and generalizations*. CRC press.
- Hudson, H. (1974). Empirical bayes estimation technical report no 58.
- Kang, S. H., W. Liao, and Y. Liu (2019). IDENT: Identifying differential equations with numerical time evolution. *arXiv preprint arXiv:1904.03538*.
- Lagergren, J. H., J. T. Nardini, G. Michael Lavigne, E. M. Rutter, and K. B. Flores (2020). Learning partial differential equations for biological transport models from noisy spatio-

REFERENCES

- temporal data. *Proceedings of the Royal Society A* 476(2234), 20190800.
- Lambert, J. D. et al. (1991). *Numerical methods for ordinary differential systems*, Volume 146. Wiley New York.
- Liang, H. and H. Wu (2008). Parameter estimation for differential equation models using a framework of measurement error in regression models. *Journal of the American Statistical Association* 103(484), 1570–1583.
- Liu, H., Y.-S. Ong, X. Shen, and J. Cai (2020). When gaussian process meets big data: A review of scalable gps. *IEEE transactions on neural networks and learning systems* 31(11).
- Loyola-Gonzalez, O. (2019). Black-box vs. white-box: Understanding their advantages and weaknesses from a practical point of view. *IEEE Access* 7, 154096–154113.
- Lu, T., H. Liang, H. Li, and H. Wu (2011). High-dimensional ODEs coupled with mixed-effects modeling techniques for dynamic gene regulatory network identification. *Journal of the American Statistical Association* 106(496), 1242–1258.
- Mack, Y.-p. and B. W. Silverman (1982). Weak and strong uniform consistency of kernel regression estimates. *Zeitschrift für Wahrscheinlichkeitstheorie und verwandte Gebiete* 61(3), 405–415.
- Mallows, C. L. (2000). Some comments on cp. *Technometrics* 42(1), 87–94.
- Mangan, N. M., J. N. Kutz, S. L. Brunton, and J. L. Proctor (2017). Model selection for dynamical systems via sparse regression and information criteria. *Proceedings of the Royal*

REFERENCES

- Society A: Mathematical, Physical and Engineering Sciences* 473(2204), 20170009.
- McKinley, S. and M. Levine (1998). Cubic spline interpolation. *College of the Redwoods* 45(1), 1049–1060.
- Messer, K. (1991). A comparison of a spline estimate to its equivalent kernel estimate. *The Annals of Statistics* 19(2), 817–829.
- Miao, H., C. Dykes, L. M. Demeter, and H. Wu (2009). Differential equation modeling of HIV viral fitness experiments: model identification, model selection, and multimodel inference. *Biometrics* 65(1), 292–300.
- Olver, P. J. (2014). *Introduction to partial differential equations*. Springer.
- Parlitz, U. and C. Merkwirth (2000). Prediction of spatiotemporal time series based on reconstructed local states. *Physical review letters* 84(9), 1890.
- Perona, P., A. Porporato, and L. Ridolfi (2000). On the trajectory method for the reconstruction of differential equations from time series. *Nonlinear Dynamics* 23(1), 13–33.
- Rashidinia, J. and R. Mohammadi (2008). Non-polynomial cubic spline methods for the solution of parabolic equations. *International Journal of Computer Mathematics* 85(5), 843–850.
- Reinsch, C. H. (1967). Smoothing by spline functions. *Numerische mathematik* 10(3), 177–183.
- Rice, J. and M. Rosenblatt (1983). Smoothing splines: regression, derivatives and deconvolution. *The annals of Statistics*, 141–156.
- Rosenblatt, M. (1952). Remarks on a multivariate transformation. *The annals of mathematical*

REFERENCES

- statistics* 23(3), 470–472.
- Rubin, S. G. and R. A. Graves Jr (1975). A cubic spline approximation for problems in fluid mechanics. *NASA STI/Recon Technical Report N 75*, 33345.
- Rudenko, O. and S. Soluian (1975). The theoretical principles of nonlinear acoustics. *Moscow Izdatel Nauka*.
- Rudy, S. H., S. L. Brunton, J. L. Proctor, and J. N. Kutz (2017). Data-driven discovery of partial differential equations. *Science Advances* 3(4), e1602614.
- Schaeffer, H. (2017). Learning partial differential equations via data discovery and sparse optimization. *Proceedings of the Royal Society A: Mathematical, Physical and Engineering Sciences* 473(2197), 20160446.
- Shridhar, M. and N. Balatoni (1974). A generalized cubic spline technique for identification of multivariable systems. *Journal of Mathematical Analysis and Applications* 47(1), 78–90.
- Silverman, B. W. (1978). Weak and strong uniform consistency of the kernel estimate of a density and its derivatives. *The Annals of Statistics*, 177–184.
- Silverman, B. W. (1984). Spline smoothing: the equivalent variable kernel method. *The Annals of Statistics*, 898–916.
- Srivastava, K., M. Ahlawat, J. Singh, and V. Kumar (2020). Learning partial differential equations from noisy data using neural networks. In *Journal of Physics: Conference Series*, Volume 1655, pp. 012075. IOP Publishing.

REFERENCES

- Tibshirani, R. (1996). Regression shrinkage and selection via the lasso. *Journal of the Royal Statistical Society: Series B (Methodological)* 58(1), 267–288.
- Tseng, P. (2001). Convergence of a block coordinate descent method for nondifferentiable minimization. *Journal of optimization theory and applications* 109(3), 475–494.
- Tusnády, G. (1977). A remark on the approximation of the sample DF in the multidimensional case. *Periodica Mathematica Hungarica* 8(1), 53–55.
- Ueberhuber, C. W. (2012). *Numerical computation 1: methods, software, and analysis*. Springer Science & Business Media.
- Wahba, G. (1975). Smoothing noisy data with spline functions. *Numerische mathematik* 24(5), 383–393.
- Wang, D., K. Liu, and X. Zhang (2019). Spatiotemporal thermal field modeling using partial differential equations with time-varying parameters. *IEEE Transactions on Automation Science and Engineering*.
- Wang, H., D. Yang, and S. Zhu (2014). Inhomogeneous Dirichlet boundary-value problems of space-fractional diffusion equations and their finite element approximations. *SIAM Journal on Numerical Analysis* 52(3), 1292–1310.
- Wei, S.-b., W. Wang, N. Liu, J. Chen, X.-y. Guo, R.-b. Tang, R.-h. Yu, D.-y. Long, C.-h. Sang, C.-x. Jiang, et al. (2018). U-shaped association between serum free triiodothyronine and recurrence of atrial fibrillation after catheter ablation. *Journal of Interventional Cardiac Electrophysiology* 51(3), 263–270.

REFERENCES

- Whitham, G. B. (2011). *Linear and nonlinear waves*. John Wiley & Sons.
- Winkelbauer, A. (2012). Moments and absolute moments of the normal distribution. *arXiv preprint arXiv:1209.4340*.
- Wu, H., H. Xue, and A. Kumar (2012). Numerical discretization-based estimation methods for ordinary differential equation models via penalized spline smoothing with applications in biomedical research. *Biometrics* 68(2), 344–352.
- Xun, X., J. Cao, B. Mallick, A. Maity, and R. J. Carroll (2013). Parameter estimation of partial differential equation models. *Journal of the American Statistical Association* 108(503), 1009–1020.

A. Supplementary Material

A.1 Overview of Our Proposed Algorithm

We give an overview our SAPDEMI method in Algorithm 1.

Algorithm 1: Overview of our proposed SAPDEMI method

Input: Data from the unknown PDE model as in (1.1); penalty parameter used in the

Lasso identify model: $\lambda > 0$; smoothing parameter used in the cubic spline:

$$\alpha, \bar{\alpha} \in (0, 1].$$

Output: The identified/recovered PDE model.

1 Functional estimation stage:

2 $\left[\begin{array}{l} \text{Estimate } \mathbf{X}, \nabla_t \mathbf{u} \text{ by cubic spline with } \alpha, \bar{\alpha} \in (0, 1]. \end{array} \right.$

3 Model identification stage:

4 $\left[\begin{array}{l} \text{The unknown PDE system is recovered as: } \frac{\partial}{\partial t} u(x, t) = \mathbf{x}^\top \hat{\boldsymbol{\beta}}, \text{ where} \\ \hat{\boldsymbol{\beta}} = \arg \min_{\boldsymbol{\beta}} \frac{1}{2MN} \|\nabla_t \mathbf{u} - \mathbf{X}\boldsymbol{\beta}\|_2^2 + \lambda \|\boldsymbol{\beta}\|_1 \text{ and } \mathbf{x} = \\ \left(1, u(x, t), \frac{\partial u(x, t)}{\partial x}, \frac{\partial^2 u(x, t)}{\partial x^2}, (u(x, t))^2, u(x, t) \frac{\partial u(x, t)}{\partial x}, \dots, \right)^\top. \end{array} \right.$

A.2 Derivation of the 0-th, First, Second Derivative of the Cubic Spline in Section 2.1

In this section, we focus on solving the derivatives of $u(x, t_n)$ with respect to x , i.e.,

$\left\{ u(x_i, t_n), \frac{\partial}{\partial x} u(x_i, t_n), \frac{\partial^2}{\partial x^2} u(x_i, t_n) \right\}_{i=0,1,\dots,M-1}$, for any $n = 0, 1, \dots, N - 1$. To realize this

objective, we first fix t as t_n for a general $n \in \{0, 1, \dots, N - 1\}$. Then we use cubic spline to fit

A.2 Derivation of the 0-th, First, Second Derivative of the Cubic Spline in Section 2.1

data $\{(x_i, u_n^i)\}_{i=0,1,\dots,M-1}$.

Suppose the cubic polynomial spline over the knots $\{(x_i, u_n^i)\}_{i=0,1,\dots,M-1}$ is $s(x)$. So under good approximation, we can regard $s(x), s'(x), s''(x)$ as the estimators of $u(x_i, t_n), \frac{\partial}{\partial x}u(x, t_n), \frac{\partial^2}{\partial x^2}u(x, t_n)$, where $s'(x), s''(x)$ is the first and second derivatives of $s(x)$, respectively.

Let's first take a look at the zero-order derivatives of $s(x)$. By introducing matrix algebra, the objective function in equation (2.4) can be rewritten as

$$J_\alpha(s) = \alpha(\mathbf{u}^n - \mathbf{f})^\top \mathbf{W}(\mathbf{u}^n - \mathbf{f}) + (1 - \alpha)\mathbf{f}^\top \mathbf{A}^\top \mathbf{M}^{-1} \mathbf{A} \mathbf{f} \quad (\text{A.17})$$

where vector

$$\mathbf{f} = \begin{pmatrix} s(x_0) \\ s(x_1) \\ \vdots \\ s(x_{M-1}) \end{pmatrix} \triangleq \begin{pmatrix} f_0 \\ f_1 \\ \vdots \\ f_{M-1} \end{pmatrix}, \mathbf{u}^n = \begin{pmatrix} u_0^n \\ u_1^n \\ \vdots \\ u_{M-1}^n \end{pmatrix}$$

and matrix $\mathbf{W} = \text{diag}(w_0, w_1, \dots, w_{M-1})$ and matrix \mathbf{A} is defined in (2.6). By taking the derivative of (A.17) with respect to \mathbf{f} and set it as zero, we have

$$\hat{\mathbf{f}} = [\alpha \mathbf{W} + (1 - \alpha) \mathbf{A}^\top \mathbf{M} \mathbf{A}]^{-1} \alpha \mathbf{W} \mathbf{u}^n. \quad (\text{A.18})$$

Then we solve the second-order derivative with respect to x . Let us first suppose that the cubic spline $s(x)$ in $[x_i, x_{i+1}]$ is denoted $s_i(x)$, and we denote $s_i''(x_i) = \sigma_i, s_i''(x_{i+1}) = \sigma_{i+1}$.

Then we have $\forall x \in [x_i, x_{i+1}]$ ($0 \leq i \leq M - 2$),

$$s_i''(x) = \sigma_i \frac{x_{i+1} - x}{h_i} + \sigma_{i+1} \frac{x - x_i}{h_i},$$

A.2 Derivation of the 0-th, First, Second Derivative of the Cubic Spline in Section 2.1

where matrix \mathbf{M} is defined in (2.7). This is because $s_i''(x)$ with $x \in [x_i, x_{i+1}]$ is a linear function.

By taking a double integral of the above equation, we have

$$s_i(x) = \frac{\sigma_i}{6h_i}(x_{i+1} - x)^3 + \frac{\sigma_{i+1}}{6h_i}(x - x_i)^3 + c_1(x - x_i) + c_2(x_{i+1} - x), \quad (\text{A.19})$$

where c_1, c_2 is the unknown parameters to be estimated. Because $s_i(x)$ interpolates two end-points (x_i, f_i) and (x_{i+1}, f_{i+1}) , if we plug x_i, x_{i+1} into the above $s_i(x)$, we have

$$\begin{cases} f_i &= s_i(x_i) = \frac{\sigma_i}{6}h_i^2 + c_2h_i \\ f_{i+1} &= s_i(x_{i+1}) = \frac{\sigma_{i+1}}{6}h_i^2 + c_1h_i, \end{cases}$$

where we can solve c_1, c_2 as

$$\begin{cases} c_1 &= (f_{i+1} - \frac{\sigma_{i+1}}{6}h_i^2)/h_i, \\ c_2 &= (f_i - \frac{\sigma_i}{6}h_i^2)/h_i. \end{cases}$$

By plugging in the value of c_1, c_2 into equation (A.19), we have ($0 \leq i \leq M - 2$)

$$s_i(x) = \frac{\sigma_i}{6h_i}(x_{i+1} - x)^3 + \frac{\sigma_{i+1}}{6h_i}(x - x_i)^3 + \left(\frac{f_{i+1}}{h_i} - \frac{\sigma_{i+1}h_i}{6}\right)(x - x_i) + \left(\frac{f_i}{h_i} - \frac{\sigma_i h_i}{6}\right)(x_{i+1} - x),$$

with its first derivative as

$$s_i'(x) = -\frac{\sigma_i}{2h_i}(x_{i+1} - x)^2 + \frac{\sigma_{i+1}}{2h_i}(x - x_i)^2 + \frac{f_{i+1} - f_i}{h_i} - \frac{h_i}{6}(\sigma_{i+1} - \sigma_i). \quad (\text{A.20})$$

Because $s'_{i-1}(x_i) = s'_i(x_i)$, for $1 \leq i \leq M - 2$, we have

$$\frac{1}{6}h_{i-1}\sigma_{i-1} + \frac{1}{3}(h_{i-1} + h_i)\sigma_i + \frac{1}{6}h_i\sigma_{i+1} = \frac{f_{i+1} - f_i}{h_i} - \frac{f_i - f_{i-1}}{h_{i-1}}. \quad (\text{A.21})$$

Equation (A.21) gives $M - 2$ equations. Recall $\sigma_0 = \sigma_{M-1} = 0$, so totally we get M equations,

which is enough to solve M parameters, i.e., $\sigma_0, \sigma_1, \dots, \sigma_{M-1}$. We write out the above system

A.2 Derivation of the 0-th, First, Second Derivative of the Cubic Spline in Section 2.1

of linear equations, where we hope to identify a fast numerical approach to solve it. The system

of linear equations is:

$$\left\{ \begin{array}{l} \frac{1}{3}(h_0 + h_1)\sigma_1 + \frac{1}{6}h_1\sigma_2 = \frac{u_2^n - u_1^n}{h_1} - \frac{f_1 - u_0}{h_0} \\ \frac{1}{6}h_1\sigma_1 + \frac{1}{3}(h_1 + h_2)\sigma_2 + \frac{1}{6}h_2\sigma_3 = \frac{f_3 - f_2}{h_1} - \frac{f_2 - f_1}{h_0} \\ \vdots \\ \frac{1}{6}h_{M-4}\sigma_{M-4} + \frac{1}{3}(h_{M-4} + h_{M-3})\sigma_{M-3} + \frac{1}{6}h_{M-3}\sigma_{M-2} = \frac{f_{M-2} - f_{M-3}}{h_{M-3}} - \frac{f_{M-3} - f_{M-4}}{h_{M-4}} \\ \frac{1}{6}h_{M-3}\sigma_{M-3} + \frac{1}{3}(h_{M-3} + h_{M-2})\sigma_{M-2} = \frac{f_{M-1} - f_{M-2}}{h_{M-2}} - \frac{f_{M-2} - f_{M-3}}{h_{M-3}} \end{array} \right.$$

From the above system of equation, we can see that the second derivative of cubic spline $s(x)$

can be solved by the above system of linear equation, i.e.,

$$\hat{\sigma} = \mathbf{M}^{-1} \mathbf{A} \hat{\mathbf{f}} \quad (\text{A.22})$$

where vector $\hat{\mathbf{f}}$ is defined in (A.18), matrix $\mathbf{A} \in \mathbb{R}^{(M-2) \times M}$ is defined in (2.6), and matrix

$\mathbf{M} \in \mathbb{R}^{(M-2) \times (M-2)}$ is defined as (2.7).

Finally, we focus on solving the first derivative of cubic spline $s(x)$. Let $\theta_i = s'(x_i)$ for

$i = 0, 1, \dots, M-1$, then we have

$$\begin{aligned} s_i(x) &= \theta_i \frac{(x_{i+1}-x)^2(x-x_i)}{h_i^2} - \theta_{i+1} \frac{(x-x_i)^2(x_{i+1}-x)}{h_i^2} + f_i \frac{(x_{i+1}-x)^2[2(x-x_i)+h_i]}{h_i^3} + \\ &\quad f_{i+1} \frac{(x-x_i)^2[2(x_{i+1}-x)+h_i]}{h_i^3}, \\ s'_i(x) &= \theta_i \frac{(x_{i+1}-x)(2x_i+x_{i+1}-3x)}{h_i^2} - \theta_{i+1} \frac{(x-x_i)(2x_{i+1}+x_i-3x)}{h_i^2} + 6 \frac{u_{i+1}^n - u_i^n}{h_i^3} (x_{i+1} - x)(x - x_i), \\ s''_i(x) &= -2\theta_i \frac{2x_{i+1}+x_i-3x}{h_i^2} - 2\theta_{i+1} \frac{2x_i+x_{i+1}-3x}{h_i^2} + 6 \frac{u_{i+1}^n - u_i^n}{h_i^3} (x_{i+1} + x_i - 2x). \end{aligned}$$

A.2 Derivation of the 0-th, First, Second Derivative of the Cubic Spline in Section 2.1

By plugging x_i into $s_i''(x)$ and $s_{i-1}''(x)$, we have

$$\begin{cases} s_i''(x) &= -2\theta_i \frac{2x_{i+1}+x_i-3x}{h_i^2} - 2\theta_{i+1} \frac{2x_i+x_{i+1}-3x}{h_i^2} + 6 \frac{f_{i+1}-f_i}{h_i^3} (x_{i+1} + x_i - 2x) \\ s_{i-1}''(x) &= -2\theta_{i-1} \frac{2x_i+x_{i-1}-3x}{h_{i-1}^2} - 2\theta_i \frac{2x_{i-1}+x_i-3x}{h_{i-1}^2} + 6 \frac{f_i-f_{i-1}}{h_{i-1}^3} (x_i + x_{i-1} - 2x) \end{cases}$$

which gives

$$\begin{cases} s_i''(x) &= \frac{-4}{h_i} \theta_i + \frac{-2}{h_i} \theta_{i+1} + 6 \frac{f_{i+1}-f_i}{h_i^2} \\ s_{i-1}''(x) &= \frac{2}{h_{i-1}} \theta_{i-1} + \frac{4}{h_{i-1}} \theta_i - 6 \frac{f_i-f_{i-1}}{h_{i-1}^2}. \end{cases}$$

Because $s_i''(x_i) = s_{i-1}''(x_i)$, we have ($\forall i = 1, 2, \dots, M-2$)

$$\begin{aligned} \frac{-4}{h_i} \theta_i + \frac{-2}{h_i} \theta_{i+1} + 6 \frac{f_{i+1}-f_i}{h_i^2} &= \frac{2}{h_{i-1}} \theta_{i-1} + \frac{4}{h_{i-1}} \theta_i - 6 \frac{f_i-f_{i-1}}{h_{i-1}^2} \\ \Leftrightarrow \frac{2}{h_{i-1}} \theta_{i-1} + \left(\frac{-4}{h_i} + \frac{4}{h_i} \right) \theta_i + \frac{2}{h_i} \theta_{i+1} &= 6 \frac{f_{i+1}-f_i}{h_i^2} + 6 \frac{f_i-f_{i-1}}{h_{i-1}^2} \\ \Leftrightarrow \frac{1}{h_{i-1}} \theta_{i-1} + \left(\frac{2}{h_{i-1}} + \frac{2}{h_i} \right) \theta_i + \frac{1}{h_i} \theta_{i+1} &= 3 \frac{f_{i+1}-f_i}{h_i^2} + 3 \frac{f_i-f_{i-1}}{h_{i-1}^2}. \end{aligned}$$

By organizing the above system of equation into matrix algebra, we have

$$\begin{pmatrix} \frac{1}{h_0} & \frac{2}{h_0} + \frac{2}{h_1} & \frac{1}{h_1} & 0 & \dots & 0 & 0 & 0 \\ 0 & \frac{1}{h_1} & \frac{2}{h_1} + \frac{2}{h_2} & 0 & \dots & 0 & 0 & 0 \\ \vdots & \vdots & \vdots & \vdots & \ddots & \vdots & \vdots & \vdots \\ 0 & 0 & 0 & 0 & \dots & \frac{1}{h_{M-3}} & \frac{2}{h_{M-3}} + \frac{2}{h_{M-2}} & \frac{1}{h_{M-2}} \end{pmatrix} \begin{pmatrix} \theta_0 \\ \theta_1 \\ \theta_2 \\ \vdots \\ \theta_{M-1} \end{pmatrix} = \begin{pmatrix} 3 \frac{f_2-f_1}{h_1^2} + 3 \frac{f_1-f_0}{h_0^2} \\ 3 \frac{f_3-f_2}{h_2^2} + 3 \frac{f_2-f_1}{h_1^2} \\ \vdots \\ 3 \frac{f_{M-1}-f_{M-2}}{h_{M-2}^2} + 3 \frac{f_{M-2}-f_{M-3}}{h_{M-3}^2} \end{pmatrix}.$$

A.2 Derivation of the 0-th, First, Second Derivative of the Cubic Spline in Section 2.1

For the endpoint θ_0 , because $s_0''(x_0) = 0$, we have

$$s_0''(x) = -2\theta_0 \frac{2x_1 + x_0 - 3x}{h_0^2} - 2\theta_1 \frac{2x_0 + x_1 - 3x}{h_0^2} + 6 \frac{f_1 - f_0}{h_0^3} (x_1 + x_0 - 2x).$$

When we take the value of x as x_0 , we have

$$\begin{aligned} s_0''(x_0) &= -2\theta_0 \frac{2x_1 + x_0 - 3x_0}{h_0^2} - 2\theta_1 \frac{2x_0 + x_1 - 3x_0}{h_0^2} + 6 \frac{f_1 - f_0}{h_0^3} (x_1 + x_0 - 2x_0) \\ &= \frac{-4}{h_0} \theta_0 + \frac{-2}{h_0} \theta_1 + 6 \frac{f_1 - f_0}{h_0^3} \\ &= 0. \end{aligned}$$

For the two endpoint θ_{M-1} , because $s_{M-2}''(x_{M-1}) = 0$, we have

$$\begin{aligned} s_{M-2}''(x) &= -2\theta_{M-2} \frac{2x_{M-1} + x_{M-2} - 3x}{h_{M-2}^2} - 2\theta_{M-1} \frac{2x_{M-2} + x_{M-1} - 3x}{h_{M-2}^2} + \\ &\quad 6 \frac{f_{M-1} - f_{M-2}}{h_{M-2}^3} (x_{M-1} + x_{M-2} - 2x). \end{aligned}$$

When we take the value of x as x_{M-1} , we have

$$\begin{aligned} s_{M-2}''(x_{M-1}) &= -2\theta_{M-2} \frac{2x_{M-1} + x_{M-2} - 3x_{M-1}}{h_{M-2}^2} - 2\theta_{M-1} \frac{2x_{M-2} + x_{M-1} - 3x_{M-1}}{h_{M-2}^2} + \\ &\quad 6 \frac{f_{M-1} - f_{M-2}}{h_{M-2}^3} (x_{M-1} + x_{M-2} - 2x_{M-1}) \\ &= \frac{2}{h_{M-2}} \theta_{M-2} + \frac{4}{h_{M-2}} \theta_{M-1} - 6 \frac{f_{M-1} - f_{M-2}}{h_{M-2}^3} \\ &= 0. \end{aligned}$$

A.2 Derivation of the 0-th, First, Second Derivative of the Cubic Spline in Section 2.1

So the first order derivative $\boldsymbol{\theta} = (\theta_0, \theta_1, \dots, \theta_{M-1})^\top$ can be solved by

$$\underbrace{\begin{pmatrix} \frac{2}{h_0} & \frac{1}{h_0} & 0 & 0 & \dots & 0 & 0 & 0 \\ \frac{1}{h_0} & \frac{2}{h_0} + \frac{2}{h_1} & \frac{1}{h_1} & 0 & \dots & 0 & 0 & 0 \\ 0 & \frac{1}{h_1} & \frac{2}{h_1} + \frac{2}{h_2} & 0 & \dots & 0 & 0 & 0 \\ \vdots & \vdots & \vdots & \vdots & \ddots & \vdots & \vdots & \vdots \\ 0 & 0 & 0 & 0 & \dots & \frac{1}{h_{M-3}} & \frac{2}{h_{M-3}} + \frac{2}{h_{M-2}} & \frac{1}{h_{M-2}} \\ 0 & 0 & 0 & 0 & \dots & 0 & \frac{1}{h_{M-2}} & \frac{2}{h_{M-2}} \end{pmatrix}}_{\mathbf{Q} \in \mathbb{R}^{M \times M}} \underbrace{\begin{pmatrix} \theta_0 \\ \theta_1 \\ \theta_2 \\ \theta_3 \\ \theta_4 \\ \vdots \\ \theta_{M-1} \end{pmatrix}}_{\boldsymbol{\theta}}$$

$$= \underbrace{\begin{pmatrix} 3 \frac{f_1 - f_0}{h_0^2} \\ 3 \frac{f_2 - f_1}{h_1^2} + 3 \frac{f_1 - f_0}{h_0^2} \\ 3 \frac{f_3 - f_2}{h_2^2} + 3 \frac{f_2 - f_1}{h_1^2} \\ \vdots \\ 3 \frac{f_{M-1} - f_{M-2}}{h_{M-2}^2} + 3 \frac{f_{M-2} - f_{M-3}}{h_{M-3}^2} \\ 3 \frac{f_{M-1} - f_{M-2}}{h_{M-2}^2} \end{pmatrix}}_{\mathbf{q}}.$$

In matrix notation, the first order derivative $\boldsymbol{\theta} = (\theta_0, \theta_1, \dots, \theta_{M-1})^\top$ can be solved by

$$\hat{\boldsymbol{\theta}} = \mathbf{Q}^{-1} \hat{\mathbf{q}} = \mathbf{Q}^{-1} \mathbf{B} \hat{\mathbf{f}}, \quad (\text{A.23})$$

A.3 Computational Complexity of Local Polynomial Regression Method

where $\hat{\mathbf{f}}$ is defined in (A.18), and matrix $\mathbf{B} \in \mathbb{R}^{M \times M}$ is defined as

$$\mathbf{B} = \begin{pmatrix} \frac{-3}{h_0^2} & \frac{3}{h_0^2} & 0 & 0 & \dots & 0 & 0 & 0 & 0 \\ \frac{-3}{h_0^2} & \frac{3}{h_0^2} - \frac{3}{h_1^2} & \frac{3}{h_1^2} & 0 & \dots & 0 & 0 & 0 & 0 \\ 0 & \frac{-3}{h_1^2} & \frac{3}{h_1^2} - \frac{3}{h_2^2} & \frac{3}{h_2^2} & \dots & 0 & 0 & 0 & 0 \\ \vdots & \vdots & \vdots & \vdots & \ddots & \vdots & \vdots & \vdots & \vdots \\ & 0 & 0 & 0 & 0 & \frac{-3}{h_{M-3}^2} & \frac{3}{h_{M-3}^2} - \frac{3}{h_{M-2}^2} & \frac{3}{h_{M-2}^2} & \\ & 0 & 0 & 0 & 0 & 0 & \frac{-3}{h_{M-2}^2} & \frac{3}{h_{M-2}^2} & \end{pmatrix}.$$

A.3 Computational Complexity of Local Polynomial Regression Method

In the functional estimation stage, the computational complexity of the local polynomial regression method is stated in the following proportion.

Proposition A.1. Given data \mathcal{D} in (1.1), if we use the local polynomial regression in the functional estimation stage, i.e., estimate $\mathbf{X} \in \mathbb{R}^{MN \times K}$, $\nabla_t \mathbf{u} \in \mathbb{R}^{MN}$ via the local polynomial regression described as in this online supplementary material, then the computation complexity of this stage is of order

$$\max\{O(q_{\max}^2 M^2 N), O(MN^2), O(q_{\max}^3 MN), O(p_{\max} MN), O(K^3)\},$$

where p_{\max} is the highest polynomial order in (1.3), q_{\max} is the highest order of derivatives in (1.3), M is the spatial resolution, N is the temporal resolution, and K is the number of columns of \mathbf{X} .

A.4 Coordinate Gradient Descent to Solve the Optimization problem in Section 2.2.

If we set $q_{\max} = 2$ to match the derivative order of the local polynomial regression to the cubic spline, then the computation complexity is of order

$$\max\{O(M^2N), O(MN^2), O(p_{\max}MN), O(K^3)\}.$$

See a proof in Section A.10.2.

As suggested by Proposition A.1, the computational complexity of local polynomial regression is much higher than that in the cubic spline. But the advantage of local polynomial regression is that it can derive any order of derivatives, i.e., $q_{\max} \geq 0$ in (1.3), while for the cubic spline, $q_{\max} = 2$. In applications, $q_{\max} = 2$ should be sufficient because most of the PDE models are governed by derivatives up to the second derivative, for instance, heat equation, wave equation, Laplace's equation, Helmholtz equation, Poisson's equation, and so on. In our paper, we mainly use cubic spline as an illustration example due to its simplification and computational efficiency. Readers can extend our proposed SAPDEMI method to the higher-order spline with $q_{\max} > 2$ if they are interested in higher-order derivatives.

A.4 Coordinate Gradient Descent to Solve the Optimization problem in Section 2.2.

In this section, we briefly review the implement of the coordinate descent algorithm in Friedman et al. (2010) to solve (2.10). The main idea of the coordinate descent is to update the estimator in a coordinate-wise fashion, which is the main difference between the coordinate descent and regular gradient descent. For instance, in the k -th iteration, the coordinate descent updates

A.4 Coordinate Gradient Descent to Solve the Optimization problem in Section 2.2.

the iterative estimator $\boldsymbol{\beta}^{(k)}$ by using partial of the gradient information, instead of the whole gradient information. Mathematically speaking, in the k -th iteration, the coordinate descent optimizes $F(\boldsymbol{\beta}) = \frac{1}{2MN} \|\nabla_t \mathbf{u} - \mathbf{X}\boldsymbol{\beta}\|_2^2 + \lambda \|\boldsymbol{\beta}\|_1$ with respect to $\boldsymbol{\beta}$ by

$$\beta_j^{(k+1)} = \arg \min_{\beta_j} F((\beta_1^{(k)}, \beta_2^{(k)}, \dots, \beta_{j-1}^{(k)}, \beta_j, \beta_{j+1}^{(k)}, \dots, \beta_K^{(k)}))$$

for all $j = 1, 2, \dots, K$. To minimize the above optimization problem, we can derive the first derivative and set it as 0:

$$\frac{\partial}{\partial \beta_j} F(\boldsymbol{\beta}^{(k)}) = \frac{1}{MN} \left(\mathbf{e}_j^\top \mathbf{X}^\top \mathbf{X} \boldsymbol{\beta}^{(k)} - \nabla_t \mathbf{u}^\top \mathbf{X} \mathbf{e}_j \right) + \lambda \text{sign}(\beta_j) = 0,$$

where \mathbf{e}_j is a vector of length K whose entries are all zero except the j -th entry is 1. By solving the above equation, we can solve $\beta_j^{(k+1)}$ by

$$\beta_j^{(k+1)} = S \left(\nabla_t \mathbf{u}^\top \mathbf{X} \mathbf{e}_j - \sum_{l \neq j} (\mathbf{X}^\top \mathbf{X})_{jl} \beta_l^{(k)}, MN\lambda \right) / (\mathbf{X}^\top \mathbf{X})_{jj},$$

where $S(\cdot)$ is the soft-thresholding function defined as

$$S(x, \alpha) = \begin{cases} x - \alpha & \text{if } x \geq \alpha \\ x + \alpha & \text{if } x \leq -\alpha \\ 0 & \text{otherwise} \end{cases} .$$

The detailed procedure of this algorithm is summarized in Algorithm 2.

A.4 Coordinate Gradient Descent to Solve the Optimization problem in
Section 2.2.

Algorithm 2: Algorithm for the coordinate descent to minimize

$F(\boldsymbol{\beta})$

Input: response vector $\nabla_t \mathbf{u}$, design matrix \mathbf{X} , and number of
iterations M

Output: coefficient estimation $\hat{\boldsymbol{\beta}}$

1 Initialize $\boldsymbol{\beta}^{(0)}$

2 for $\ell = 1, \dots, \mathcal{L}$ do

3 for $j = 1, \dots, K$ do

4 $\boldsymbol{\beta}_j^{(\ell)} =$
 $S\left(\nabla_t \mathbf{u}^\top \mathbf{X} \mathbf{e}_j - \sum_{l \neq j} (\mathbf{X}^\top \mathbf{X})_{jl} \boldsymbol{\beta}_l^{(\ell-1)}, MN\lambda\right) / (\mathbf{X}^\top \mathbf{X})_{jj}$

5 $\hat{\boldsymbol{\beta}} = \boldsymbol{\beta}^{(\mathcal{L})}$

A.5 A review of methods to select the smoothing parameter in the cubic spline literature

A.5 A review of methods to select the smoothing parameter in the cubic spline literature

We consider a noisy data $\{(x_i, y_i)\}_{i=1, \dots, n}$, where

$$y_i = g(x_i) + \epsilon_i,$$

with $\epsilon_i \sim N(0, \sigma^2)$. To fit this noisy data, the cubic spline use a spline function $s(x)$ to approximate $g(x)$. And the function $s(x)$ can be solved as the minimizer of the following optimization problem:

$$J_\lambda(s) = \frac{1}{n} \sum_{i=1}^n [y_i - s(x_i)]^2 + \lambda \int_{x_1}^{x_n} s''(x)^2 dx,$$

where the first term $\sum_{i=1}^n [y_i - s(x_i)]^2$ is the sum of squares for residuals. And this term is commonly called *infidelity* of the data. In the second term $\lambda \int_{x_1}^{x_n} s''(x)^2 dx$, the function $s''(x)$ is the second derivative of $s(x)$, and this term is the penalty of the smoothness. In the above optimization problem, the parameter $\lambda > 0$ controls the trade off between the goodness of fit and the smoothness of the cubic spline.

We will discuss the selection of λ under two scenarios: σ is known and σ is unknown.

- **Scenario 1: σ is known.** As suggested by Reinsch (1967), a good value of λ should be the one make the infidelity $(\frac{1}{n} \sum_{i=1}^n [y_i - s(x_i)]^2)$ equals to σ^2 , i.e.,

$$\lambda^* = \left\{ \lambda : \frac{1}{n} \sum_{i=1}^n [y_i - s(x_i)]^2 = \sigma^2 \right\}.$$

A.5 A review of methods to select the smoothing parameter in the cubic spline literature

An alternative way to select λ is to choose the optimal λ which minimizes the true mean square error averaged over the data points (Wahba, 1975; Craven and Wahba, 1978).

And the true mean square error $R(\lambda)$ is defined as

$$R(\lambda) = \frac{1}{n} \sum_{i=1}^n [g(x_i) - s(x_i)]^2.$$

So the optimal λ is

$$\lambda^* = \arg \min_{\lambda} R(\lambda).$$

In practice, the above two approaches from Reinsch (1967); Wahba (1975); Craven and Wahba (1978) are not feasible, because σ is commonly unknown.

- **Scenario 2: σ is unknown.**

The first representative method is from Mallows (2000); Hudson (1974), where the optimal λ^* is

$$\begin{aligned} \lambda^* &= \arg \min_{\lambda} E \left(\frac{1}{n} A(\lambda) y - g \right) \\ &= \arg \min_{\lambda} \frac{1}{n} \| [I - A(\lambda)] g \|^2 + \frac{\sigma^2}{n} \text{tr}(A^2(\lambda)). \end{aligned}$$

Here the matrix $A(\lambda) \in \mathbb{R}^{n \times n}$ depends on λ and is defined by the following equation:

$$\begin{pmatrix} s(x_1) \\ s(x_2) \\ \vdots \\ s(x_n) \end{pmatrix} = A(\lambda) \begin{pmatrix} y_1 \\ y_2 \\ \vdots \\ y_n \end{pmatrix}.$$

A.6 Some Important Lemmas

In the above equation, the vectors y and g are defined $y = (y_1, \dots, y_n)^\top$ and $g = (g(x_1), \dots, g(x_n))^\top$. And the norm $\|\cdot\|^2$ is the Euclidean norm.

The second representative method is generalized cross-validation (GCV) (Craven and Wahba, 1978; Aydin et al., 2013). Mathematically, it takes the optimal λ as the minimizer of $V(\lambda)$, i.e.,

$$\begin{aligned} \lambda^* &= \arg \min_{\lambda} V(\lambda) \\ &= \arg \min_{\lambda} \frac{1}{n} \| [I - A(\lambda)]y \|^2 \bigg/ \left[\frac{1}{n} \text{tr}(I - A(\lambda)) \right]^2. \end{aligned}$$

A.6 Some Important Lemmas

In this section, we present some important preliminaries, which are important blocks for the proofs of the main theories. To begin with, we first give the upper bound of $\widehat{u(x, t_n)} - u(x, t_n)$ for $x \in \{x_0, x_1, \dots, x_{M-1}\}$, which is distance between the ground truth $u(x, t_n)$ and the estimated zero-order derivatives by cubic spline $\widehat{u(x, t_n)}$.

Lemma A.2. Assume that

1. for any fixed $n = 0, 1, \dots, N-1$, we have the spatial variable x is sorted in nondecreasing order, i.e., $x_0 < x_1 < \dots < x_{M-1}$;
2. for any fixed $n = 0, 1, \dots, N-1$, we have the ground truth function $f^*(x) := u(x, t_n) \in C^4$, where C^4 refers to the set of functions that is fourth-time differentiable;

A.6 Some Important Lemmas

3. for any fixed $n = 0, 1, \dots, N - 1$, we have $\frac{\partial^2}{\partial x^2} u(x_0, t_n) = \frac{\partial^2}{\partial x^2} u(x_{M-1}, t_n) = 0$, and

$$\frac{\partial^3}{\partial x^3} u(x_0, t_n) \neq 0, \frac{\partial^3}{\partial x^3} u(x_{M-1}, t_n) = 0;$$

4. for any fixed $n = 0, 1, \dots, N - 1$, the value of third order derivative of function $f^*(x) :=$

$$u(x, t_n) \text{ at point } x = 0 \text{ is bounded, i.e., } \frac{d^3}{dx^3} f^*(0) < +\infty;$$

5. for any U_i^n generated by the underlying PDE system $U_i^n = u(x_i, t_n) + w_i^n$ with $w_i^n \stackrel{i.i.d}{\sim}$

$$N(0, \sigma^2), \text{ we have } \eta^2 := \max_{i=0, \dots, M-1, n=0, \dots, N-1} E(U_i^n)^2 \text{ is bounded};$$

6. for function $K(x) = \frac{1}{2} e^{-|x|/\sqrt{2}} [\sin(|x|\sqrt{2}) + \pi/4]$, we assume that it is uniformly con-

tinuous with modulus of continuity w_K and of bounded variation $V(K)$ and we also

assume that $\int |K(x)| dx$, $\int |x|^{1/2} |dK(x)|$, $\int |x \log |x||^{1/2} |dK(x)|$ are bounded and denote

$$K_{\max} := \max_{x \in \max_{x \in [0, X_{\max}] \cup [0, T_{\max}]}} K(x);$$

7. the smoothing parameter in (2.4) is set as $\alpha = (1 + M^{-4/7})^{-1}$;

8. the Condition 3.3 - Condition 3.4 hold.

Then there exist finite positive constant $\mathcal{C}_{(\sigma, \|u\|_{L^\infty(\Omega)})} > 0$, $C_{(\sigma, \|u\|_{L^\infty(\Omega)})} > 0$, $\tilde{C}_{(\sigma, \|u\|_{L^\infty(\Omega)})} >$

0 , $Q_{(\sigma, \|u\|_{L^\infty(\Omega)})} > 0$, $\gamma_{(M)} > 0$, $\omega_{(M)} > 1$, such that for any ϵ satisfying

$$\begin{aligned} \epsilon > \mathcal{C}_{(\sigma, \|u\|_{L^\infty(\Omega)})} \max \left\{ 4K_{\max} M^{-3/7}, 4AM^{-3/7}, 4\sqrt{2} \frac{d^3}{dx^3} f^*(0) M^{-3/7}, \right. \\ \left. \frac{16 \left[C_{(\sigma, \|u\|_{L^\infty(\Omega)})} \log(M) + \gamma_{(M)} \right] \log(M)}{M^{3/7}}, \right. \\ \left. 16 \sqrt{\frac{\omega_{(M)}}{7}} \tilde{C}_{(\sigma, \|u\|_{L^\infty(\Omega)})} \frac{\sqrt{\log(M)}}{M^{3/7}} \right\}, \end{aligned}$$

A.6 Some Important Lemmas

there exist a $\dot{M} > 0$, such that when $M > \dot{M}$, we have

$$\begin{aligned}
 & P \left[\sup_{x \in [0, X_{\max}]} \left| \frac{\partial^k}{\partial x^k} \widehat{u(x, t_n)} - \frac{\partial^k}{\partial x^k} u(x, t_n) \right| > \epsilon \right] \\
 & < 2M e^{-\frac{(M^{3/7} - \|u\|_{L^\infty(\Omega)})^2}{2\sigma^2}} + Q_{(\sigma, \|u\|_{L^\infty(\Omega)})} e^{-L\gamma(M)} + 4\sqrt{2}\eta^4 M^{-\omega(M)/7}
 \end{aligned}$$

for $k = 0, 1, 2$. Here $A = \sup_{\alpha} \int |u|^s f_M(\alpha, u) du \times \int_{x \in [0, X_{\max}]} |K(x)| dx$.

Proof. See in Section A.10.3 in this file. □

In the above lemma, we add $(\sigma, \|u\|_{L^\infty(\Omega)})$ as the subscript of constants $\mathcal{C}, C, \tilde{C}, Q$ to emphasize that these constant are independent of the temporal resolution N and spatial resolution M , and only depends on the noisy data \mathcal{D} in (1.1) itself. We add M as the subscript of constants γ, ω to emphasize that γ, ω are function of the spatial resolution M , and we will discuss the value of γ, ω in Lemma A.3.

The above lemma show the closeness between $\frac{\partial^k}{\partial x^k} \widehat{u(x, t_n)}$ and $\frac{\partial^k}{\partial x^k} u(x, t_n)$ for $k = 0, 1, 2$. This results can be easily extend of the closeness between $\frac{\partial}{\partial t} \widehat{u(x_i, t)}$ and $\frac{\partial}{\partial t} u(x_i, t)$, which is shown in the following corollary.

Corollary A.1. Assume that

1. for any fixed $i = 0, 1, \dots, M-1$, we have the spatial variable t is sorted in nondecreasing order, i.e., $t_0 < t_1 \dots < t_{N-1}$;
2. for any fixed $i = 0, 1, \dots, M-1$, we have the ground truth function $f^*(t) := u(x_i, t) \in C^4$,
where C^4 refers to the set of functions that is forth-time differentiable;

A.6 Some Important Lemmas

3. for any fixed $i = 0, 1, \dots, M - 1$, we have $\frac{\partial^2}{\partial t^2} u(x_i, t_0) = \frac{\partial^2}{\partial t^2} u(x_i, t_{N-1}) = 0$, and

$$\frac{\partial^3}{\partial t^3} u(x_i, t_0) \neq 0, \frac{\partial^3}{\partial t^3} u(x_i, t_{N-1}) = 0;$$

4. for any fixed $i = 0, 1, \dots, M - 1$, the value of third order derivative of function $\bar{f}^*(x) :=$

$$u(x_i, t) \text{ at point } t = 0 \text{ is bounded, i.e., } \frac{d^3}{dt^3} \bar{f}^*(0) < +\infty;$$

5. for any U_i^n generated by the underlying PDE system $U_i^n = u(x_i, t_n) + w_i^n$ with $w_i^n \stackrel{i.i.d}{\sim}$

$$N(0, \sigma^2), \text{ we have } \max_{i=0, \dots, M-1, n=0, \dots, N-1} E(U_i^n)^2 \text{ is bounded};$$

6. for function $K(x) = \frac{1}{2} e^{-|x|/\sqrt{2}} [\sin(|x|\sqrt{2}) + \pi/4]$, we have $K(x)$ is uniformly continuous

with modulus of continuity w_K and of bounded variation $V(K)$, and we also assume

that $\int_{x \in [0, X_{\max}]} |K(x)| dx, \int |x|^{1/2} |dK(x)|, \int |x \log |x||^{1/2} |dK(x)|$ are bounded and denote

$$K_{\max} := \max_{x \in [0, X_{\max}] \cup [0, T_{\max}]} K(x);$$

7. the smoothing parameter in (2.4) is set as $\bar{\alpha} = O\left(\left(1 + N^{-4/7}\right)^{-1}\right)$;

8. the Condition 3.3 - Condition 3.4 hold.

then there exist finite positive constant $\mathcal{C}_{(\sigma, \|u\|_{L^\infty(\Omega)})} > 0, C_{(\sigma, \|u\|_{L^\infty(\Omega)})} > 0, \tilde{C}_{(\sigma, \|u\|_{L^\infty(\Omega)})} >$

$0, Q_{(\sigma, \|u\|_{L^\infty(\Omega)})} > 0, \gamma_{(N)} > 0, \omega_{(N)} > 1$, such that for any ϵ satisfying

$$\begin{aligned} \epsilon > \mathcal{C}_{(\sigma, \|u\|_{L^\infty(\Omega)})} \max \left\{ 4K_{\max} N^{-3/7}, 4\bar{A} N^{-3/7}, 4\sqrt{2} \frac{d^3}{dx^3} f^*(0) N^{-3/7}, \right. \\ & \frac{16 \left[C_{(\sigma, \|u\|_{L^\infty(\Omega)})} \log(N) + \gamma_{(N)} \right] \log(N)}{N^{3/7}}, \\ & \left. 16 \sqrt{\frac{\omega_{(N)}}{7}} \tilde{C}_{(\sigma, \|u\|_{L^\infty(\Omega)})} \frac{\sqrt{\log(N)}}{N^{3/7}} \right\}, \end{aligned}$$

A.7 Justification of $\alpha, \bar{\alpha}$ in Theorem 3.1

there exist a $\dot{N} > 0$, such that when $N > \dot{N}$, we have

$$P \left[\sup_{t \in [0, T_{\max}]} \left| \frac{\partial}{\partial t} \widehat{u}(x_i, t) - \frac{\partial}{\partial t} u(x_i, t) \right| > \epsilon \right] < 2Ne^{-\frac{(N^{3/7} - \|u\|_{L^\infty(\Omega)})^2}{2\sigma^2}} + Q_{(\sigma, \|u\|_{L^\infty(\Omega)})} e^{-L\gamma(N)} + 4\sqrt{2}\eta^4 N^{-\omega(N)/7}.$$

Here $\bar{A} = \sup_{\alpha} \int |u|^s \bar{f}_N(\alpha, u) du \times \int_{t \in [0, T_{\max}]} |K(x)| dx$.

After bounding the error of all the derivatives, we then aim to bound $\|\nabla_t \mathbf{u} - \mathbf{X}\beta^*\|_\infty$. It is important to bound $\|\nabla_t \mathbf{u} - \mathbf{X}\beta^*\|_\infty$, with the reason described as follows in Lemma A.3.

Lemma A.3. Suppose the conditions in Lemma A.2 and Corollary A.1 hold and we set $M = O(N)$, then there exist finite positive constant $\mathcal{C}_{(\sigma, \|u\|_{L^\infty(\Omega)})} > 0$ such that for any ϵ satisfying

$$\epsilon > \mathcal{C}_{(\sigma, \|u\|_{L^\infty(\Omega)})} \frac{\log(N)}{N^{3/7-r}},$$

and any $r \in (0, \frac{3}{7})$, there exist $\dot{N} > 0$, such that when $N > \dot{N}$, we have

$$P(\|\nabla_t \mathbf{u} - \mathbf{X}\beta^*\|_\infty > \epsilon) < Ne^{-N^r},$$

where $\mathcal{C}_{(\sigma, \|u\|_{L^\infty(\Omega)})}$ is a constant which do not depend on the temporal resolution M and spatial resolution N .

Proof. See Section A.10. □

A.7 Justification of $\alpha, \bar{\alpha}$ in Theorem 3.1

We acknowledge that our way to select the smoothing parameters $\alpha, \bar{\alpha}$ is different from that in the cubic spline literature (see a detailed literature review in the supplementary material). The

A.8 Tables to draw the curve in Fig. 2 and Fig. 8

root cause of the difference lies in the different objectives in theory. For the existing methods in the cubic spline literature, the objective is to minimize the fitting error when one fits the data (similar to *single objective optimization*). However, for our proposed SAPDEMI method, the objective is to maximize the accuracy when one identifies the underlying PDE models. To build a path to this objective, we apply the cubic spline as an important block. And the selection of the smoothing parameter is required to, on the one hand, have a relatively small fitting error; on the other hand, leads to a high identification accuracy (similar to *multiple objective optimizations*).

A.8 Tables to draw the curve in Fig. 2 and Fig. 8

In this section, we present the table to draw the curves in Fig. 2,8 in Table 2, 3, respectively.

Table 2: Computational complexity of the functional estimation by cubic spline and local polynomial regression in transport equation

	M = 20						
	N=200	N=400	N=800	N=1000	N=1200	N=1600	N=2000
cubic spline	374,389	748,589	1,496,989	1,871,189	2,245,389	2,993,789	3,742,189
local poly	14,136,936	45,854,336	162,089,136	246,606,536	348,723,936	605,758,736	933,193,536
	N = 20						
	M=200	M=400	M=800	M=1000	M=1200	M=1600	M=2000
cubic spline	398,573	875,773	207,0173	2,787,373	3,584,573	5,418,973	7,573,373
local poly	33,046,336	125,596,136	489,255,736	760,365,536	1,090,995,336	1,930,814,936	3,008,714,536

A.8 Tables to draw the curve in Fig. 2 and Fig. 8

Table 3: Correct identification probability of transport equation, inviscid Burgers equation and viscous Burgers's equation

	σ											
	0.01	0.05	0.1	0.25	0.3	0.4	0.5	0.7	0.75	0.8	0.9	1
	transport equation											
$M = N = 100$	100%	100%	100%	100%	100%	100%	100%	100%	100%	100%	100%	100%
$M = N = 150$	100%	100%	100%	100%	100%	100%	100%	100%	100%	100%	100%	100%
$M = N = 200$	100%	100%	100%	100%	100%	100%	100%	100%	100%	100%	100%	100%
	inviscid Burgers equation											
$M = N = 100$	100%	100%	100%	100%	100%	100%	100%	99.9%	99.8%	99.8%	99.8%	99.1%
$M = N = 150$	100%	100%	100%	100%	100%	100%	100%	100%	99.8%	99.7%	99.7%	99.7%
$M = N = 200$	100%	100%	100%	100%	100%	100%	100%	100%	100%	100%	100%	100%
	viscous Burgers equation											
$M = N = 100$	100%	99.4%	89.8%	78.0%	71.4%	82.0%	91.6%	72.8%	79.0%	72.9%	57.9%	51.3%
$M = N = 150$	100%	100%	100%	97.3%	96.5%	96.2%	97.6%	95.6%	93.3%	86.6%	79.9%	73.6%
$M = N = 200$	100%	100%	100%	100%	99.6%	99.6%	98.2%	98.8%	98.2%	97.0%	94.3%	91.3%

¹ The simulation results are based on 1000 times of simulations.

A.9 The reasons why the RK4 is not feasible.

A.9 The reasons why the RK4 is not feasible.

In this section, we discuss the reasons why the RK4 is not feasible. Generally speaking, RK4 is used to approximate solutions of ordinary differential equations. In our content, it aims at solving the solution of the following differential equation with fixed $i \in \{0, \dots, M-1\}$:

$$\begin{cases} \frac{\partial}{\partial t} u(x_i, t) = p(u, t) \\ u(x_i, t_0) = u_i^0 \end{cases}, \quad (\text{A.24})$$

where $p(u, t)$ is the function interpolated through data set

$$\left\{ t_n, u_i^n, \frac{u(x_i, t_n + \Delta t) - u(x_i, t_n)}{\Delta t} \right\}_{n=0, \dots, N-2}.$$

Then as shown by Chapter 5 in Lambert et al. (1991), the solution can be approximate by

$$u(x_i, t_{n+1}) = u(x_i, t_n) + \frac{\Delta t}{6}(k_1 + k_2 + k_3 + k_4),$$

where $\Delta t = t_{n+1} - t_n$ and k_1, k_2, k_3, k_4 are defined as

$$\begin{cases} k_1 = p(t_n, u_i^n) \\ k_2 = p(t_n + \Delta t/2, u_i^n + k_1 \Delta t/2) \\ k_3 = p(t_n + \Delta t/2, u_i^n + k_2 \Delta t/2) \\ k_4 = p(t_n + \Delta t, u_i^n + k_3 \Delta t). \end{cases} \quad (\text{A.25})$$

Given the above implementation of RK4, we find it is infeasible to be used in our case study due to the following two reasons. First, it is infeasible to obtain $p(u, t)$ in (A.24), even though the interpolation methods. Second, it is infeasible to get the value of k_3 in (A.25).

Because the calculation of k_3 depends on the value of k_2 and k_2 needs to be obtained (at least) by interpolation, it is complicated to calculate k_1, k_2, k_3, k_4 through one-time operation. Given the complicated implementation of RK4, we use the explicit Euler method in our case study.

A.10 Proofs

A.10.1 Proof of Proposition 2.1

Proof. The computational complexity in the functional estimation stage lies in calculating all elements in matrix \mathbf{X} and vector $\nabla_i \mathbf{u}$, including

$$\left\{ \widehat{u(x_i, t_n)}, \widehat{\frac{\partial}{\partial x} u(x_i, t_n)}, \widehat{\frac{\partial^2}{\partial x^2} u(x_i, t_n)}, \widehat{\frac{\partial}{\partial t} u(x_i, t_n)} \right\}_{i=0, \dots, M-1, n=0, \dots, N-1}.$$

by cubic spline in (2.4).

We divide our proof into two scenarios: (1) $\alpha = 1$ and (2) $\alpha \in (0, 1)$.

- First of all, we discuss a very simple case, i.e., $\alpha = 1$. When $\alpha = 1$, we call the cubic spline as *interpolating cubic spline* since there is no penalty on the smoothness.

For the zero-order derivative, i.e., $\left\{ \widehat{u(x_i, t_n)} \right\}_{i=0, \dots, M-1, n=0, \dots, N-1}$, it can be estimated

as $\widehat{u(x_i, t_n)} = u_i^n$ for $i = 0, 1, \dots, M-1, n = 0, 1, \dots, N-1$. So there is no computational complexity involved.

For the second order derivatives, i.e., $\left\{ \widehat{\frac{\partial^2}{\partial x^2} u(x_i, t_n)} \right\}_{i=0, \dots, M-1}$, with $n \in \{0, \dots, N-1\}$

fixed, it can be solved in a closed-form, i.e.,

$$\widehat{\boldsymbol{\sigma}} = \mathbf{M}^{-1} \mathbf{A} \mathbf{u}^n$$

where $\widehat{\boldsymbol{\sigma}} = \left(\frac{\partial^2}{\partial x^2} \widehat{u}(x_0, t_n), \frac{\partial^2}{\partial x^2} \widehat{u}(x_1, t_n), \dots, \frac{\partial^2}{\partial x^2} \widehat{u}(x_{M-1}, t_n) \right)^\top$. So the main computational load lies in the calculation of \mathbf{M}^{-1} . Recall $\mathbf{M} \in \mathbb{R}^{(M-2) \times (M-2)}$ is a tri-diagonal matrix:

$$\mathbf{M} = \begin{pmatrix} \frac{h_0+h_1}{3} & \frac{h_1}{6} & 0 & \dots & 0 & 0 \\ \frac{h_1}{6} & \frac{h_1+h_2}{3} & \frac{h_2}{6} & \dots & 0 & 0 \\ 0 & \frac{h_2}{6} & \frac{h_2+h_3}{3} & \ddots & 0 & 0 \\ \vdots & \vdots & \ddots & \ddots & \ddots & \vdots \\ 0 & 0 & 0 & \ddots & \frac{h_{M-4}+h_{M-3}}{3} & \frac{h_{M-3}}{6} \\ 0 & 0 & 0 & \dots & \frac{h_{M-3}}{6} & \frac{h_{M-3}+h_{M-2}}{3} \end{pmatrix}.$$

For this type of tri-diagonal matrix, there exist a fast algorithm to calculate its inverse.

The main idea of this fast algorithm is to decompose \mathbf{M} through Cholesky decomposition

as

$$\mathbf{M} = \mathbf{L}\mathbf{D}\mathbf{L}^\top,$$

where $\mathbf{L} \in \mathbb{R}^{(M-2) \times (M-2)}$, $\mathbf{D} \in \mathbb{R}^{(M-2) \times (M-2)}$ has the form of

$$\mathbf{L} = \begin{pmatrix} 1 & 0 & 0 & \dots & 0 \\ l_1 & 1 & 0 & \dots & 0 \\ 0 & l_2 & 1 & \dots & 0 \\ \vdots & \vdots & \ddots & \ddots & \vdots \\ 0 & 0 & 0 & l_{M-3} & 1 \end{pmatrix}, \mathbf{D} = \begin{pmatrix} d_1 & 0 & \dots & 0 \\ 0 & d_2 & \dots & 0 \\ \vdots & \vdots & \ddots & \vdots \\ 0 & 0 & \dots & d_{M-2} \end{pmatrix}.$$

After decomposing matrix \mathbf{M} into \mathbf{LDL}^\top , the second derivatives $\hat{\boldsymbol{\sigma}}$ can be solved as

$$\hat{\boldsymbol{\sigma}} = (\mathbf{L}^\top)^{-1} \mathbf{D}^{-1} \mathbf{L}^{-1} \underbrace{\mathbf{A} \mathbf{u}^n}_{\boldsymbol{\xi}}.$$

In the remaining of the proof in this scenario, we will verify the following two issues:

1. the computational complexity to decompose \mathbf{M} into \mathbf{LDL}^\top is $O(M)$ with $n \in \{0, \dots, N-1\}$ fixed;
2. the computational complexity to compute $\hat{\boldsymbol{\sigma}} = (\mathbf{L}^\top)^{-1} \mathbf{D}^{-1} \mathbf{L}^{-1} \boldsymbol{\xi}$ is $O(M)$ with $n \in \{0, \dots, N-1\}$ fixed and \mathbf{L}, \mathbf{D} available.

For the decomposition of $\mathbf{M} = \mathbf{LDL}^\top$, its essence is to derive l_1, \dots, l_{M-3} in matrix \mathbf{L} and d_1, \dots, d_{M-2} in matrix \mathbf{D} . By utilizing the method of undetermined coefficients to

inequality $\mathbf{M} = \mathbf{LDL}^\top$, we have:

$$= \begin{bmatrix} d_1 & d_1 l_1 & 0 & \dots & 0 & 0 \\ d_1 l_1 & d_2 & d_2 l_2 & \dots & 0 & 0 \\ 0 & d_2 l_2 & d_3 & \dots & 0 & 0 \\ \vdots & \vdots & \vdots & \ddots & \vdots & \vdots \\ 0 & 0 & 0 & \dots & d_{M-3} l_{M-3} & d_{M-3} l_{M-3}^2 + d_{M-2} \end{bmatrix} \\ = \begin{bmatrix} M_{11} & M_{12} & \dots & 0 \\ M_{21} & M_{22} & \dots & 0 \\ 0 & M_{32} & \dots & 0 \\ \vdots & \vdots & \ddots & \vdots \\ 0 & 0 & \dots & M_{M-2, M-2} \end{bmatrix},$$

where $M_{i,j}$ is the (i,j) th entry in matrix \mathbf{M} . Through the above method of undetermined coefficients, we can solve the exact value of the entries in matrix \mathbf{L}, \mathbf{D} , which is summarized in Algorithm 3. It can be seen from Algorithm 3 that, the computational complexity of solve \mathbf{L}, \mathbf{D} is of order $O(M)$.

For the calculation of $\hat{\boldsymbol{\sigma}} = (\mathbf{L}^\top)^{-1} \mathbf{D}^{-1} \mathbf{L}^{-1} \boldsymbol{\xi}$ with matrix \mathbf{L}, \mathbf{D} available, we will first verify that the computational complexity to solve $\bar{\boldsymbol{\xi}} = \mathbf{L}^{-1} \boldsymbol{\xi}$ is $O(M)$. Then, we will verify that the computational complexity to solve $\bar{\bar{\boldsymbol{\xi}}} = \mathbf{D}^{-1} \bar{\boldsymbol{\xi}}$ is $O(M)$. Finally, we will verify that the computational complexity to solve $\bar{\bar{\bar{\boldsymbol{\xi}}}} = (\mathbf{L}^\top)^{-1} \bar{\bar{\boldsymbol{\xi}}}$ is $O(M)$. First, the computational complexity of calculating $\bar{\boldsymbol{\xi}} = \mathbf{L}^{-1} \boldsymbol{\xi}$ is $O(M)$, this is because by $\mathbf{L} \bar{\boldsymbol{\xi}} = \boldsymbol{\xi}$,

we have the following system of equations:

$$\begin{cases} \xi_1 = \bar{\xi}_1 \\ \xi_2 = \bar{\xi}_2 + l_1 \bar{\xi}_1 \\ \vdots \\ \xi_{M-2} = \bar{\xi}_{M-2} + l_{M-3} \bar{\xi}_{M-3}, \end{cases}$$

where $\xi_i, \bar{\xi}_i$ is the i -th entry in $\boldsymbol{\xi}, \bar{\boldsymbol{\xi}}$, respectively. Through the above system of equations, we can solve the values of all entries in $\bar{\boldsymbol{\xi}}$, which is summarized in Algorithm 4. From Algorithm 4, we know that the computational complexity of solving $\mathbf{L}^{-1}\boldsymbol{\xi}$ is $O(M)$. Next, it is obvious that the computational complexity of $\bar{\boldsymbol{\xi}} = \mathbf{D}^{-1}\bar{\boldsymbol{\xi}}$ is $O(M)$, because \mathbf{D} is a diagonal matrix. Finally, with the similar logic flow, we can verify that the computational complexity of $\bar{\bar{\boldsymbol{\xi}}} = (\mathbf{L}^\top)^{-1}\bar{\boldsymbol{\xi}}$ is still $O(M)$. So, the computational complexity is to calculate $\hat{\boldsymbol{\sigma}} = (\mathbf{L}^\top)^{-1}\mathbf{D}^{-1}\mathbf{L}^{-1}\boldsymbol{\xi}$, with known \mathbf{L}, \mathbf{D} is $O(M)$.

As a summary, the computational complexity is to calculate $\left\{ \widehat{\frac{\partial^2}{\partial x^2} u(x_i, t_n)} \right\}_{i=0, \dots, M-1}$ with a fixed $n \in \{0, 1, \dots, N-1\}$ is $O(M)$. Accordingly, the computational complexity to solve $\left\{ \widehat{\frac{\partial^2}{\partial x^2} u(x_i, t_n)} \right\}_{i=0, \dots, M-1, n=0, \dots, N-1}$ is $O(MN)$.

For the first order derivatives, i.e., $\left\{ \frac{\partial}{\partial x} u(x_i, t_n), \frac{\partial}{\partial x} u(x_i, t_n) \right\}_{i=0, \dots, M-1, n=0, \dots, N-1}$, we can verify the computational complexity to solve them is also $O(MN)$ with the similar

logic as that in the second order derivatives.

Algorithm 3: Pseudo code to solve \mathbf{L}, \mathbf{D}

Input: matrix \mathbf{M}

Output: matrix \mathbf{L}, \mathbf{D}

```

1 Initialize  $d_1 = M_{1,1}$ 
2 for  $i = 1, 2, \dots, M - 3$  do
3    $l_i = M_{i,i+1}/d_i$ 
4    $d_{i+1} = M_{i+1,i+1} - d_i l_i^2$ 

```

Algorithm 4: Pseudo code to solve $\mathbf{L}^{-1}\boldsymbol{\xi}$

Input: matrix $\mathbf{L}, \boldsymbol{\xi}$

Output: matrix $\bar{\boldsymbol{\xi}}$

```

1 Initialize  $\bar{\xi}_1 = \xi_1$ 
2 for  $i = 2, \dots, M - 2$  do
3    $\bar{\xi}_i = \xi_i - l_{i-1}\bar{\xi}_{i-1}$ 

```

- Next, we discuss the scenario when $\alpha \in (0, 1)$.

Since all the derivatives has similar closed-form formulation as shown in (2.5), (A.23),

(A.22), we take the zero-order derivative $\{u(x_i, t_n)\}_{i=0, \dots, M-1, n=0, \dots, N-1}$ as an illustra-

tion example, and other derivatives can be derived similarly.

Recall that in Section 2.1, the zero-order derivative $\{u(x_i, t_n)\}_{i=0, \dots, M-1}$ with $n \in$

$\{0, 1, \dots, N-1\}$ fixed can be estimated through cubic spline as in equation (2.5):

$$\hat{\mathbf{f}} = \underbrace{[\alpha \mathbf{W} + (1-\alpha) \mathbf{A}^\top \mathbf{M} \mathbf{A}]}_{\mathbf{Z}}^{-1} \underbrace{\alpha \mathbf{W} \mathbf{u}^n}_{\mathbf{y}},$$

where $\alpha \in (0, 1)$ trades off the fitness of the cubic spline and the smoothness of the cubic

spline, vector $\hat{\mathbf{f}} = (u(\widehat{x_0, t_n}), u(\widehat{x_1, t_n}), \dots, u(\widehat{x_{M-1}, t_n}))^\top$, vector $\mathbf{u}^n = (u_0^n, \dots, u_{M-1}^n)^\top$,

matrix $\mathbf{W} = \text{diag}(w_0, w_1, \dots, w_{M-1})$, matrix $\mathbf{A} \in \mathbb{R}^{(M-2) \times M}$, $\mathbf{M} \in \mathbb{R}^{(M-2) \times (M-2)}$ are

defined as

$$\mathbf{A} = \begin{pmatrix} \frac{1}{h_0} & -\frac{1}{h_0} - \frac{1}{h_1} & \frac{1}{h_1} & 0 & \dots & 0 & 0 & 0 \\ 0 & \frac{1}{h_1} & -\frac{1}{h_1} - \frac{1}{h_2} & \frac{1}{h_2} & \dots & 0 & 0 & 0 \\ \vdots & \vdots & \vdots & \vdots & \ddots & \vdots & \vdots & \vdots \\ 0 & 0 & 0 & 0 & \dots & \frac{1}{h_{M-3}} & -\frac{1}{h_{M-3}} - \frac{1}{h_{M-2}} & \frac{1}{h_{M-2}} \end{pmatrix},$$

$$\mathbf{M} = \begin{pmatrix} \frac{h_0+h_1}{3} & \frac{h_1}{6} & 0 & \dots & 0 & 0 \\ \frac{h_1}{6} & \frac{h_1+h_2}{3} & \frac{h_2}{6} & \dots & 0 & 0 \\ 0 & \frac{h_2}{6} & \frac{h_2+h_3}{3} & \dots & 0 & 0 \\ \vdots & \vdots & \vdots & \ddots & \vdots & \vdots \\ 0 & 0 & 0 & \dots & \frac{h_{M-4}+h_{M-3}}{3} & \frac{h_{M-3}}{6} \\ 0 & 0 & 0 & \dots & \frac{h_{M-3}}{6} & \frac{h_{M-3}+h_{M-2}}{3} \end{pmatrix}$$

with $h_i = x_{i+1} - x_i$ for $i = 0, 1, \dots, M-2$.

By simple calculation, we know that matrix $\mathbf{Z} = \alpha \mathbf{W} + (1-\alpha) \mathbf{A}^\top \mathbf{M} \mathbf{A} \in \mathbb{R}^{M \times M}$ is a

2. the computational complexity to compute $(\mathbf{P}^\top)^{-1}\mathbf{\Sigma}^{-1}\mathbf{P}^{-1}\mathbf{y}$ is $O(M)$ with $n \in \{0, \dots, N-1\}$ fixed.

First of all, we verify that the computational complexity to decompose \mathbf{Z} into $\mathbf{P}\mathbf{\Sigma}\mathbf{P}^\top$ is $O(M)$ when $n \in \{0, \dots, N-1\}$ fixed. By applying method of undetermined coefficients to equality $\mathbf{Z} = \mathbf{P}\mathbf{\Sigma}\mathbf{P}^\top$, we have

$$\begin{bmatrix} s_1 & s_1\ell_1 & s_1\gamma_1 & \dots & 0 \\ s_1\ell_1 & s_1\ell_1^2 + s_2 & s_1\ell_1\gamma_1 + s_2\ell_2 & \dots & 0 \\ s_1\gamma_1 & s_1\ell_1\gamma_1 + s_2\ell_2 & s_1\gamma_1^2 + s_2\ell_2^2 + s_3 & \dots & 0 \\ s_1\eta_1 & s_1\eta_1\ell_1 + s_2\gamma_2 & s_1\eta_1\gamma_1 + s_2\gamma_2\ell_2 + s_3\ell_3 & \dots & 0 \\ 0 & s_2\eta_2 & s_2\eta_2\ell_2 + s_3\gamma_3 & \dots & 0 \\ 0 & 0 & s_3\eta_3 & \dots & 0 \\ \vdots & \vdots & \vdots & \ddots & \vdots \\ 0 & 0 & 0 & \dots & s_{M-3}\eta_{M-3}^2 + s_{M-2}\gamma_{M-2}^2 \\ & & & & + s_{M-1}\gamma_{M-1}\ell_{M-1}^2 + s_M \end{bmatrix} = [z_{i,j}],$$

where $[z_{i,j}]$ denotes matrix \mathbf{Z} with its (i, j) th entry as $z_{i,j}$. Through the above method of undetermined coefficients, we can solve the explicit value of all entries in matrix \mathbf{P} , $\mathbf{\Sigma}$, i.e., $\ell_1, \dots, \ell_{M-1}, \gamma_1, \dots, \gamma_{M-2}, \eta_1, \dots, \eta_{M-3}$ in matrix \mathbf{P} and s_1, \dots, s_M in matrix $\mathbf{\Sigma}$, which is summarized in Algorithm 5. From Algorithm 5, we can see that the computational complexity to decompose \mathbf{Z} into $\mathbf{P}\mathbf{\Sigma}\mathbf{P}^\top$ is $O(M)$ with $n \in \{0, \dots, N-1\}$ fixed.

Second, we verify the computational complexity to compute $(\mathbf{P}^\top)^{-1}\mathbf{\Sigma}^{-1}\mathbf{P}^{-1}\mathbf{y}$ is $O(M)$

with $n \in \{0, \dots, N-1\}$ fixed and matrix $\mathbf{P}, \mathbf{\Sigma}$ available. To realize this objective, we will first verify that the computational complexity to calculate $\bar{\mathbf{y}} = \mathbf{P}^{-1}\mathbf{y}$ is $O(M)$. Then, we will first verify that the computational complexity to calculate $\bar{\bar{\mathbf{y}}} = \mathbf{\Sigma}^{-1}\bar{\mathbf{y}}$ is $O(M)$. Finally, we will first verify that the computational complexity to calculate $\bar{\bar{\bar{\mathbf{y}}}} = (\mathbf{P}^\top)^{-1}\bar{\bar{\mathbf{y}}}$ is $O(M)$. First of all, let us verify the computational complexity to compute $\bar{\mathbf{y}} = \mathbf{P}^{-1}\mathbf{y}$ is $O(M)$ with $n \in \{0, \dots, N-1\}$ fixed. Because we have a system of equations derived from $\mathbf{P}\bar{\mathbf{y}} = \mathbf{y}$:

$$\left\{ \begin{array}{l} \bar{y}_1 = y_1 \\ \bar{y}_2 = y_2 - \ell_1 \bar{y}_1 \\ \bar{y}_3 = y_3 - \gamma_1 \bar{y}_1 - \ell_2 \bar{y}_2 \\ \bar{y}_4 = y_4 - \eta_1 \bar{y}_1 - \gamma_2 \bar{y}_2 - \ell_3 \bar{y}_3 \\ \bar{y}_5 = y_5 - \eta_2 \bar{y}_3 - \gamma_3 \bar{y}_3 - \ell_4 \bar{y}_4 \\ \vdots \\ \bar{y}_M = y_M - \eta_{M-3} \bar{y}_{M-3} - \gamma_{M-2} \bar{y}_{M-2} - \ell_{M-1} \bar{y}_{M-1}, \end{array} \right.$$

we can solve vector $\bar{\mathbf{y}} = (\bar{y}_1, \bar{y}_2, \dots, \bar{y}_M)^\top$ explicitly through Algorithm 6, which only requires $O(M)$ computational complexity. After deriving $\bar{\mathbf{y}} = \mathbf{P}^{-1}\mathbf{y}$, we can easily verify that the computational complexity to derive $\bar{\bar{\mathbf{y}}} = \mathbf{\Sigma}^{-1}\bar{\mathbf{y}}$ is still $O(M)$ because $\mathbf{\sigma}$ is a diagonal matrix. Finally, after deriving $\bar{\bar{\bar{\mathbf{y}}}} = \mathbf{\Sigma}^{-1}\bar{\bar{\mathbf{y}}}$, we can verify that the computational complexity to derive $\bar{\bar{\bar{\mathbf{y}}}} = (\mathbf{P}^\top)^{-1}\bar{\bar{\mathbf{y}}}$ is still $O(M)$ with the similar logic as that in $\bar{\mathbf{y}} = \mathbf{P}^{-1}\mathbf{y}$.

From the above discussion, we know that the computational complexity to calculate

$$\widehat{\mathbf{f}} = (u(\widehat{x_0, t_n}), u(\widehat{x_1, t_n}), \dots, u(\widehat{x_{M-1}, t_n}))^\top, \text{ is } O(M) \text{ with } n \in \{0, 1, \dots, N-1\} \text{ fixed.}$$

In other words, the computational complexity to derive $\{u(\widehat{x_i, t_n})\}_{i=0, \dots, M-1}$ is $O(M)$.

According, the computational complexity to derive $\{u(\widehat{x_i, t_n})\}_{i=0, \dots, M-1, n=0, \dots, N-1}$ is $O(MN)$.

Algorithm 5: Pseudo code to solve \mathbf{P}, Σ

Input: matrix \mathbf{Z}

Output: matrix \mathbf{P}, Σ

- 1 **Initialize** $s_j = \eta_j = \gamma_j = \ell_j = 0 \forall j \leq 0$
 - 2 **for** $i = 1, 2, \dots, M$ **do**
 - 3 $s_i = z_{ii} - s_{i-3}\eta_{i-3}^2 - s_{i-2}\gamma_{i-2}^2 - s_{i-1}\ell_{i-1}^2$
 - 4 $\ell_i = (z_{i, i+1} - s_{i-2}\gamma_{i-2}\eta_{i-2} - s_{i-1}\gamma_{i-1}\ell_{i-1})/s_i$
 - 5 $\eta_i = a_{i, i+3}/s_i$
-

Algorithm 6: Pseudo code to solve $\mathbf{P}^{-1}\mathbf{y}$

Input: matrix \mathbf{P}, \mathbf{y}

Output: vector $\bar{\mathbf{y}}$

- 1 **Initialize** $\eta_i = \gamma_i = \ell_i = 0 \forall i \leq 0$
 - 2 **for** $i = 1, \dots, M$ **do**
 - 3 $\bar{y}_i = y_i - \eta_{i-3}\bar{y}_{i-3} - \gamma_{i-2}\bar{y}_{i-2} - \ell_{i-1}\bar{y}_{i-1}$
-

□

A.10.2 Proof of Proposition A.1

Proof. We have discussed how to use cubic spline to derive derivatives of $u(x, t)$. In this section, we discuss how to use local polynomial regression to derive derivatives, as a benchmark method.

Recall that the derivatives can be estimated by local polynomial regression includes $u(x_i, t_n), \frac{\partial}{\partial x}u(x_i, t_n), \frac{\partial^2}{\partial x^2}u(x_i, t_n), \dots$. And here we take the derivation $\frac{\partial^l}{\partial x^l}u(x, t_n)$ as an example ($l = 0, 1, 2, \dots$), and the other derivatives can be derived with the same logic flow. To derive the estimation of $\frac{\partial^l}{\partial x^l}u(x, t_n)$, we fix the temporal variable t_n for a general $n \in \{0, 1, \dots, N-1\}$.

Then we locally fit a degree \check{p} polynomial over the data $\{(x_i, u_i^n)\}_{i=0, \dots, M-1}$, i.e.,

$$\left\{ \begin{array}{l} u(x_0, t_n) = u(x, t_n) + \frac{\partial}{\partial x}u(x, t_n)(x_0 - x) + \dots + \frac{\partial^{\check{p}}}{\partial x^{\check{p}}}u(x, t_n)(x_0 - x)^{\check{p}} \\ u(x_1, t_n) = u(x, t_n) + \frac{\partial}{\partial x}u(x, t_n)(x_1 - x) + \dots + \frac{\partial^{\check{p}}}{\partial x^{\check{p}}}u(x, t_n)(x_1 - x)^{\check{p}} \\ \vdots \quad \quad \quad \vdots \\ u(x_{M-1}, t_n) = u(x, t_n) + \frac{\partial}{\partial x}u(x, t_n)(x_{M-1} - x) + \dots + \frac{\partial^{\check{p}}}{\partial x^{\check{p}}}u(x, t_n)(x_{M-1} - x)^{\check{p}} \end{array} \right. .$$

For the choice of \check{p} , we choose $\check{p} = l + 3$ to realize minmax efficiency (see Fan et al., 1997). If we

denote $\mathbf{b}(x) = \left(u(x, t_n), \frac{\partial}{\partial x}u(x, t_n), \dots, \frac{\partial^{\check{p}}}{\partial x^{\check{p}}}u(x, t_n) \right)^\top$, then $\frac{\partial^l}{\partial x^l}u(x, t_n)$ can be obtained as the

$(l + 1)$ -th entry of the vector $\widehat{\mathbf{b}}(x)$, and $\widehat{\mathbf{b}}(x)$ is obtained by the following optimization problem:

$$\widehat{\mathbf{b}}(x) = \arg \min_{\mathbf{b}(x)} \sum_{i=0}^{M-1} \left[u_i^n - \sum_{j=0}^{\check{p}} \frac{\partial^j}{\partial x^j}u(x, t_n)(x_i - x)^j \right]^2 \mathcal{K} \left(\frac{x_i - x}{h} \right), \quad (\text{A.26})$$

where h is the bandwidth parameter, and \mathcal{K} is a kernel function, and in our paper, we use the

Epanechnikov kernel $\mathcal{K}(x) = \frac{3}{4} \max\{0, 1 - x^2\}$ for $x \in \mathbb{R}$. Essentially, the optimization problem

in equation (A.26) is a weighted least squares model, where $\mathbf{b}(x)$ can be solved in a close form:

$$\mathbf{b}(x) = \left(\mathbf{X}_{\text{spa}}^\top \mathbf{W}_{\text{spa}} \mathbf{X}_{\text{spa}} \right)^{-1} \mathbf{X}_{\text{spa}}^\top \mathbf{W}_{\text{spa}} \mathbf{u}^n, \quad (\text{A.27})$$

where

$$\mathbf{X}_{\text{spa}} = \begin{bmatrix} 1 & (x_0 - x) & \dots & (x_0 - x)^{\bar{p}} \\ 1 & (x_1 - x) & \dots & (x_1 - x)^{\bar{p}} \\ \vdots & \vdots & \ddots & \vdots \\ 1 & (x_{M-1} - x) & \dots & (x_{M-1} - x)^{\bar{p}} \end{bmatrix}, \quad \mathbf{u}^n = \begin{bmatrix} u_0^n \\ u_1^n \\ \vdots \\ u_{M-1}^n \end{bmatrix}$$

and $\mathbf{W}_{\text{spa}} = \text{diag} \left(\mathcal{K} \left(\frac{x_0 - x}{h} \right), \dots, \mathcal{K} \left(\frac{x_{M-1} - x}{h} \right) \right)$.

By implementing the local polynomial in this way, the computational complexity is much higher than our method, and we summarize its computational complexity in the following proposition.

Following please find the proof.

Similar to the proof of the computational complexity in cubic spline, the proof of the computational complexity of local polynomial regression in the functional estimation stage lies in calculating all elements in matrix \mathbf{X} and vector $\nabla_t \mathbf{u}$, including

$$\left\{ \widehat{u(x_i, t_n)}, \widehat{\frac{\partial}{\partial x} u(x_i, t_n)}, \widehat{\frac{\partial^2}{\partial x^2} u(x_i, t_n)}, \widehat{\frac{\partial}{\partial t} u(x_i, t_n)} \right\}_{i=0, \dots, M-1, n=0, \dots, N-1}.$$

We will take the estimation of $\widehat{\frac{\partial^p}{\partial x^p} u(x_i, t_n)}$ with a general $p \in \mathbb{N}$ as an example. To solve $\left\{ \widehat{\frac{\partial^p}{\partial x^p} u(x_i, t_n)} \right\}_{i=0, \dots, M-1, n=0, \dots, N-1}$, we first focus on $\left\{ \widehat{\frac{\partial^p}{\partial x^p} u(x_i, t_n)} \right\}_{i=0, \dots, M-1}$, with $n \in \{0, \dots, N-1\}$ fixed. To solve it, the main idea of local polynomial regression is to do Taylor

expansion:

$$\left\{ \begin{array}{l} u(x_0, t_n) = u(x, t_n) + \frac{\partial}{\partial x} u(x, t_n)(x_0 - x) + \dots + \frac{\partial^{\check{p}}}{\partial x^{\check{p}}} u(x, t_n)(x_0 - x)^{\check{p}} \\ u(x_1, t_n) = u(x, t_n) + \frac{\partial}{\partial x} u(x, t_n)(x_1 - x) + \dots + \frac{\partial^{\check{p}}}{\partial x^{\check{p}}} u(x, t_n)(x_1 - x)^{\check{p}} \\ \vdots \\ u(x_{M-1}, t_n) = u(x, t_n) + \frac{\partial}{\partial x} u(x, t_n)(x_{M-1} - x) + \dots + \frac{\partial^{\check{p}}}{\partial x^{\check{p}}} u(x, t_n)(x_{M-1} - x)^{\check{p}} \end{array} \right. ,$$

where \check{p} is usually set as $\check{p} = p + 3$ to obtain asymptotic minimax efficiency (see Fan et al., 1997). In the above system of equations, if we denote

$$\mathbf{b}(x) = \left(u(x, t_n), \frac{\partial}{\partial x} u(x, t_n), \dots, \frac{\partial^{\check{p}}}{\partial x^{\check{p}}} u(x, t_n) \right)^\top ,$$

then we can solve $\mathbf{b}(x)$ through the optimization problem in (A.26) with a closed-form solution shown in (A.27):

$$\mathbf{b}(x) = \left(\mathbf{X}_{\text{spa}}^\top \mathbf{W}_{\text{spa}} \mathbf{X}_{\text{spa}} \right)^{-1} \mathbf{X}_{\text{spa}}^\top \mathbf{W}_{\text{spa}} \mathbf{u}^n, \quad (\text{A.28})$$

where

$$\mathbf{X}_{\text{spa}} = \begin{bmatrix} 1 & (x_0 - x) & \dots & (x_0 - x)^{\check{p}} \\ 1 & (x_1 - x) & \dots & (x_1 - x)^{\check{p}} \\ \vdots & \vdots & \ddots & \vdots \\ 1 & (x_{M-1} - x) & \dots & (x_{M-1} - x)^{\check{p}} \end{bmatrix}, \quad \mathbf{u}^n = \begin{bmatrix} u_0^n \\ u_1^n \\ \vdots \\ u_{M-1}^n \end{bmatrix}$$

and $\mathbf{W}_{\text{spa}} = \text{diag} \left(\mathcal{K} \left(\frac{x_0 - x}{h} \right), \dots, \mathcal{K} \left(\frac{x_{M-1} - x}{h} \right) \right)$.

The main computational complexity to derive $\mathbf{b}(x)$ lies in the computation of inverse of

matrix $\mathbf{X}_{\text{spa}}^\top \mathbf{W}_{\text{spa}} \mathbf{X}_{\text{spa}} \in \mathbb{R}^{(\check{p}+1) \times (\check{p}+1)}$, where

$$\mathbf{X}_{\text{spa}}^\top \mathbf{W}_{\text{spa}} \mathbf{X}_{\text{spa}} = \begin{bmatrix} \sum_{i=0}^{M-1} w_i & \sum_{i=0}^{M-1} w_i(x_i - x) & \sum_{i=0}^{M-1} w_i(x_i - x)^2 & \dots & \sum_{i=0}^{M-1} w_i(x_i - x)^{\check{p}} \\ \sum_{i=0}^{M-1} w_i(x_i - x) & \sum_{i=0}^{M-1} w_i(x_i - x)^2 & \sum_{i=0}^{M-1} w_i(x_i - x)^3 & \dots & \sum_{i=0}^{M-1} w_i(x_i - x)^{\check{p}+1} \\ \sum_{i=0}^{M-1} w_i(x_i - x)^2 & \sum_{i=0}^{M-1} w_i(x_i - x)^3 & \sum_{i=0}^{M-1} w_i(x_i - x)^4 & \dots & \sum_{i=0}^{M-1} w_i(x_i - x)^{\check{p}+2} \\ \vdots & \vdots & \vdots & \ddots & \vdots \\ \sum_{i=0}^{M-1} w_i(x_i - x)^{\check{p}} & \sum_{i=0}^{M-1} w_i(x_i - x)^{\check{p}+1} & \sum_{i=0}^{M-1} w_i(x_i - x)^{\check{p}+2} & \dots & \sum_{i=0}^{M-1} w_i(x_i - x)^{2\check{p}} \end{bmatrix}$$

and

$$\mathbf{X}_{\text{spa}}^\top \mathbf{W}_{\text{spa}} \mathbf{u}^n = \begin{pmatrix} \sum_{i=0}^{M-1} w_i u_i^n \\ \sum_{i=0}^{M-1} w_i(x_i - x) u_i^n \\ \sum_{i=0}^{M-1} w_i(x_i - x)^2 u_i^n \\ \sum_{i=0}^{M-1} w_i(x_i - x)^3 u_i^n \\ \sum_{i=0}^{M-1} w_i(x_i - x)^4 u_i^n \end{pmatrix},$$

we know that for a fixed $n \in \{0, \dots, N-1\}$ and $x \in \{x_0, \dots, x_{M-1}\}$, the computational

complexity of computing $\mathbf{X}_{\text{spa}}^\top \mathbf{W}_{\text{spa}} \mathbf{X}_{\text{spa}}$ and $\mathbf{X}_{\text{spa}}^\top \mathbf{W}_{\text{spa}} \mathbf{u}^n$ is $O(\check{p}^2 M)$. Besides, the compu-

tational complexity to derive $(\mathbf{X}_{\text{spa}}^\top \mathbf{W}_{\text{spa}} \mathbf{X}_{\text{spa}})^{-1}$ is $O(\check{p}^3)$. So we know that for a fixed $n \in$

$\{0, \dots, N-1\}$ and $x \in \{x_0, \dots, x_{M-1}\}$, the computational complexity of computing $\frac{\partial^p}{\partial x^p} u(x_i, t_n)$

is $\max\{O(\check{p}^2 M), O(\check{p}^3)\}$ with \check{p} usually set as $\check{p} = p + 3$. Accordingly, the computational

complexity of computing $\left\{ \frac{\partial^p}{\partial x^p} u(x_i, t_n) \right\}_{i=0, \dots, M-1, n=0, \dots, N-1}$ is $\max\{O(\check{p}^2 M^2 N), O(\check{p}^3 MN)\}$.

Because $p \leq q_{\max}$, we know that the computational complexity of computing all derivatives

with respect to x with highest order as q_{\max} is $\max\{O(q_{\max}^2 M^2 N), O(q_{\max}^3 MN)\}$. Similarly,

the computational complexity of computing the first order derivatives with respect to t is $\max\{O(MN^2), O(MN)\}$. In conclusion, the computational complexity to derive all elements in matrix \mathbf{X} and vector $\nabla_t \mathbf{u}$, including

$$\left\{ \widehat{u(x_i, t_n)}, \frac{\partial}{\partial x} \widehat{u(x_i, t_n)}, \frac{\partial^2}{\partial x^2} \widehat{u(x_i, t_n)}, \frac{\partial}{\partial t} \widehat{u(x_i, t_n)} \right\}_{i=0, \dots, M-1, n=0, \dots, N-1}.$$

by local polynomial regression in (2.4) is $\max\{O(q_{\max}^2 M^2 N), O(MN^2), O(q_{\max}^3 MN)\}$, where q_{\max} is the highest order of derivatives desired in (1.3). \square

A.10.3 Proof of Lemma A.2

Proof. In this proof, we take $k = 0$ as an illustration example, i.e., prove that when

$$\epsilon > \mathcal{C}(\sigma, \|u\|_{L^\infty(\Omega)}) \max \left\{ \frac{4K_{\max}}{M^{3/7}}, 4AM^{-3/7}, 4\sqrt{2} \frac{d^3}{dx^3} f^*(0) M^{-3/7}, \frac{16(C \log M + \gamma) \log(M)}{M^{3/7}}, 16\sqrt{\frac{\omega}{7}} \tilde{C}(\sigma, \|u\|_{L^\infty(\Omega)}) \frac{\sqrt{\log(M)}}{M^{3/7}} \right\},$$

we have

$$P \left[\sup_{x \in [0, X_{\max}]} \left| \widehat{u(x, t_n)} - u(x, t_n) \right| > \epsilon \right] < 2Me^{-\frac{M^{2/7}}{2\sigma^2}} + Qe^{-L\gamma} + 4\sqrt{2}\eta^4 M^{-\frac{2}{7}\omega}$$

for a fixed t_n with $n \in \{0, 1, \dots, N-1\}$. For $k = 1, 2$, it can be derived with the same logic flow.

Recall in Section 2.1, the fitted value of the smoothing cubic spline $s(x)$ is the minimizer of the optimization problem in (2.4). From Theorem A in Silverman (1984) (also mentioned by Messer (1991) in the Section 1, and equation (2.2) in Craven and Wahba (1978)) that when

Condition 3.3 - Condition 3.4 hold and for large M and small $\tilde{\lambda} = \frac{1-\alpha}{\alpha}$, we have

$$\hat{f}_i = \frac{1}{M\tilde{\lambda}^{1/4}} \sum_{j=0}^{M-1} K\left(\frac{x_i - x_j}{\tilde{\lambda}^{1/4}}\right) u_j^n,$$

where $\hat{f}_i = u(\widehat{x_i, t_n})$, $\tilde{\lambda}$ trades off the goodness-of-fit and smoothness of the cubic spline in (2.4)

and $K(\cdot)$ is a fixed kernel function defined as

$$K(x) = \frac{1}{2} e^{-|x|/\sqrt{2}} \left[\sin(|x|/\sqrt{2} + \pi/4) \right].$$

For a general spatial variable x and fixed $n \in \{0, 1, \dots, N-1\}$, we denote

$$f^*(x) = u(x, t_n),$$

which is the ground truth of the underlying dynamic function $u(x, t_n)$ with t_n fixed. Besides,

we denote $\hat{f}(x) = u(\widehat{x, t_n})$, which is an estimation of the ground truth of $f^*(x) = u(x, t_n)$ with

t_n fixed. Accordingly to the above discussion, this estimation of $\hat{f}(x)$ can be written as

$$\hat{f}(x) = \frac{1}{M\tilde{\lambda}^{1/4}} \sum_{j=0}^{M-1} K\left(\frac{x - x_j}{\tilde{\lambda}^{1/4}}\right) u_j^n,$$

where $\hat{f}_i = \hat{f}(x_i)$ for $i \in \{0, 1, \dots, M-1\}$

In order to bound $P\left(\sup|\widehat{f}(x) - f^*(x)| > \epsilon\right)$ for a general x , we decompose it as follows:

$$\begin{aligned}
& P\left(\sup|\widehat{f}(x) - f^*(x)| > \epsilon\right) \\
&= P\left(\sup|\widehat{f}(x) - \widehat{f}^B(x) + \widehat{f}^B(x) - f^*(x)| > \epsilon\right) \\
&= P\left(\sup|\widehat{f}(x) - \widehat{f}^B(x) - E(\widehat{f}(x) - \widehat{f}^B(x)) + E(\widehat{f}(x) - \widehat{f}^B(x)) + \widehat{f}^B(x) - f^*(x)| > \epsilon\right) \\
&= P\left(\sup\left|\underbrace{\widehat{f}(x) - \widehat{f}^B(x)}_{\mathcal{A}} - \underbrace{E(\widehat{f}(x) - \widehat{f}^B(x))}_{\mathcal{B}} + \underbrace{E(\widehat{f}(x) - \widehat{f}^B(x))}_{\mathcal{C}} + \underbrace{\widehat{f}^B(x) - E(\widehat{f}^B(x))}_{\mathcal{D}}\right| > \epsilon\right) \\
&\leq P\left(\sup|\mathcal{A}| > \frac{\epsilon}{4}\right) + P\left(\sup|\mathcal{B}| > \frac{\epsilon}{4}\right) + P\left(\sup|\mathcal{C}| > \frac{\epsilon}{4}\right) + P\left(\sup|\mathcal{D}| > \frac{\epsilon}{4}\right)
\end{aligned} \tag{A.29}$$

where the $\widehat{f}^B(x)$ in (A.29) the truncated estimator defined as

$$\widehat{f}^B(x) = \frac{1}{M\widehat{\lambda}^{1/4}} \sum_{j=0}^{M-1} K\left(\frac{x - x_j}{\widehat{\lambda}^{1/4}}\right) u_j^n \mathbb{1}\{u_j^n < B_M\}.$$

Here $\{B_M\}$ is an increasing sequence and $B_M \rightarrow +\infty$ as $M \rightarrow +\infty$, i.e., $B_M = M^b$ with constant $b > 0$, and we will discuss the value of b at the end of this proof.

In the remaining of the proof, we work on the upper bound of the four decomposed terms, i.e., $P\left(\sup|\mathcal{A}| > \frac{\epsilon}{4}\right)$, $P\left(\sup|\mathcal{B}| > \frac{\epsilon}{4}\right)$, $P\left(\sup|\mathcal{C}| > \frac{\epsilon}{4}\right)$, $P\left(\sup|\mathcal{D}| > \frac{\epsilon}{4}\right)$.

First, let us discuss the upper bound of $P\left(\sup|\mathcal{A}| > \frac{\epsilon}{4}\right)$.

Because

$$\begin{aligned}
P\left(\sup |\mathcal{A}| > \frac{\epsilon}{4}\right) &= P\left(\sup \left|\widehat{f}(x) - \widehat{f}^B(x)\right| > \frac{\epsilon}{4}\right) \\
&= P\left(\sup \left|\frac{1}{M\widetilde{\lambda}^{1/4}} \sum_{j=0}^{M-1} K\left(\frac{x-x_j}{\widetilde{\lambda}^{1/4}}\right) u_j^n \mathbb{1}\{u_j^n \geq B_M\}\right| > \frac{\epsilon}{4}\right) \\
&\leq P\left(\sup \left|\frac{K_{\max}}{M\widetilde{\lambda}^{1/4}} \sum_{j=0}^{M-1} u_j^n \mathbb{1}\{u_j^n \geq B_M\}\right| > \frac{\epsilon}{4}\right),
\end{aligned}$$

where $K_{\max} = \max_{x \in [0, X_{\max}] \cup [0, T_{\max}]} K(x)$. If we let $\frac{\epsilon}{4} > \frac{K_{\max}}{M\widetilde{\lambda}^{1/4}} B_M$, then we have

$$\begin{aligned}
P\left(\sup |\mathcal{A}| > \frac{\epsilon}{4}\right) &\leq P(\exists i = 0, \dots, M-1, \text{ s.t. } |u_i^n| \geq B_M) \\
&= P\left(\max_{i=0, \dots, M-1} |u_i^n| \geq B_M\right).
\end{aligned}$$

Let $C_M = B_M - \|U\|_{L^\infty(\Omega)}$, where U is the random variable generated from the unknown

dynamic system, i.e., $U = u(x, t) + \epsilon$ with $\epsilon \sim N(0, \sigma^2)$. Then we have

$$\begin{aligned}
P\left(\sup |\mathcal{A}| > \frac{\epsilon}{4}\right) &= P\left(\sup \left|\widehat{f}(x) - \widehat{f}^B(x)\right| > \frac{\epsilon}{4}\right) \\
&\leq P\left(\max_{i=0, \dots, M-1} |U_i^n - u_i^n| \geq C_M\right) \\
&\leq 2Me^{-C_M^2/(2\sigma^2)}.
\end{aligned}$$

Next, let us discuss the upper bound of $P\left(\sup |\mathcal{B}| > \frac{\epsilon}{4}\right)$.

$$\begin{aligned}
\mathcal{B} &= E\left(|\widehat{f}(x) - \widehat{f}^B(x)|\right) \\
&= E\left(\left|\frac{1}{M\widetilde{\lambda}^{1/4}} \sum_{j=0}^{M-1} K\left(\frac{x-x_j}{\widetilde{\lambda}^{1/4}}\right) u_j^n \mathbb{1}\{u_j^n \geq B_M\}\right|\right) \\
&\leq E\left(\frac{1}{M\widetilde{\lambda}^{1/4}} \sum_{j=0}^{M-1} \left|K\left(\frac{x-x_j}{\widetilde{\lambda}^{1/4}}\right)\right| |u_j^n| \mathbb{1}\{u_j^n \geq B_M\}\right) \\
&= \frac{1}{\widetilde{\lambda}^{1/4}} \int \int_{|u| \geq B_M} \left|K\left(\frac{x-a}{\widetilde{\lambda}^{1/4}}\right)\right| |u| dF_M(a, u) \tag{A.30} \\
&\leq \int |K(\xi)| d\xi \times \underbrace{\sup_{\alpha} \int_{|u| \geq B_M} |u| f_M(\alpha, u) du}_{\mathcal{V}}. \tag{A.31}
\end{aligned}$$

Here in (A.30), $F_M(\cdot, \cdot)$ is the empirical c.d.f. of (x, u) 's, and in (A.31), $f_M(\cdot, \cdot)$ is the empirical p.d.f. of (x, u) 's.

Now let us take a look at the upper bound of \mathcal{V} . For any $s > 0$, we have

$$\begin{aligned}
\sup_{\alpha} \int_{|u| \geq B_M} \frac{|u|}{B_M} f_M(\alpha, u) du &\leq \sup_{\alpha} \int_{|u| \geq B_M} \left(\frac{|u|}{B_M}\right)^s f_M(\alpha, u) du \\
&\leq \sup_{\alpha} \int \left(\frac{|u|}{B_M}\right)^s f_M(\alpha, u) du,
\end{aligned}$$

which gives

$$\mathcal{V} := \sup_{\alpha} \int_{|u| \geq B_M} |u| f_M(\alpha, u) du \leq B_M^{1-s} \underbrace{\sup_{\alpha} \int |u|^s f_M(\alpha, u) du}_{\pi_s}.$$

From the lemma statement we know that when $s = 2$, we have $\pi_s := \sup_{\alpha} \int |u|^s f_M(\alpha, u) du <$

$+\infty$. If we set $A = \pi_s \int |K(\xi)| d\xi$, then we have

$$\mathcal{B} \leq AB_M^{1-s}.$$

So when $\frac{\epsilon}{4} > AB_M^{1-s}$, we have

$$P\left(\sup |\mathcal{B}| > \frac{\epsilon}{4}\right) = P\left(E\left(|\widehat{f}(x) - \widehat{f}^B(x)|\right) \geq \frac{\epsilon}{4}\right) = 0.$$

Then, let us discuss the upper bound of $P(\sup |\mathcal{C}| > \frac{\epsilon}{4})$. According to Lemma 5 in

Rice and Rosenblatt (1983), when

$$f^*(x) \in C^4, \frac{d^2}{dx^2} f^*(x_0) = \frac{d^2}{dx^2} f^*(x_{M-1}) = 0 \text{ and } \frac{d^3}{dx^3} f^*(x_0) \neq 0, \frac{d^3}{dx^3} f^*(x_{M-1}) = 0, \text{ we}$$

have

$$\begin{aligned} & E(\widehat{f}(x)) - f^*(x) \\ &= \sqrt{2} \frac{d^3}{dx^3} f^*(0) \widetilde{\lambda}^{3/4} \exp\left(\frac{-x}{\sqrt{2}} \widetilde{\lambda}^{-1/4}\right) \cos\left(\frac{x}{\sqrt{2}} \widetilde{\lambda}^{-1/4}\right) + \ell(x), \end{aligned}$$

where the error term $\ell(x)$ satisfies

$$\int [\ell(x)]^2 dx = o\left(\int [E(\widehat{f}(x)) - f^*(x)]^2 dx\right).$$

So when $\frac{\epsilon}{4} > \sqrt{2} \frac{d^3}{dx^3} f^*(0) \widetilde{\lambda}^{3/4}$ and M is sufficiently large then we have

$$P\left(\sup |\mathcal{C}| > \frac{\epsilon}{4}\right) = 0.$$

Finally, let us discuss the upper bound of $P(\sup |\mathcal{D}| > \frac{\epsilon}{4})$.

In order to bound $P(\sup |D| > \frac{\epsilon}{4})$, we further decompose \mathcal{D} into two components, i.e.,

$$\mathcal{D} := \widehat{f}^B(x) - E(\widehat{f}^B(x)) = e_M(x, t_n) + \frac{1}{\sqrt{M}} \rho_M(x, t_n).$$

The decomposition procedure and the definition of $e_M(x, t_n), \rho_M(x, t_n)$ are described in the

following system of equations (see Mack and Silverman, 1982, Proposition 2):

$$\begin{aligned}
\mathcal{D} &= \widehat{f}^B(x) - E(\widehat{f}^B(x)) \\
&= \frac{1}{M\widetilde{\lambda}^{1/4}} \sum_{j=0}^{M-1} K\left(\frac{x-x_j}{\widetilde{\lambda}^{1/4}}\right) u_j^n \mathbb{1}\{u_j^n < B_M\} - \\
&\quad E\left(\frac{1}{M\widetilde{\lambda}^{1/4}} \sum_{j=0}^{M-1} K\left(\frac{x-x_j}{\widetilde{\lambda}^{1/4}}\right) u_j^n \mathbb{1}\{u_j^n < B_M\}\right) \\
&= \frac{1}{\sqrt{M}\widetilde{\lambda}^{1/4}} \int_{a \in \mathbb{R}} \int_{|u| < B_M} K\left(\frac{x-a}{\widetilde{\lambda}^{1/4}}\right) u \underbrace{d\left(\sqrt{M}(F_M(a,u) - F(a,u))\right)}_{Z_M(a,u)} \quad (\text{A.32}) \\
&= \frac{1}{\sqrt{M}\widetilde{\lambda}^{1/4}} \int_{a \in \mathbb{R}} K\left(\frac{x-a}{\widetilde{\lambda}^{1/4}}\right) \int_{|u| < B_M} u \, d(Z_M(a,u)) \\
&= \frac{1}{\sqrt{M}\widetilde{\lambda}^{1/4}} \int_{a \in \mathbb{R}} K\left(\frac{x-a}{\widetilde{\lambda}^{1/4}}\right) \left[\int_{|u| < B_M} u \, d(Z_M(a,u) - B_0(T(a,u))) + \right. \\
&\quad \left. \int_{|u| < B_M} u \, dB_0(T(a,u)) \right] \quad (\text{A.33}) \\
&= \frac{1}{\sqrt{M}\widetilde{\lambda}^{1/4}} \int_{a \in \mathbb{R}} \int_{|u| < B_M} \underbrace{K\left(\frac{x-a}{\widetilde{\lambda}^{1/4}}\right) u \, d(Z_M(a,u) - B_0(T(a,u)))}_{e_M(x,t_n)} \\
&\quad + \frac{1}{\sqrt{M}} \frac{1}{\widetilde{\lambda}^{1/4}} \int_{a \in \mathbb{R}} \int_{|u| < B_M} \underbrace{K\left(\frac{x-a}{\widetilde{\lambda}^{1/4}}\right) u \, dB_0(T(a,u))}_{\rho_M(x,t_n)}.
\end{aligned}$$

In (A.32), $F_M(\cdot, \cdot) := F_M(\cdot, \cdot | t_n)$ is the empirical c.d.f of (x, u) with a fixed t_n , and $Z_M(a, u) =$

$\sqrt{M}(F_M(a, u) - F(a, u))$ is a two-dimensional empirical process (see Tusnády, 1977; Mack and Silverman,

1982). In (A.33), $B_0(T(a, u))$ is a sample path of two-dimensional Brownian bride. And

$T(a, u) : \mathbb{R}^2 \rightarrow [0, 1]^2$ is the transformation defined by Rosenblatt (1952), i.e., $T(a, u) =$

$(F_A(x), F_{U|A}(u|a))$, where F_A is the marginal c.d.f of A and $F_{U|A}$ is the conditional c.d.f of

U given A (see Mack and Silverman, 1982, Proposition 2).

Through the above decomposition of \mathcal{D} , we have

$$P\left(\sup |D| > \frac{\epsilon}{4}\right) \leq P\left(\sup |e_M(x, t_n)| > \frac{\epsilon}{8}\right) + P\left(\sup \frac{1}{\sqrt{M}} |\rho_M(x, t_n)| > \frac{\epsilon}{8}\right).$$

For $e_M(x, t_n)$, we have

$$\begin{aligned} & P\left(\sup |e_M(x, t_n)| > \frac{\epsilon}{8}\right) \\ = & P\left(\sup \left| \frac{1}{\sqrt{M\tilde{\lambda}^{1/4}}} \int_{a \in \mathbb{R}} \int_{|u| < B_M} K\left(\frac{x-a}{\tilde{\lambda}^{1/4}}\right) u d(Z_M(a, u) - B_0(T(a, u))) \right| > \frac{\epsilon}{8}\right) \\ \leq & P\left(\frac{2B_M K_{\max}}{\sqrt{M\tilde{\lambda}^{1/4}}} \sup_{a, u} |Z_M(a, u) - B_0(T(a, u))| > \frac{\epsilon}{8}\right). \end{aligned}$$

Proved by Theorem 1 in Tusnady (1977), we know that, for any γ , we have

$$P\left(\sup_{a, u} |Z_M(a, u) - B_0(T(a, u))| > \frac{(C \log M + \gamma) \log M}{\sqrt{M}}\right) \leq Qe^{-L\gamma},$$

where C, Q, L are absolute positive constants which is independent of temporal resolution N

and spatial resolution M . Thus, when $\frac{\epsilon}{8} \geq \frac{2B_M K_{\max}}{\sqrt{M\tilde{\lambda}^{1/4}}} \frac{(C \log M + \gamma) \log M}{\sqrt{M}}$, we have

$$P\left(\sup |e_M(x, t_n)| > \frac{\epsilon}{8}\right) < Qe^{-L\gamma}.$$

For $\rho_M(x, t_n)$, by equation (7) in Mack and Silverman (1982), we have

$$\begin{aligned} \frac{\tilde{\lambda}^{1/8} \sup |\rho_M(x, t_n)|}{\sqrt{\log(1/\tilde{\lambda}^{1/4})}} & \leq \underbrace{16(\log V)^{1/2} S^{1/2} \left(\log\left(\frac{1}{\tilde{\lambda}^{1/4}}\right)\right)^{-1/2} \int |\xi|^{1/2} |dK(\xi)|}_{\mathcal{W}_{1, M}} + \\ & \underbrace{16\sqrt{2}\tilde{\lambda}^{-1/8} \left(\log\left(\frac{1}{\tilde{\lambda}^{1/4}}\right)\right)^{-1/2} \int q(S\tilde{\lambda}^{1/4}|\tau|) |d(K(\tau))|}_{\mathcal{W}_{2, M}}, \end{aligned}$$

where V is a random variable satisfying $E(V) \leq 4\sqrt{2}\eta^4$ for $\eta^2 = \max_{i=0, \dots, M-1, n=0, \dots, N-1} E(U_i^n)^2$,

$S = \sup_x \int u^2 f(x, u) du$ with $f(\cdot, \cdot)$ as the distribution function of (x_i, u_i^n) , and $q(z) = \int_0^z \frac{1}{2} \sqrt{\frac{1}{y} \log\left(\frac{1}{y}\right)} dy$.

So we have the following system of equations:

$$\begin{aligned}
& P\left(\sup \frac{1}{\sqrt{M}} |\rho_M(x, t_n)| > \frac{\epsilon}{8}\right) \\
&= P\left(\frac{\tilde{\lambda}^{1/8} \sup |\rho_M(x, t_n)|}{\sqrt{\log(1/\tilde{\lambda}^{1/4})}} > \frac{\sqrt{M\tilde{\lambda}^{1/8}\epsilon}}{8\sqrt{\log(1/\tilde{\lambda}^{1/4})}}\right) \\
&\leq P\left(\mathcal{W}_{1,M} + \mathcal{W}_{2,M} > \frac{\sqrt{M\tilde{\lambda}^{1/8}\epsilon}}{8\sqrt{\log(1/\tilde{\lambda}^{1/4})}}\right) \\
&\leq P\left(\mathcal{W}_{1,M} \geq \frac{\sqrt{M\tilde{\lambda}^{1/8}\epsilon}}{16\sqrt{\log(1/\tilde{\lambda}^{1/4})}}\right) + P\left(\mathcal{W}_{2,M} \geq \frac{\sqrt{M\tilde{\lambda}^{1/8}\epsilon}}{16\sqrt{\log(1/\tilde{\lambda}^{1/4})}}\right) \quad (\text{A.34})
\end{aligned}$$

Now let us bound $P\left(\mathcal{W}_{1,M} \geq \frac{\sqrt{M\tilde{\lambda}^{1/8}\epsilon}}{16\sqrt{\log(1/\tilde{\lambda}^{1/4})}}\right)$, $P\left(\mathcal{W}_{2,M} \geq \frac{\sqrt{M\tilde{\lambda}^{1/8}\epsilon}}{16\sqrt{\log(1/\tilde{\lambda}^{1/4})}}\right)$ in (A.34) separately.

1. For the first term in (A.34), we have

$$\begin{aligned}
& P\left(\mathcal{W}_{1,M} \geq \frac{\sqrt{M\tilde{\lambda}^{1/8}\epsilon}}{16\sqrt{\log(1/\tilde{\lambda}^{1/4})}}\right) \\
&= P\left(16(\log V)^{1/2} S^{1/2} \left(\log\left(\frac{1}{\tilde{\lambda}^{1/4}}\right)\right)^{-1/2} \int |\xi|^{1/2} |dK(\xi)| \geq \frac{\sqrt{M\tilde{\lambda}^{1/8}\epsilon}}{16\sqrt{\log(1/\tilde{\lambda}^{1/4})}}\right) \\
&= P\left((\log V)^{1/2} \geq \frac{\sqrt{M\tilde{\lambda}^{1/8}\epsilon}}{16^2 S^{1/2} \int |\xi|^{1/2} |dK(\xi)|}\right) \\
&= P\left(\log V \geq \left(\frac{\sqrt{M\tilde{\lambda}^{1/8}\epsilon}}{16^2 S^{1/2} \int |\xi|^{1/2} |dK(\xi)|}\right)^2\right) \\
&= P\left(V \geq \exp\left[\left(\frac{\sqrt{M\tilde{\lambda}^{1/8}\epsilon}}{16^2 S^{1/2} \int |\xi|^{1/2} |dK(\xi)|}\right)^2\right]\right) \\
&\leq \frac{E(V)}{\exp\left[\left(\frac{\sqrt{M\tilde{\lambda}^{1/8}\epsilon}}{16^2 S^{1/2} \int |\xi|^{1/2} |dK(\xi)|}\right)^2\right]} \quad (\text{A.35})
\end{aligned}$$

$$\leq \frac{4\sqrt{2}\eta^4}{\exp\left[\left(\frac{\sqrt{M\tilde{\lambda}^{1/8}\epsilon}}{16^2 S^{1/2} \int |\xi|^{1/2} |dK(\xi)|}\right)^2\right]} \quad (\text{A.36})$$

$$= 4\sqrt{2}\eta^4 \tilde{\lambda}^{\omega/4} \quad (\text{A.37})$$

Here inequality (A.35) is due to Markov's inequality, and inequality (A.36) is due to the fact that $E(V) \leq 4\sqrt{2}\eta^4$. Equality (A.37) is because we set $\frac{\sqrt{M}\lambda^{1/8}\epsilon}{16\sqrt{\log(1/\lambda^{1/4})}} = \sqrt{\omega}\tilde{C}(t_n, \sigma, \|u\|_{L^\infty(\Omega)})$, where

$$\tilde{C}(t_n, \sigma, \|u\|_{L^\infty(\Omega)}) := 16\sqrt{S} \int |\xi|^{1/2} |dK(\xi)|$$

and $\omega > 1$ is an arbitrary scaler.

2. For the second term of (A.34), it converges to $\tilde{C}(t_n, \sigma, \|u\|_{L^\infty(\Omega)})$ by using arguments similar to Silverman (1978) (page. 180-181) under the condition in Lemma A.2 that $\int \sqrt{|x \log(|x|)|} |dK(x)| < +\infty$. Here we add $(t_n, \sigma, \|u\|_{L^\infty(\Omega)})$ after \tilde{C} to emphasize that the constant $\tilde{C}(t_n, \sigma, \|u\|_{L^\infty(\Omega)})$ is dependent on $t_n, \sigma, \|u\|_{L^\infty(\Omega)}$.

It should be noted that

$$\tilde{C}(t_n, \sigma, \|u\|_{L^\infty(\Omega)}) < +\infty, \tag{A.38}$$

given the reasons listed as follows. First, it can be easily verified that the term $\int |\xi|^{1/2} |dK(\xi)|$ in $\tilde{C}(t_n, \sigma, \|u\|_{L^\infty(\Omega)})$ is bounded. Second, for $S = \sup_x \int u^2 f(x, u) du$, it is also bounded.

The reasons are described as follows. For a general $\varrho > 0$, we have

$$\begin{aligned} & \sup_{x \in [0, X_{\max}]} \int |u|^\varrho f(x, u) du \\ &= \sup_{x \in [0, X_{\max}]} \int |u|^\varrho \frac{1}{\sqrt{2\pi\sigma^2}} \exp\left(-\frac{(u - u(x, t_n))^2}{2\sigma^2}\right) du \\ &= \sup_{x \in [0, X_{\max}]} \frac{1}{\sqrt{2}} \sigma^2 2^{\varrho/2} \Gamma\left(\frac{1+\varrho}{2}\right) G\left(-\frac{\varrho}{2}, \frac{1}{2}, -\frac{1}{2} \left(\frac{u(x, t_n)}{\sigma}\right)^2\right), \end{aligned}$$

where $G(a, b, z)$ is Kummer's confluent hypergeometric function of $z \in \mathbb{C}$ with parameters $a, b \in \mathbb{C}$ (see Winkelbauer, 2012). Because $G(-\frac{\varrho}{2}, \frac{1}{2}, \cdot)$ is an entire function for fixed

parameters, we have

$$\begin{aligned}
 & \sup_{x \in [0, X_{\max}]} \int |u|^\varrho f(x, u) du \\
 \leq & \sup_{x \in [0, X_{\max}]} \frac{1}{\sqrt{2}} \sigma^2 2^{\varrho/2} \Gamma\left(\frac{1+\varrho}{2}\right) \sup_{z \in \left[-\frac{\max_{t \in \Omega} u^2(x, t)}{2\sigma^2}, -\frac{\min_{t \in \Omega} u^2(x, t)}{2\sigma^2}\right]} G\left(-\frac{\varrho}{2}, \frac{1}{2}, z\right) \\
 < & +\infty.
 \end{aligned}$$

So we can bound $\sup_{x \in [0, X_{\max}]} \int |u|^\varrho f(x, u) du$ by a constant. If we take $\varrho = 2$, we can obtain $S = \sup_x \int u^2 f(x, u) du$ bounded by a constant. So we can declare the statement in (A.38).

We would also like to declare that there exist a constant $\tilde{C}(\sigma, \|u\|_{L^\infty(\Omega)}) > 0$ such that for any $N \geq 1$, we have

$$\max_{n=0, \dots, N-1} \tilde{C}(t_n, \sigma, \|u\|_{L^\infty(\Omega)}) \leq \tilde{C}(\sigma, \|u\|_{L^\infty(\Omega)}),$$

where $\tilde{C}(\sigma, \|u\|_{L^\infty(\Omega)})$ is independent of t_n, x_i, M, N , and only depends on the noisy data \mathcal{D} itself.

From the above discussion, we learn that $\mathcal{W}_{2, M}$ converges to $\tilde{C}(t_n, \sigma, \|u\|_{L^\infty(\Omega)})$, which can be bounded by $\tilde{C}(\sigma, \|u\|_{L^\infty(\Omega)})$. If we set $\frac{\sqrt{M\tilde{\lambda}^{1/8}\epsilon}}{16\sqrt{\log(1/\tilde{\lambda}^{1/4})}} > \sqrt{\omega}\tilde{C}(\sigma, \|u\|_{L^\infty(\Omega)})$ with $\omega > 1$, then there exists a positive integer $\dot{M}(\omega)$ such that as long as $M > \dot{M}(\omega)$, we have $P\left(\mathcal{W}_{2, M} \geq \frac{\sqrt{M\tilde{\lambda}^{1/8}\epsilon}}{16\sqrt{\log(1/\tilde{\lambda}^{1/4})}}\right) = 0$.

For the value of ω , we set it as $\omega = M^{2r}$ with $r > 0$. And we will discuss the value of r later.

By combining $P\left(\mathcal{W}_{1,M} \geq \frac{\sqrt{M}\tilde{\lambda}^{1/8}\epsilon}{16\sqrt{\log(1/\tilde{\lambda}^{1/4})}}\right)$, $P\left(\mathcal{W}_{2,M} \geq \frac{\sqrt{M}\tilde{\lambda}^{1/8}\epsilon}{16\sqrt{\log(1/\tilde{\lambda}^{1/4})}}\right)$ together, we have when $\frac{\epsilon}{16} > \sqrt{\omega}\tilde{C}(\sigma, \|u\|_{L^\infty(\Omega)})\sqrt{\frac{\log(1/\tilde{\lambda}^{1/4})}{M\tilde{\lambda}^{1/4}}}$ and $M > \dot{M}(\omega)$, we have

$$P\left(\sup\left|\frac{1}{\sqrt{M}}\rho_M(x, t_n)\right| > \frac{\epsilon}{8}\right) < 4\sqrt{2}\eta^4\tilde{\lambda}^{\omega/4}.$$

By combining the discussion on $P(\sup|\mathcal{A}| > \frac{\epsilon}{4})$, $P(\sup|\mathcal{B}| > \frac{\epsilon}{4})$, $P(\sup|\mathcal{C}| > \frac{\epsilon}{4})$, and $P(\sup|\mathcal{D}| > \frac{\epsilon}{4})$, we can conclude that when

- $\frac{\epsilon}{4} > \frac{K_{\max}}{M\tilde{\lambda}^{1/4}}B_M$
- $\frac{\epsilon}{4} > AB_M^{1-s}$ ($s = 2$)
- $\frac{\epsilon}{4} > \sqrt{2}\frac{d^3}{dx^3}f^*(0)\tilde{\lambda}^{3/4}$
- $\frac{\epsilon}{8} > \frac{2B_M K_{\max}(C \log M + \gamma) \log M}{\tilde{\lambda}^{1/4}M}$
- $\frac{\epsilon}{16} > \sqrt{\omega}\tilde{C}(\sigma, \|u\|_{L^\infty(\Omega)})\sqrt{\frac{\log(1/\tilde{\lambda}^{1/4})}{M\tilde{\lambda}^{1/4}}}$

we have

$$P(\sup|\mathcal{A} + \mathcal{B} + \mathcal{C} + \mathcal{D}| > \epsilon) < \underbrace{2Me^{-\frac{C^2M}{2\sigma^2}}}_{\mathcal{Z}_1} + \underbrace{Qe^{-L\gamma}}_{\mathcal{Z}_2} + \underbrace{4\sqrt{2}\eta^4\tilde{\lambda}^{\omega/4}}_{\mathcal{Z}_3}. \quad (\text{A.39})$$

Let

$$\left\{ \begin{array}{l} E_1 = \frac{4K_{\max}}{M\tilde{\lambda}^{1/4}}B_M \\ E_2 = 4AB_M^{1-s} \\ E_3 = 4\sqrt{2}\frac{d^3}{dx^3}f^*(0)\tilde{\lambda}^{3/4} \\ E_4 = \frac{16B_M K_{\max}(C \log M + \gamma) \log M}{\tilde{\lambda}^{1/4}M} \\ E_5 = 16\sqrt{\omega}\tilde{C}(\sigma, \|u\|_{L^\infty(\Omega)})\sqrt{\frac{\log(1/\tilde{\lambda}^{1/4})}{M\tilde{\lambda}^{1/4}}} \end{array} \right. ,$$

by setting $\tilde{\lambda} = M^{-a}$, $B_M = M^b$ with $a, b > 0$, we have

$$\left\{ \begin{array}{l} E_1 = \frac{4K_{\max}}{M\tilde{\lambda}^{1/4}} B_M = \frac{4K_{\max}}{M^{1-a/4-b}} \\ E_2 = 4AB_M^{1-s} = 4A \frac{1}{M^{b(s-1)}} \\ E_3 = 4\sqrt{2} \frac{d}{dx} f^*(0) \tilde{\lambda}^{3/4} = 4\sqrt{2} \frac{d}{dx} f^*(0) M^{-3a/4} \\ E_4 = \frac{16B_M K_{\max} (C \log M + \gamma) \log M}{\tilde{\lambda}^{1/4} M} = \frac{16K_{\max} (C \log M + \gamma) \log(M)}{M^{1-a/4-b}} \\ E_5 = 16\sqrt{\omega} \tilde{C}(\sigma, \|u\|_{L^\infty(\Omega)}) \sqrt{\frac{\log(1/\tilde{\lambda}^{1/4})}{M\tilde{\lambda}^{1/4}}} = 8\sqrt{a\omega} \tilde{C}(\sigma, \|u\|_{L^\infty(\Omega)}) \sqrt{\frac{\log(M)}{M^{1-a/4}}}. \end{array} \right.$$

To guarantee that $E_1, E_2, E_3, E_4, E_5 \rightarrow 0$ as $M \rightarrow +\infty$, we can set

$$\left\{ \begin{array}{l} 1 - a/4 - b = 3a/4 \\ b(s-1) > 0 \\ \frac{1}{2}(1 - a/4) = 3a/4 \\ a, b > 0 \\ s = 2 \end{array} \right. \cdot$$

then we have

$$\left\{ \begin{array}{l} a = 4/7 \\ b = 3/7 \\ s = 2 \end{array} \right. \cdot$$

Accordingly, we have

$$\left\{ \begin{array}{l} E_1 = \frac{4K_{\max}}{M^{3/7}} \\ E_2 = 4AM^{-3/7} \\ E_3 = 4\sqrt{2} \frac{d^3}{dx^3} f^*(0) M^{-3/7} \\ E_4 = \frac{16K_{\max}(C \log M + \gamma) \log(M)}{M^{3/7}} \\ E_5 = 16\sqrt{\frac{\omega}{7}} \tilde{C}(\sigma, \|u\|_{L^\infty(\Omega)}) \frac{\sqrt{\log(M)}}{M^{3/7}} \end{array} \right. ,$$

where

$$E_1, E_2, E_3, E_5 \lesssim E_4$$

as $M \rightarrow +\infty$. Here, the operator \lesssim means that when $M \rightarrow +\infty$, the order of the left side hand of \lesssim will be much smaller than that on the right side hand. So we can declare that when M is sufficiently large and

$$\epsilon > \max \left\{ \frac{4K_{\max}}{M^{3/7}}, 4AM^{-3/7}, 4\sqrt{2} \frac{d^3}{dx^3} f^*(0) M^{-3/7}, \frac{16K_{\max}(C \log M + \gamma) \log(M)}{M^{3/7}}, 16\sqrt{\frac{\omega}{7}} \tilde{C}(\sigma, \|u\|_{L^\infty(\Omega)}) \frac{\sqrt{\log(M)}}{M^{3/7}} \right\},$$

we have

$$\begin{aligned} P(\sup |\mathcal{A} + \mathcal{B} + \mathcal{C} + \mathcal{D}| > \epsilon) &\leq 2Me^{-\frac{C_M^2}{2\sigma^2}} + Qe^{-L\gamma} + 4\sqrt{2}\eta^4 \tilde{\lambda}^{\omega/4} \\ &= 2Me^{-\frac{(M^{3/7} - \|U\|_{L^\infty(\Omega)})^2}{2\sigma^2}} + Qe^{-L\gamma} + 4\sqrt{2}\eta^4 M^{-\omega/7}. \end{aligned}$$

□

A.10.4 Proof of Lemma C.2

Proof. For the estimation error $\|\nabla_t \mathbf{u} - \mathbf{X}\boldsymbol{\beta}^*\|_\infty$, we have

$$\begin{aligned}
 \|\nabla_t \mathbf{u} - \mathbf{X}\boldsymbol{\beta}^*\|_\infty &= \|\nabla_t \mathbf{u} - \nabla_t \mathbf{u}^* + \nabla_t \mathbf{u}^* - \mathbf{X}\boldsymbol{\beta}^*\|_\infty \\
 &= \|\nabla_t \mathbf{u} - \nabla_t \mathbf{u}^* + \mathbf{X}^* \boldsymbol{\beta}^* - \mathbf{X}\boldsymbol{\beta}^*\|_\infty \\
 &\leq \|\nabla_t \mathbf{u} - \nabla_t \mathbf{u}^*\|_\infty + \|(\mathbf{X}^* - \mathbf{X})\boldsymbol{\beta}^*\|_\infty. \tag{A.40}
 \end{aligned}$$

So accordingly, we have

$$P(\|\nabla_t \mathbf{u} - \mathbf{X}\boldsymbol{\beta}^*\|_\infty > \epsilon) \leq P\left(\|\nabla_t \mathbf{u} - \nabla_t \mathbf{u}^*\|_\infty > \frac{\epsilon}{2}\right) + P(\|(\mathbf{X}^* - \mathbf{X})\boldsymbol{\beta}^*\|_\infty).$$

In the remaining of the proof, we will discuss the bound of $P(\|\nabla_t \mathbf{u} - \nabla_t \mathbf{u}^*\|_\infty > \frac{\epsilon}{2})$ and $P(\|(\mathbf{X}^* - \mathbf{X})\boldsymbol{\beta}^*\|_\infty)$ separately.

- First let us discuss the bound of $P(\|\nabla_t \mathbf{u} - \nabla_t \mathbf{u}^*\|_\infty > \frac{\epsilon}{2})$. Because

$$\begin{aligned}
 P\left(\|\nabla_t \mathbf{u} - \nabla_t \mathbf{u}^*\|_\infty > \frac{\epsilon}{2}\right) &\leq P\left(\max_{i=0, \dots, M-1} \sup_{t \in [0, T_{\max}]} \left| \widehat{\frac{\partial}{\partial t} u(x_i, t)} - \frac{\partial}{\partial t} u(x_i, t) \right| > \frac{\epsilon}{2}\right) \\
 &\leq \sum_{i=0}^{M-1} P\left(\sup_{t \in [0, T_{\max}]} \left| \widehat{\frac{\partial}{\partial t} u(x_i, t)} - \frac{\partial}{\partial t} u(x_i, t) \right| > \frac{\epsilon}{2}\right),
 \end{aligned}$$

if we set

$$\begin{aligned}
 \frac{\epsilon}{2} &> \mathcal{C}_{(\sigma, \|u\|_{L^\infty(\Omega)})} \max \left\{ 4K_{\max} N^{-3/7}, 4\bar{A} N^{-3/7}, 4\sqrt{2} \frac{d^3}{dx^3} \bar{f}^*(0) N^{-3/7}, \right. \\
 &\quad \frac{16K_{\max} \left[C_{(\sigma, \|u\|_{L^\infty(\Omega)})} \log(N) + \gamma(N) \right] \log(N)}{N^{3/7}}, \tag{A.41} \\
 &\quad \left. 16\sqrt{\frac{\omega(N)}{7}} \tilde{C}_{(\sigma, \|u\|_{L^\infty(\Omega)})} \frac{\sqrt{\log(N)}}{N^{3/7}} \right\},
 \end{aligned}$$

then we have

$$\begin{aligned}
& P\left(\|\nabla_t \mathbf{u} - \nabla_t \mathbf{u}^*\|_\infty > \frac{\epsilon}{2}\right) \\
& \leq M \left[2N e^{-\frac{(N^{3/7} - \|U\|_{L^\infty(\Omega)})^2}{2\sigma^2}} + Q_{(\sigma, \|u\|_{L^\infty(\Omega)})} e^{-L\gamma(N)} + 4\sqrt{2}\eta^4 N^{-\omega(N)/7} \right] \quad (\text{A.42})
\end{aligned}$$

where inequity (A.42) is derived according to Corollary A.1.

- Second, let us discuss the bound of $P(\|(\mathbf{X}^* - \mathbf{X})\beta^*\|_\infty)$. Because

$$\begin{aligned}
& P\left(\|(\mathbf{X}^* - \mathbf{X})\beta^*\|_\infty > \frac{\epsilon}{2}\right) \\
& \leq P\left(\|\beta^*\|_\infty \max_{n=0, \dots, N-1} \sup_{x \in [0, X_{\max}]} \sum_{k=1}^K \|(\mathbf{X}_k^*(x, t_n) - \mathbf{X}_k(x, t_n))\|_\infty > \frac{\epsilon}{2}\right) \\
& = P\left(\max_{n=0, \dots, N-1} \sup_{x \in [0, X_{\max}]} \sum_{k=1}^K \|(\mathbf{X}_k^*(x, t_n) - \mathbf{X}_k(x, t_n))\|_\infty > \frac{\epsilon}{2\|\beta^*\|_\infty}\right) \\
& \leq \sum_{n=0}^{N-1} \sum_{k=1}^K P\left(\sup_{x \in [0, X_{\max}]} \|(\mathbf{X}_k^*(x, t_n) - \mathbf{X}_k(x, t_n))\|_\infty > \frac{\epsilon}{2K\|\beta^*\|_\infty}\right),
\end{aligned}$$

if we set

$$\begin{aligned}
\frac{\epsilon}{2K\|\beta^*\|_\infty} & > \mathcal{C}_{(\sigma, \|u\|_{L^\infty(\Omega)})} \max \left\{ 4K_{\max} M^{-3/7}, 4AM^{-3/7}, 4\sqrt{2} \frac{d^3}{dx^3} f^*(0) M^{-3/7}, \right. \\
& \quad \frac{16 \left[C_{(\sigma, \|u\|_{L^\infty(\Omega)})} \log M + \gamma(M) \right] \log(M)}{M^{3/7}}, \\
& \quad \left. 16\sqrt{\frac{\omega(M)}{7}} \tilde{C}(\sigma, \|u\|_{L^\infty(\Omega(M))}) \frac{\sqrt{\log(M)}}{M^{3/7}} \right\}, \quad (\text{A.43})
\end{aligned}$$

then we have

$$\begin{aligned}
& P\left(\|(\mathbf{X}^* - \mathbf{X})\beta^*\|_\infty > \frac{\epsilon}{2}\right) \\
& \leq NK \left[2M e^{-\frac{(M^{3/7} - \|U\|_{L^\infty(\Omega)})^2}{2\sigma^2}} + Q_{(\sigma, \|u\|_{L^\infty(\Omega)})} e^{-L\gamma(M)} + 4\sqrt{2}\eta^4 M^{-\omega(M)/7} \right] \quad (\text{A.44})
\end{aligned}$$

Inequality (A.44) is derived by Lemma A.2.

By combining the results in (A.41), (A.42), (A.43), (A.44), we have that when

$$\begin{aligned}
\frac{\epsilon}{2} &> \mathcal{C}_{(\sigma, \|u\|_{L^\infty(\Omega)})} \max \left\{ 4K_{\max} M^{-3/7}, 4KK_{\max} \|\beta^*\|_\infty N^{-3/7}, \right. \\
&4AM^{-3/7}, 4K\|\beta^*\|_\infty \bar{A}N^{-3/7}, \\
&4\sqrt{2} \frac{d^3}{dx^3} f^*(0) M^{-3/7}, 4\sqrt{2} K \|\beta^*\|_\infty \frac{d^3}{dx^3} \bar{f}^*(0) N^{-3/7}, \\
&\frac{16KK_{\max} \|\beta^*\|_\infty \left[C_{(\sigma, \|u\|_{L^\infty(\Omega)})} \log(M) + \gamma(M) \right] \log(M)}{M^{3/7}}, \\
&\frac{16K_{\max} \left[C_{(\sigma, \|u\|_{L^\infty(\Omega)})} \log(N) + \gamma(N) \right] \log(N)}{N^{3/7}}, \\
&16\sqrt{\frac{\omega(M)}{7}} \tilde{C}_{(\sigma, \|u\|_{L^\infty(\Omega)})} \frac{\sqrt{\log(M)}}{M^{3/7}}, \\
&\left. 16K \|\beta^*\|_\infty \sqrt{\frac{\omega(N)}{7}} \tilde{C}_{(\sigma, \|u\|_{L^\infty(\Omega)})} \frac{\sqrt{\log(N)}}{N^{3/7}} \right\},
\end{aligned}$$

we have

$$\begin{aligned}
&P(\|\nabla_t \mathbf{u} - \mathbf{X}\beta^*\|_\infty > \epsilon) \\
&\leq M \left[2Ne^{-\frac{(N^{3/7} - \|U\|_{L^\infty(\Omega)})^2}{2\sigma^2}} + Q_{(\sigma, \|u\|_{L^\infty(\Omega)})} e^{-L\gamma(N)} + 4\sqrt{2}\eta^4 N^{-\omega(N)/7} \right] + \\
&NK \left[2Me^{-\frac{(M^{3/7} - \|U\|_{L^\infty(\Omega)})^2}{2\sigma^2}} + Q_{(\sigma, \|u\|_{L^\infty(\Omega)})} e^{-L\gamma(M)} + 4\sqrt{2}\eta^4 M^{-\omega(M)/7} \right]
\end{aligned}$$

Now, let us do some simplification of the above results. Let $M = N^\kappa, \gamma(M) = \gamma(N) =$

$\frac{1}{L}N^r, \omega_{(M)} = \omega_{(N)} = N^{2r}$, and

$$\left\{ \begin{array}{l} \mathcal{J}_1 = 4KK_{\max}\|\beta^*\|_{\infty}N^{-3\kappa/7} \\ \mathcal{J}'_1 = 4K_{\max}N^{-3/7} \\ \mathcal{J}_2 = 4AK\|\beta^*\|_{\infty}N^{-3\kappa/7} \\ \mathcal{J}'_2 = 4\bar{A}N^{-3/7} \\ \mathcal{J}_3 = 4\sqrt{2}K\|\beta^*\|_{\infty}\frac{d^3}{dx^3}f^*(0)N^{-3\kappa/7} \\ \mathcal{J}'_3 = 4\sqrt{2}\frac{d^3}{dx^3}\bar{f}^*(0)N^{-3/7} \\ \mathcal{J}_4 = \frac{16KK_{\max}\|\beta^*\|_{\infty}\left[C_{(\sigma,\|u\|_{L^{\infty}(\Omega)})}(\log(\kappa)+\log(N))+N^r/L\right](\log(\kappa)+\log(N))}{N^{3\kappa/7}} \\ \mathcal{J}'_4 = \frac{16K_{\max}\left[C_{(\sigma,\|u\|_{L^{\infty}(\Omega)})}\log(N)+N^r\right]\log(N)}{N^{3/7}} \\ \mathcal{J}_5 = 16K\|\beta^*\|_{\infty}\sqrt{\frac{N^{2r}}{7}}\tilde{C}_{(\sigma,\|u\|_{L^{\infty}(\Omega)})}\frac{\sqrt{\log(\kappa)+\log(N)}}{N^{3\kappa/7}} \\ \mathcal{J}'_5 = 16\sqrt{\frac{N^{2r}}{7}}\tilde{C}_{(\sigma,\|u\|_{L^{\infty}(\Omega)})}\frac{\sqrt{\log(N)}}{N^{3/7}} \end{array} \right.$$

To guarantee that $\mathcal{J}_1, \mathcal{J}'_1, \mathcal{J}_2, \mathcal{J}'_2, \mathcal{J}_3, \mathcal{J}'_3, \mathcal{J}_4, \mathcal{J}'_4, \mathcal{J}_5, \mathcal{J}'_5 \rightarrow 0$, as $N \rightarrow +\infty$, we need

$$\left\{ \begin{array}{l} 3\kappa/7 - r > 0 \\ 3/7 - r > 0 \end{array} \right. ,$$

where the optimal κ is $\kappa = 1$. Accordingly, we have

$$\mathcal{J}_1, \mathcal{J}'_1, \mathcal{J}_2, \mathcal{J}'_2, \mathcal{J}_3, \mathcal{J}'_3, \mathcal{J}_5, \mathcal{J}'_5 \lesssim \mathcal{J}_4, \mathcal{J}'_4.$$

Based on the above discussion, we can declare that when N is sufficiently large, with

$$\epsilon > \mathcal{C}_{(\sigma,\|u\|_{L^{\infty}(\Omega)})}\frac{\log(N)}{N^{3/7-r}}$$

for any $r \in (0, \frac{3}{7})$ and $M = O(N)$, we have

$$\begin{aligned}
& P \|\nabla_t \mathbf{u} - \mathbf{X}\boldsymbol{\beta}^*\|_\infty > \epsilon) \\
& \leq M \left[2Ne^{-\frac{(N^{3/7} - \|U\|_{L^\infty(\Omega)})^2}{2\sigma^2}} + Q_{(\sigma, \|u\|_{L^\infty(\Omega)})} e^{-L\gamma(N)} + 4\sqrt{2}\eta^4 N^{-\omega(N)/7} \right] + \\
& \quad NK \left[2Me^{-\frac{(M^{3/7} - \|U\|_{L^\infty(\Omega)})^2}{2\sigma^2}} + Q_{(\sigma, \|u\|_{L^\infty(\Omega)})} e^{-L\gamma(M)} + 4\sqrt{2}\eta^4 M^{-\omega(M)/7} \right] \\
& = M \left[2Ne^{-\frac{(N^{3/7} - \|U\|_{L^\infty(\Omega)})^2}{2\sigma^2}} + Q_{(\sigma, \|u\|_{L^\infty(\Omega)})} e^{-N^r} + 4\sqrt{2}\eta^4 N^{-N^{2r}/7} \right] + \\
& \quad NK \left[2Me^{-\frac{(M^{3/7} - \|U\|_{L^\infty(\Omega)})^2}{2\sigma^2}} + Q_{(\sigma, \|u\|_{L^\infty(\Omega)})} e^{-N^r} + 4\sqrt{2}\eta^4 M^{-N^{2r}/7} \right] \\
& = O(Ne^{-N^r}).
\end{aligned}$$

Thus, we finish the proof of the theorem. \square

A.10.5 Proof of Theorem 3.1

Proof. By KKT-condition, any minimizer $\boldsymbol{\beta}$ of (2.10) must satisfies:

$$-\frac{1}{MN} \mathbf{X}^\top (\nabla_t \mathbf{u} - \mathbf{X}\boldsymbol{\beta}) + \lambda \mathbf{z} = 0 \text{ for } \mathbf{z} \in \partial \|\boldsymbol{\beta}\|_1,$$

where $\partial \|\boldsymbol{\beta}\|_1$ is the sub-differential of $\|\boldsymbol{\beta}\|_1$. The above equation can be equivalently transformed

into

$$\mathbf{X}^\top \mathbf{X}(\boldsymbol{\beta} - \boldsymbol{\beta}^*) + \mathbf{X}^\top [(\mathbf{X} - \mathbf{X}^*)\boldsymbol{\beta}^* - (\nabla_t \mathbf{u} - \nabla_t \mathbf{u}^*)] + \lambda MN \mathbf{z} = 0. \quad (\text{A.45})$$

Here matrix $\mathbf{X} \in \mathbb{R}^{MN \times K}$ is defined in (2.9), and matrix $\mathbf{X}^* \in \mathbb{R}^{MN \times K}$ is defined as

$$\mathbf{X}^* = (\mathbf{x}_0^0 \quad \mathbf{x}_1^0 \quad \dots \quad \mathbf{x}_{M-1}^0 \quad \mathbf{x}_1^0 \quad \dots \quad \mathbf{x}_{M-1}^{N-1})^\top,$$

with

$$\mathbf{x}_i^n = \left(1, u(x_i, t_n), \frac{\partial u(x_i, t_n)}{\partial x}, \frac{\partial^2 u(x_i, t_n)}{\partial x^2}, \left(\widehat{u(x_i, t_n)} \right)^2, \dots, \left(\frac{\partial^2 u(x_i, t_n)}{\partial x^2} \right)^{p_{\max}} \right)^\top \in \mathbb{R}^K.$$

And vector $\boldsymbol{\beta}^* = (\beta_1, \dots, \beta_K) \in \mathbb{R}^K$ is the ground truth coefficients. Besides, vector $\nabla_t \mathbf{u} \in \mathbb{R}^{MN}$ is defined in (2.8), and vector $\nabla_t \mathbf{u}^* \in \mathbb{R}^K$ is the ground truth, i.e.,

$$\nabla_t \mathbf{u}^* = \left(\frac{\partial u(x_0, t_0)}{\partial t}, \frac{\partial u(x_1, t_0)}{\partial t}, \dots, \frac{\partial u(x_{M-1}, t_0)}{\partial t}, \frac{\partial u(x_0, t_1)}{\partial t}, \dots, \frac{\partial u(x_{M-1}, t_{N-1})}{\partial t} \right)^\top.$$

Let us denote $\mathcal{S} = \{i : \beta_i^* \neq 0 \forall i = 0, 1, \dots, K\}$, then we can decompose \mathbf{X} into $\mathbf{X}_{\mathcal{S}}$ and $\mathbf{X}_{\mathcal{S}^c}$, where $\mathbf{X}_{\mathcal{S}}$ is the columns of \mathbf{X} whose indices are in \mathcal{S} and $\mathbf{X}_{\mathcal{S}^c}$ is the complement of $\mathbf{X}_{\mathcal{S}}$. And we can also decompose $\boldsymbol{\beta}$ into $\boldsymbol{\beta}_{\mathcal{S}}$ and $\boldsymbol{\beta}_{\mathcal{S}^c}$, where $\boldsymbol{\beta}_{\mathcal{S}}$ is the subvector of $\boldsymbol{\beta}$ only contains elements whose indices are in \mathcal{S} and $\boldsymbol{\beta}_{\mathcal{S}^c}$ is the complement of $\boldsymbol{\beta}_{\mathcal{S}}$.

By using the decomposition, we can rewrite (A.45) as

$$\begin{aligned} \begin{pmatrix} \mathbf{0} \\ \mathbf{0} \end{pmatrix} &= \begin{pmatrix} \mathbf{X}_{\mathcal{S}}^\top \mathbf{X}_{\mathcal{S}} & \mathbf{X}_{\mathcal{S}}^\top \mathbf{X}_{\mathcal{S}^c} \\ \mathbf{X}_{\mathcal{S}^c}^\top \mathbf{X}_{\mathcal{S}} & \mathbf{X}_{\mathcal{S}^c}^\top \mathbf{X}_{\mathcal{S}^c} \end{pmatrix} \begin{pmatrix} \boldsymbol{\beta}_{\mathcal{S}} - \boldsymbol{\beta}_{\mathcal{S}}^* \\ \boldsymbol{\beta}_{\mathcal{S}^c} \end{pmatrix} + \begin{pmatrix} \mathbf{X}_{\mathcal{S}}^\top \\ \mathbf{X}_{\mathcal{S}^c}^\top \end{pmatrix} [(\mathbf{X} - \mathbf{X}^*)_{\mathcal{S}} \boldsymbol{\beta}_{\mathcal{S}}^* - (\nabla_t \mathbf{u} - \nabla_t \mathbf{u}^*)] + \\ &\quad \lambda MN \begin{pmatrix} \mathbf{z}_{\mathcal{S}} \\ \mathbf{z}_{\mathcal{S}^c} \end{pmatrix} \end{aligned} \tag{A.46}$$

Suppose the primal-dual witness (PDW) construction gives us an solution $(\check{\boldsymbol{\beta}}, \check{\mathbf{z}}) \in \mathbb{R}^K \times \mathbb{R}^K$,

where $\check{\boldsymbol{\beta}}_{\mathcal{S}^c} = \mathbf{0}$ and $\check{\mathbf{z}} \in \partial \|\check{\boldsymbol{\beta}}\|_1$. By plugging $(\check{\boldsymbol{\beta}}, \check{\mathbf{z}})$ into the above equation, we have

$$\begin{aligned} \check{\mathbf{z}}_{\mathcal{S}^c} &= \mathbf{X}_{\mathcal{S}^c}^\top \mathbf{X}_{\mathcal{S}} (\mathbf{X}_{\mathcal{S}}^\top \mathbf{X}_{\mathcal{S}})^{-1} \mathbf{z}_{\mathcal{S}} - \mathbf{X}_{\mathcal{S}^c}^\top \underbrace{(\mathbf{I} - \mathbf{X}_{\mathcal{S}} (\mathbf{X}_{\mathcal{S}}^\top \mathbf{X}_{\mathcal{S}})^{-1} \mathbf{X}_{\mathcal{S}}^\top)}_{\mathbf{H}_{X_{\mathcal{S}}}} \frac{[(\mathbf{X} - \mathbf{X}^*)_{\mathcal{S}} \boldsymbol{\beta}_{\mathcal{S}}^* - (\nabla_t \mathbf{u} - \nabla_t \mathbf{u}^*)]}{\lambda MN} \\ &= \mathbf{X}_{\mathcal{S}^c}^\top \mathbf{X}_{\mathcal{S}} (\mathbf{X}_{\mathcal{S}}^\top \mathbf{X}_{\mathcal{S}})^{-1} \mathbf{z}_{\mathcal{S}} - \frac{1}{\lambda MN} \mathbf{X}_{\mathcal{S}^c}^\top \mathbf{H}_{X_{\mathcal{S}}} \underbrace{(\mathbf{X}_{\mathcal{S}} \boldsymbol{\beta}_{\mathcal{S}}^* - \nabla_t \mathbf{u})}_{\boldsymbol{\tau}}. \end{aligned} \tag{A.47}$$

From (A.47), we have

$$\begin{aligned}
P(\|\tilde{\mathbf{z}}_{S^c}\|_\infty \geq 1) &= P\left(\left\|\mathbf{X}_{S^c}^\top \mathbf{X}_S (\mathbf{X}_S^\top \mathbf{X}_S)^{-1} \mathbf{z}_S - \frac{1}{\lambda MN} \mathbf{X}_{S^c}^\top \mathbf{H}_{X_s} \boldsymbol{\tau}\right\|_\infty > 1\right) \\
&\leq P\left(\left\|\mathbf{X}_{S^c}^\top \mathbf{X}_S (\mathbf{X}_S^\top \mathbf{X}_S)^{-1} \mathbf{z}_S\right\|_\infty > 1 - \mu\right) + \\
&\quad P\left(\left\|\frac{1}{\lambda MN} \mathbf{X}_{S^c}^\top \mathbf{H}_{X_s} \boldsymbol{\tau}\right\|_\infty > \mu\right).
\end{aligned}$$

If we denote $\tilde{Z}_j = \frac{1}{\lambda MN} (\mathbf{X}_{S^c})_j^\top \mathbf{H}_{X_s} \boldsymbol{\tau}$, where $(\mathbf{X}_{S^c})_j$ is the j -th column of \mathbf{X}_{S^c} , then we have

$$P(\|\tilde{\mathbf{z}}_{S^c}\|_\infty \geq 1) \leq P\left(\left\|\mathbf{X}_{S^c}^\top \mathbf{X}_S (\mathbf{X}_S^\top \mathbf{X}_S)^{-1} \mathbf{z}_S\right\|_\infty > 1 - \mu\right) + P\left(\max_{j \in S^c} |\tilde{Z}_j| > \mu\right). \quad (\text{A.48})$$

Now let us discuss the upper bound of the second term, i.e., $P\left(\max_{j \in S^c} |\tilde{Z}_j| > \mu\right)$. Because

$$\begin{aligned}
P\left(\max_{j \in S^c} |\tilde{Z}_j| > \mu\right) &= P\left(\left\|\frac{1}{\lambda MN} \mathbf{X}_{S^c}^\top \mathbf{H}_{X_s} \boldsymbol{\tau}\right\|_\infty > \mu\right) \\
&\leq P\left(\left\|\frac{1}{\lambda MN} \mathbf{X}_{S^c}^\top \mathbf{H}_{X_s} \boldsymbol{\tau}\right\|_2 > \mu\right) \\
&\leq P\left(\left\|\frac{1}{\lambda MN} \mathbf{X}^\top \mathbf{H}_{X_s} \boldsymbol{\tau}\right\|_2 > \mu\right) \\
&\leq P\left(\frac{1}{\lambda MN} \|\mathbf{X}\|_2 \|\boldsymbol{\tau}\|_2 > \mu\right) \\
&\leq P\left(\|\boldsymbol{\tau}\|_2 > \lambda \mu \sqrt{\frac{MN}{K}}\right) \\
&\leq P\left(\|\boldsymbol{\tau}\|_\infty > \lambda \mu \frac{1}{\sqrt{K}}\right). \quad (\text{A.49})
\end{aligned}$$

By Lemma A.3, we know when

$$\lambda \mu \frac{1}{\sqrt{K}} > \mathcal{C}(\sigma, \|u\|_{L^\infty(\Omega)}) \frac{\log(N)}{N^{3/7-r}},$$

we have

$$P(\|\nabla_t \mathbf{u} - \mathbf{X} \boldsymbol{\beta}^*\|_\infty > \epsilon) < N e^{-N^r}.$$

So we know that

$$\begin{aligned}
P\left(\|\boldsymbol{\tau}\|_\infty > \lambda\mu\frac{1}{\sqrt{K}}\right) &= P\left(\|\nabla_t \mathbf{u} - \mathbf{X}_S \boldsymbol{\beta}_S^*\|_\infty > \lambda\mu\frac{1}{\sqrt{K}}\right) \\
&\leq P\left(\|\nabla_t \mathbf{u} - \mathbf{X} \boldsymbol{\beta}^*\|_\infty > \lambda\mu\frac{1}{\sqrt{K}}\right) \\
&< Ne^{-N^r}.
\end{aligned} \tag{A.50}$$

By plugging the results in (A.49) and (A.50) into (A.48), we have

$$\begin{aligned}
P(\|\check{\mathbf{z}}_{S^c}\|_\infty \geq 1) &\leq P\left(\left\|\mathbf{X}_{S^c}^\top \mathbf{X}_S (\mathbf{X}_S^\top \mathbf{X}_S)^{-1}\right\|_\infty > 1 - \mu\right) + P\left(\max_{j \in S^c} |\widetilde{Z}_j| > \mu\right) \\
&\leq P\left(\left\|\mathbf{X}_{S^c}^\top \mathbf{X}_S (\mathbf{X}_S^\top \mathbf{X}_S)^{-1}\right\|_\infty > 1 - \mu\right) + P\left(\|\boldsymbol{\tau}\|_\infty > \lambda\mu\frac{1}{\sqrt{K}}\right) \\
&\leq P\left(\left\|\mathbf{X}_{S^c}^\top \mathbf{X}_S (\mathbf{X}_S^\top \mathbf{X}_S)^{-1}\right\|_\infty > 1 - \mu\right) + Ne^{-N^r}.
\end{aligned}$$

The probability for proper support set recovery is

$$\begin{aligned}
P(\|\check{\mathbf{z}}_{S^c}\|_\infty < 1) &= 1 - P(\|\check{\mathbf{z}}_{S^c}\|_\infty \geq 1) \\
&\geq 1 - \left[P\left(\left\|\mathbf{X}_{S^c}^\top \mathbf{X}_S (\mathbf{X}_S^\top \mathbf{X}_S)^{-1}\right\|_\infty > 1 - \mu\right) + Ne^{-N^r}\right] \\
&= P\left(\left\|\mathbf{X}_{S^c}^\top \mathbf{X}_S (\mathbf{X}_S^\top \mathbf{X}_S)^{-1}\right\|_\infty \leq 1 - \mu\right) - Ne^{-N^r} \\
&\leq P_\mu - Ne^{-N^r}.
\end{aligned}$$

Thus, we finish the proof. \square

A.10.6 Proof of Theorem 3.2

Proof. By equation (A.46), we can solve $\boldsymbol{\beta}_S - \boldsymbol{\beta}_S^*$ as

$$\boldsymbol{\beta}_S - \boldsymbol{\beta}_S^* = (\mathbf{X}_S^\top \mathbf{X}_S)^{-1} \left[-\mathbf{X}_S^\top (\mathbf{X}_S - \mathbf{X}_S^*) \boldsymbol{\beta}_S^* + \mathbf{X}_S^\top (\nabla_t \mathbf{u} - \nabla_t \mathbf{u}^*) - \lambda MN \mathbf{z}_S \right].$$

Thus, we have the following series of equations:

$$\begin{aligned}
& \max_{k \in \mathcal{S}} |\beta_k - \beta_k^*| \\
& \leq \left\| (\mathbf{X}_S^\top \mathbf{X}_S)^{-1} \right\|_\infty \left\| \mathbf{X}_S^\top [\nabla_t \mathbf{u} - \nabla_t \mathbf{u}^* - (\mathbf{X}_S - \mathbf{X}_S^*) \beta_S^*] - \lambda MN \mathbf{z}_S \right\|_\infty \\
& \leq \left\| (\mathbf{X}_S^\top \mathbf{X}_S)^{-1} \right\|_\infty \left[\left\| \mathbf{X}_S^\top [\nabla_t \mathbf{u} - \nabla_t \mathbf{u}^* - (\mathbf{X}_S - \mathbf{X}_S^*) \beta_S^*] \right\|_\infty + \lambda MN \|\mathbf{z}_S\|_\infty \right] \\
& = \left\| (\mathbf{X}_S^\top \mathbf{X}_S)^{-1} \right\|_\infty \left[\left\| \mathbf{X}_S^\top (\nabla_t \mathbf{u} - \mathbf{X}_S \beta_S^*) \right\|_\infty + \lambda MN \|\mathbf{z}_S\|_\infty \right] \tag{A.51}
\end{aligned}$$

$$\leq \left\| \left(\frac{\mathbf{X}_S^\top \mathbf{X}_S}{MN} \right)^{-1} \right\|_\infty \left(\frac{\left\| \mathbf{X}_S^\top (\nabla_t \mathbf{u} - \mathbf{X}_S \beta_S^*) \right\|_\infty}{MN} + \lambda \right) \tag{A.52}$$

$$\leq \sqrt{K} C_{\min} \left(\frac{\left\| \mathbf{X}_S^\top (\nabla_t \mathbf{u} - \mathbf{X}_S \beta_S^*) \right\|_\infty}{MN} + \lambda \right) \tag{A.53}$$

$$\leq \sqrt{K} C_{\min} \left(\frac{\|\mathbf{X}_S\|_{\infty, \infty} \|\nabla_t \mathbf{u} - \mathbf{X}_S \beta_S^*\|_\infty}{MN} + \lambda \right) \tag{A.54}$$

$$\begin{aligned}
& \leq \sqrt{K} C_{\min} \left(\frac{\|\mathbf{X}_S\|_F \|\nabla_t \mathbf{u} - \mathbf{X}_S \beta_S^*\|_\infty}{\sqrt{MN}} + \lambda \right) \\
& \leq \sqrt{K} C_{\min} \left(\frac{\sqrt{MNK} \|\nabla_t \mathbf{u} - \mathbf{X}_S \beta_S^*\|_\infty}{\sqrt{MN}} + \lambda \right) \tag{A.55}
\end{aligned}$$

$$\begin{aligned}
& = \sqrt{K} C_{\min} \left(\sqrt{K} \|\nabla_t \mathbf{u} - \mathbf{X}_S \beta_S^*\|_\infty + \lambda \right) \\
& \leq \sqrt{K} C_{\min} \left(\sqrt{K} \mathcal{E}_{(\sigma, \|u\|_{L^\infty(\Omega)})} \frac{\log(N)}{N^{3/7-r}} + \lambda \right) \tag{A.56}
\end{aligned}$$

Equation (A.51) is because $\nabla_t \mathbf{u}^* = \mathbf{X}_S \beta_S^*$. Inequality (A.52) is because $\|\mathbf{z}_S\|_\infty = 1$. Inequality (A.53) is because of Condition 3.2. Inequality (A.54) is because for a matrix \mathbf{A} and a vector \mathbf{x} , we have $\|\mathbf{A}\mathbf{x}\|_q \leq \|\mathbf{A}\|_{p,q} \|\mathbf{x}\|_p$. Here the matrix norm for matrix $\mathbf{A} \in \mathbb{R}^{m \times n}$ in $\|\mathbf{A}\|_{\infty, \infty} = \|\text{vector}(\mathbf{A})\|_\infty$. In inequality (A.55), the norm of matrix $\mathbf{A} \in \mathbb{R}^{m \times n}$ is that $\|\mathbf{A}\|_F = \sqrt{\sum_{i=1}^m \sum_{j=1}^n |A_{ij}|^2}$, and the norm of vector $\mathbf{a} \in \mathbb{R}^d$ is $\|\mathbf{a}\|_\infty = \max_{1 \leq i \leq d} |a_i|$. Inequality (A.55) is because we normalized columns of \mathbf{X} . Inequality (A.56) is due to Lemma Lemma A.3 under probability $1 - O(Ne^{-N^r}) \rightarrow 1$. \square

A.11 The full model used in Section 4

The full model used in Section 4 is

$$\begin{aligned}
 \frac{\partial}{\partial t} u(x, t) &= \beta_1^* + \beta_2^* u(x, t) + \beta_3^* \frac{\partial}{\partial x} u(x, t) + \beta_4^* \frac{\partial^2}{\partial x^2} u(x, t) + \\
 &\beta_5^* [u(x, t)]^2 + \beta_6^* \left[\frac{\partial}{\partial x} u(x, t) \right]^2 + \beta_7^* \left[\frac{\partial}{\partial x} u(x, t) \right]^2 + \\
 &\beta_8^* u(x, t) \frac{\partial}{\partial x} u(x, t) + \beta_9^* u(x, t) \frac{\partial^2}{\partial x^2} u(x, t) + \\
 &\beta_{10}^* \frac{\partial}{\partial x} u(x, t) \frac{\partial^2}{\partial x^2} u(x, t)
 \end{aligned}$$

A.12 Checking Conditions of Example 1,2,3

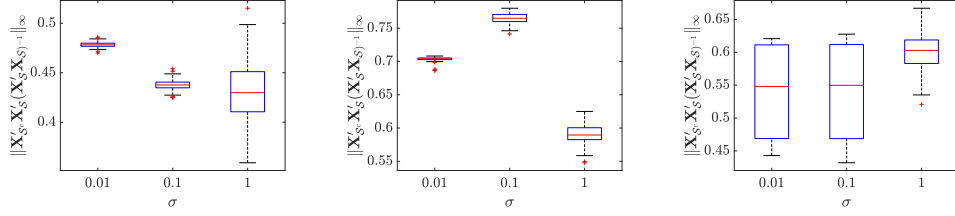
In this section, we check Condition 3.1 - Condition 3.5 of the above three examples: (1) example 1 (the transport equation), (2) example 2 (the inviscid Burgers' equation) and (3) example 3 (the viscous Burgers' equation).

A.12.1 Verification of Condition 3.1, 3.2

In this section, we check the Condition 3.1 - Condition 3.2 under example 1,2,3, though the applicability of the results is by no means restricted to these.

The verification results can be found in Fig. 11 and Fig. 12, where (a),(b),(c) are the box plot of $\|\mathbf{X}_{S^c}^\top \mathbf{X}_S (\mathbf{X}_S^\top \mathbf{X}_S)^{-1}\|_\infty$ and the minimal eigenvalue of matrix $\frac{1}{NM} \mathbf{X}_S^\top \mathbf{X}_S$ of these three examples under $\sigma = 0.01, 0.1, 1$, respectively. From Fig. 11, we find the value of $\|\mathbf{X}_{S^c}^\top \mathbf{X}_S (\mathbf{X}_S^\top \mathbf{X}_S)^{-1}\|_\infty$ is smaller than 1, so there exist a $\mu \in (0, 1]$ such that Condition 3.1 is met. From Fig. 12, we find the minimal eigenvalue of matrix $\frac{1}{MN} \mathbf{X}_S^\top \mathbf{X}$ are all strictly larger than 0, so we declare Condition 3.2 is satisfied.

A.12 Checking Conditions of Example 1,2,3

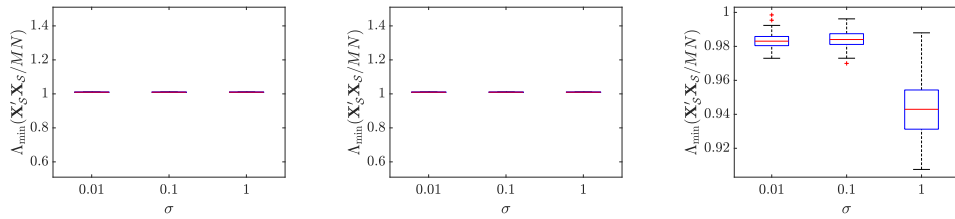


(a) example 1:

(b) example 2:

(c) example 3:

Figure 11: Box plots of $\|\mathbf{X}_{\mathcal{S}^c}^\top \mathbf{X}_{\mathcal{S}} (\mathbf{X}_{\mathcal{S}}^\top \mathbf{X}_{\mathcal{S}})^{-1}\|_\infty$ under $\sigma = 0.01, 0.1, 1$ when $M = N = 100$.



(a) example 1:

(b) example 2:

(c) example 3:

Figure 12: Box plots of the minimal eigenvalue of matrix $\frac{1}{NM} \mathbf{X}_{\mathcal{S}}^\top \mathbf{X}_{\mathcal{S}}$ under $\sigma = 0.01, 0.1, 1$ when $M = N = 100$.

A.12.2 Verification of Condition 3.3 and Condition 3.4

In example 1,2,3, the design points x_0, x_1, \dots, x_{M-1} and t_0, t_1, \dots, t_{N-1} are equally spaced, i.e., $x_0 = 1/M, x_1 = 2/M, \dots, x_{M-1} = 1$ and $t_0 = 0.1/N, t_1 = 0.2/N, \dots, t_{N-1} = 0.1$. Under this scenario, there exist an absolutely continuous distribution $F(x) = x$ for $x \in [1/M, 1]$ and $G(t) = 0.1t$ for $t \in [0.1/N, 0.1]$, where the empirical c.d.f. of the design points x_0, x_1, \dots, x_{M-1} and t_0, t_1, \dots, t_{N-1} will converge to $F(x), G(t)$, respectively, as $M, N \rightarrow +\infty$. For the $F(x), G(t)$, we know their first derivatives is bounded for $x \in [1/M, 1]$ and $t \in [0.1/N, 0.1]$, respectively. In the simulation of this paper, we take the equally spaced design points as an illustration example, and its applicability is by no means restricted to this case.

A.12.3 Verification of Condition 3.5.

The Condition 3.5 ensures that the smoothing parameter does not tend to zero too rapidly. Silverman (1984) shows that for the equally spaced design points, this condition meets. For other types of design points, for instance, randomly and independently distributed design points, it can also be verified that Condition 3.5 is satisfied (see Silverman, 1984, Section 2).

A.13 Details of the Case Study

The header of the CALIPSP dataset and its visualization can be found in Table 4 and Fig. 9(a), respectively. Fig. 9(a) shows presents the curves of the dynamic in the CALIPSP dataset, where the x-axis is the longitude and the y-axis is the value of the observed temperature. Here the

A.14 More details of Fig. 10

black curve plots the observed temperature in January 2017, and the lighter color presents the later month. As seen from Fig. 9, we find overall there is an increasing trend of the temperature in the first half-year and then the temperature decreases.

Table 4: The header of the CALIPSP dataset

	longitude						
	-177.5	-172.5	-167.5	...	167.5	172.5	177.5
Jan 2017	-46.5103	-48.4720	-44.6581	...	-44.2778	-47.3354	-44.0146
Feb 2017	-46.2618	-43.1994	-47.6370	...	-46.8409	-46.2727	-40.5556
⋮	⋮	⋮	⋮	⋮	⋮	⋮	⋮
Dec 2017	-47.3145	-47.6505	-50.8332	...	-43.9705	-43.0475	-46.0618

¹ The data is downloaded from https://asdc.larc.nasa.gov/data/CALIPSO/LID_L3_Tropospheric_APro_CloudFree-Standard-V (registration is required).

² The negative and positive longitude refer to the west and east longitude, respectively.

A.14 More details of Fig. 10

The three-dimension surface plot of the observed temperature in 2017 can be found in Fig. 10(a.1), whose fitted value can be found in Fig. 10(a.2). The three-dimension surface plot of the residual between the observed temperature and the fitted temperature can be found in Fig. 10(a.3). Seeing from Fig. 10(a.1)-(a.3), we find the fitted temperature captures the dynamic trend of the raw data well. Although the magnitude of the residual is not small, it is still satisfying given the following reasons. The fitted value by using the explicit Euler method only

serves as the baseline method, which is not accurate enough for fitting. In this paper, we focus on PDE identification, so we use the most simple method – the explicit Euler method – to check if the identified PDE model in (5.16) can capture the features of the underlying PDE model. The more advanced method – Runge-Kutta fourth order method (RK4) – is not implementable in our content, and the reasons are explained in online supplementary material.

The value to plot Fig. 10(a.2) is calculated as follows. First, we use the identified PDE model in (5.16) to predict the value of $\frac{\partial}{\partial t}u(x, t)$ in January 2017. Then, we use the explicit Euler method (Butcher and Goodwin, 2008) to predict the future value from February 2017 to December 2017, i.e., we have $u(x, t + \Delta t) = u(x, t) + \frac{\partial}{\partial t}u(x, t)\Delta t$.